FCT Fundação para a Ciência e a Tecnologia
MINISTÉRIO DA CIÊNCIA, TECNOLOGIA E ENSINO SUPERIOR

POPH
QUALIFICAR É CRESCER.

QREN
QUADRO DE REFERÊNCIA ESTRATÉGICO NACIONAL
PORTUGAL 2007.2013

GOVERNO DA REPÚBLICA PORTUGUESA

UNIÃO EUROPEIA
Fundo Social Europeu

Rita Daniela Nogueira Rebelo   Fibrous Braided Stents with Antibacterial Properties

UMinho | 2017

Universidade do Minho
Escola de Engenharia

Rita Daniela Nogueira Rebelo

Fibrous Braided Stents with Antibacterial Properties

fevereiro de 2017

Universidade do Minho
Escola de Engenharia

Rita Daniela Nogueira Rebelo

Fibrous Braided Stents with Antibacterial Properties

Tese de Doutoramento
Programa Doutoral em Engenharia Biomédica

Trabalho efectuado sob a orientação de
Professor Doutor Raul Manuel Esteves Sousa Fangueiro
Professora Doutora Sandra Maria Fernandes Carvalho
Professora Doutora Mariana Contente Rangel Henriques

fevereiro de 2017

STATEMENT OF INTEGRITY

I hereby declare having conducted my thesis with integrity. I confirm that I have not used plagiarism or any form of falsification of results in the process of the thesis elaboration.
I further declare that I have fully acknowledged the Code of Ethical Conduct of the University of Minho.

University of Minho, February, 2017

Full name: Rita Daniela Nogueira Rebelo

Signature: Rita Daniela Nogueira Rebelo

“Se o conhecimento pode criar problemas, não é através da ignorância que podemos solucioná-los.”

Isaac Asimov

Agradecimentos

A realização de uma tese de doutoramento nunca é um processo solitário e só é possível graças ao contributo de inúmeras pessoas e instituições, às quais não posso deixar de expressar o meu profundo agradecimento.

Em primeiro lugar quero agradecer ao meu orientador, Professor Raul Fangueiro, por ter acreditado e pela colaboração, não só durante o doutoramento, mas ao longo dos últimos 6 anos de trabalho em conjunto.

À Professora Sandra Carvalho, minha co-orientadora, um enorme obrigada pela paciência, confiança, apoio e disponibilidade sempre demonstrada ao longo da realização da tese. Este trabalho teria sido extremamente mais difícil sem a presença da professora.

À Professora Mariana Henriques, igualmente minha co-orientadora, gostaria de agradecer pelo auxílio, motivação e pela alegria que sempre partilhou comigo, mesmo nas horas mais complicadas.

A todos os elementos do grupo Fibernamics, aos que fazem e aos que já fizeram parte desta equipa, o meu sincero agradecimento, em especial ao Fernando Cunha e à Nívea Vila pela ajuda e paciência, na fase inicial deste trabalho.

À Catarina Guise, pela partilha de conhecimento, quer pessoal quer científico, ao longo destes anos. Obrigada, essencialmente, pela amizade e por me teres ajudado a manter o foco.

À Sílvia Carvalho, a maior otimista e motivadora que eu conheço, obrigada pelo incentivo, pela amizade e por me motivares sempre.

Aos meus colegas do “Surface Modification and Functionalization – Research Group”: Cristiana Alves, Edgar Carneiro, Isabel Carvalho, Isabel Ferreri, Mariana Marques, Noora Manninen, Sebastian Calderon e Simone Rodrigues, um enorme obrigada por me terem acolhido tão bem e pelos inúmeros *inputs* científicos, ao longo destes 4 anos, bem como pela paciência e amizade.

À Fundação para a Ciência e Tecnologia pelo financiamento da bolsa individual de doutoramento SFRH / BD / 90321/2012.

Ao André Castro, ao Manuel Pinheiro e ao Nuno Domingues, acima de tudo pela amizade, mas também pelo contributo e discussão científica ao longo do doutoramento.

A todos meus amigos, e não mencionando nomes, pois temo esquecer-me de alguém, um enorme obrigada por estarem sempre lá, por não me deixarem desistir, por acreditarem e por me

perdoarem os dias maus e os dias em que não pude estar presente. Convosco é tudo muito mais fácil!

Por fim, à minha família, em especial ao meu irmão e aos meus pais. Obrigada por me terem mostrado que vale sempre a pena, pelo carinho, pela paciência e pela inesgotável confiança que sempre depositaram em mim. Nada disto seria possível sem vós.

Obrigada mãe, obrigada pai…por tudo, e por tanto!!!

POPH QUALIFICAR É CRESCER.
QREN QUADRO DE REFERÊNCIA ESTRATÉGICO NACIONAL PORTUGAL 2007.2013
Governo da República Portuguesa
UNIÃO EUROPEIA Fundo Social Europeu
FCT Fundação para a Ciência e a Tecnologia
MINISTÉRIO DA CIÊNCIA, TECNOLOGIA E ENSINO SUPERIOR

Abstract

Nowadays, cardiovascular diseases are reported as a major cause of death and disability in developed countries. Therefore, stents have emerged as a solution to overcome this problem. However, common commercialize stents, are metallic, which present several disadvantages as corrosion, higher risk of restenosis and infection. In order to minimize the disadvantages associated with these stents, new materials, like fibrous materials, have begun to be used as well as surface modifications of biomaterials begun to be applied, in order to avoid those drawbacks, especially infection. Therefore, the main objective of this work was the development of a fibrous stent, able to compete with the mechanical properties of the commercial ones, with the advantaged of being coated with an antibacterial agent, able to avoid infections.

For this purpose, braided stents were produced by varying materials, structural and process parameters, such as monofilament type and diameter, braiding angle and mandrel diameter. The influence of these design parameters on mechanical behavior, as well as stent's porosity, was thoroughly investigated, and suitable parameters were selected for developing a stent with mechanical characteristics and porosity matching with the commercial stents. According to the experimental results, suitable performance was achieved with a polyester stent designed with: monofilament diameter of 270 μm, braiding angle of 35°; and mandrel diameter of 6 mm, providing similar properties to commercial Nitinol stents (porosity above 70%, unchanged diameter during bending tests above 75%, force for longitudinal compression between [0.16-5.28] N and force for radial compression between [1.13-2.90] N).

After the stent's development, silver and silver oxide thin films were deposited by non-reactive and reactive pulsed dc magnetron sputtering. The coatings were characterized chemical, physical and structurally. This first approach in stent's functionalization revealed that silver thin film formed a continuous layer, while silver oxide layer was composed of islands with hundreds of nanometers surrounded by small nanoparticles with tens of nanometers. In order to verify the antibacterial behavior of the coatings, halo inhibition zone tests were realized for *Staphylococcus epidermidis* and *Staphylococcus aureus*. Silver coatings did not show antibacterial behavior, contrarily to silver oxide coatings, which presented antibacterial properties against the studied bacteria. The presence of silver oxide phase along with the development of different morphology were pointed as the main factors in the origin of the antibacterial effect found in silver oxide thin film.

With the purpose of understand the influence of oxygen species in the physical, chemical and structural properties of thin films new silver and silver oxide thin films were deposited, by non-reactive and reactive pulsed dc magnetron sputtering, with the variation of oxygen content. The resulted coatings revealed that silver coating forms a continuous layer. The incorporation of oxygen leads to the formation of a mixture of Ag_2O + AgO phases. However, with the increase of the oxygen fraction, the mixture of oxides disappear and the resultant thin film became only AgO.

Cytotoxicity tests were performed, demonstrating that in the silver oxide coating no cytotoxicity was found, making this coating able to be used in stents applications.

The antibacterial behavior of coatings was, quantitatively, tested against *Staphylococcus epidermis*, showing that Ag_xO unlike Ag coating presented antibacterial behavior. The presence of silver oxide is the main reason for the antibacterial effect, probably due to the increased production of reactive oxygen species (ROS).

Finally, and in order to evaluate the coating's behavior when subjected to mechanical forces, coated silver and silver oxide stents were, again, mechanically tested, and no loss of adhesion or delamination were observed, indicating that coatings will support, adequately, the mechanical forces and the dangerous of delivering parts of coating in blood current will not occur.

In conclusion, fibrous stents coated with silver oxide, present a good mechanical behavior, when compared with nitinol commercial stents, possess antibacterial properties and are no cytotoxic, which made this stent a promising candidate as a biomaterial and a viable substitute to metallic stents.

Resumo

Atualmente, as doenças cardiovasculares são consideradas a principal causa de morte e incapacidade nos países desenvolvidos. Os *stents* surgiram como uma solução para este problema, contudo, os que se encontram no mercado são metálicos, pelo que apresentam várias desvantagens como: corrosão, maior risco de reestenose e infeção. A fim de minimizar as desvantagens associadas a estes *stent*s, novos materiais, como materiais fibrosos, começaram a ser utilizados, assim como, a modificação da superfície dos biomateriais, de forma a evitar a infeção. Consequentemente, o principal objetivo deste trabalho foi o desenvolvimento de um *stent* fibroso, capaz de competir com as propriedades mecânicas dos *stents* comerciais, com a vantagem de ser revestido com um agente antibacteriano, evitando, deste modo, a possibilidade de infeção.

Para este efeito, foram produzidos diferentes *stents* entrançados, através da variação dos materiais, parâmetros estruturais e de processo, tais como: o tipo de monofilamento e o seu diâmetro, ângulo de entrançamento e diâmetro do mandril. A influência destes parâmetros no comportamento mecânico, bem como a porosidade dos *stents* foram estudadas detalhadamente. Para o desenvolvimento do *stent* foram selecionados os parâmetros adequados com o objetivo de obter caraterísticas mecânicas e porosidade compatíveis com os *stents* comerciais. De acordo com os resultados experimentais, a melhor performance foi obtida com um *stent* de poliéster com diâmetro de monofilamento de 270 μm, ângulo de entrançamento de 35° e o diâmetro do mandril de 6 mm, proporcionando propriedades semelhantes ao *stent*s comerciais de nitinol (porosidade acima de70%, diâmetro inalterado durante os testes de dobragem acima de 75%, força de compressão longitudinal compreendida entre [0.16-5.28] N e força de compressão radial compreendida entre [1.13-2.90] N).

Após a produção do *stent*, foram depositados filmes finos de prata e óxidos de prata, através da pulverização catódica pulsada em magnetrão, em regime não-reativo e reativo.

Os revestimentos foram caracterizados química, física e estruturalmente. Esta primeira abordagem na funcionalização do *stent* revelou que o revestimento de prata formou um filme contínuo, enquanto o filme de óxido de prata era composto de ilhas, com centenas de nanómetros rodeadas por nanopartículas com dezenas de nanómetros. A fim de verificar o comportamento antibacteriano dos revestimentos, foram realizados testes de halo para *Staphylococcus epidermidis* e *Staphylococcus aureus*. Como resultado, o revestimento de prata não apresentou comportamento antibacteriano, ao contrário do revestimento de óxido de prata, que apresentou propriedades antibacterianas contra as bactérias estudadas. A presença da fase de óxido de prata juntamente com o desenvolvimento de morfologias diferentes foram apontados como os principais fatores na origem do efeito antibacteriano encontrado no revestimento de óxido de prata.

Com o propósito de compreender a influência das espécies de oxigênio nas propriedades físicas, químicas e estruturais dos filmes finos, foram depositados novos revestimentos de prata e óxido de prata, por pulverização catódica em magnetrão, em regime não-reativo e reativo, com variação do teor de oxigénio. Os revestimentos resultantes revelaram que os revestimentos de prata formaram uma camada contínua. A incorporação do oxigénio levou à formação de uma mistura de fases de Ag_2O + AgO. Contudo, com o aumento da fração de oxigénio, a mistura de óxidos desapareceu e os filmes finos resultantes apresentaram apenas a fase de AgO.

Foram realizados ensaios de citotoxicidade, demonstrando que o revestimento de óxido de prata escolhido não é tóxico, tornando-o adequado para ser aplicado em *stent*s.

O comportamento antibacteriano dos revestimentos foi, quantitativamente, testado contra *Staphylococcus epidermis*, revelando que os revestimentos de Ag_xO, ao contrário dos revestimentos de Ag, apresentam um comportamento antibacteriano. A presença do óxido de prata é um dos principais fatores para o efeito antibacteriano, provavelmente, devido ao aumento da produção de espécies reativas de oxigénio (ROS).

Finalmente, e de modo a avaliar o comportamento do revestimento quando submetido a forças mecânicas, os *stent*s revestidos com prata e óxido de prata foram, novamente, testados mecanicamente, e não se observou perda de adesão ou a delaminação do filme. Estes resultados indicam que os revestimentos conseguem suportar, de forma adequada, as forças mecânicas e que não haverá risco de perda de revestimento para a corrente sanguínea.

Em conclusão, os *stent*s fibrosos revestidos com óxido de prata, apresentam um bom comportamento mecânico, quando comparado com os *stent*s comerciais de nitinol, além de apresentarem propriedades antibacterianas e não serem citotóxicos, o que torna este *stent* um candidato promissor como substituto para os *stent*s metálicos atuais.

Contents

Agradecimentos iii

Abstract v

Resumo vii

Contents ix

List of Figures xiii

List of Tables xvii

Nomenclature xix

Scope of the thesis xxiii

Structure of the Thesis xxv

CHAPTER I – STATE OF THE ART 2

1. Introduction 3
   1.1. Coronary diseases 3
   1.2. Stents 5
   1.3. Metallic Stents 7
   1.4. Fibrous Stents 10
      1.4.1. Methods of stent’s production 12

2. Infection 16

3. Functionalization of stents 18
   3.1. Antibacterial Coatings 19
   3.2. Functionalization techniques 24

CHAPTER II- DEVELOPMENT AND MECHANICAL BEHAVIUOR OF FIBROUS STENTS 29

1. Introduction 31

2. Materials and Methods 33
   2.1. Characterization of raw materials 33
   2.2. Braiding Conditions 33
   2.3. Cover Factor and Porosity Evaluations 34
   2.4. Measurement of Radial Compression 34
   2.5. Determination of Longitudinal Compression 36
   2.6. Determination of Bending Properties 37

3. Results and Discussion 39
  3.1. Development of braided fibrous stents 39
  3.2. Mechanical behavior of fibrous stents 44
    3.2.1. Cover Factor and Porosity 44
    3.2.2. Radial Compression 49
    3.2.3. Longitudinal Compression 56
    3.2.4. Bending properties 61
  3.3. Discussion 61
    3.3.1. Selection of fiber type and design parameters 63

4. Partial Conclusion 64

CHAPTER III – DEVELOPMENT AND CHARACTERIZATION OF ANTIBACTERIAL COATINGS 67

1. Introduction 69
  1.1. Silver-based Coatings 70

2. Materials and Methods 71
  2.1. Production of silver and silver oxide coatings 71
  2.2. Characterization of silver and silver oxide coatings 73
  2.3. Preliminary antibacterial evaluation 75

3. Results and Discussion 77
  3.1. Characterization of silver and silver oxide coatings 77
  3.2. Preliminary antibacterial evaluation: Halo Test 84

4. Partial Conclusion 87

CHAPTER IV – INFUENCE OF OXYGEN CONTENT ON THE ANTIBACTERIAL COATINGS 89

1. Introduction 91

2. Materials and Methods 92
  2.1. Production of silver and silver oxide coatings 92
  2.2. Characterization of silver and silver oxide coatings 93
  2.3. Preliminary antibacterial evaluation 94

3. Results and Discussion 95
  3.1. Characterization of silver and silver oxide coatings 95
  3.2. Preliminary antibacterial evaluation 106

4. Partial Conclusions 109

CHAPTER V – FIBROUS STENTS WITH ANTIBACTERIAL COATINGS:FUNCTIONAL PROPERTIES STUDY 111

1. Introduction 113

2. Materials and Methods 113
  2.1. Production of silver and silver oxide coatings 113
  2.2. Characterization of silver and silver oxide coatings 114

3. Results and Discussion 116
  3.1. Coating's Characterization 116

4. Partial Conclusions 123

CHAPTER VI - CONCLUSIONS AND FUTURE WORK 125

1. Main Conclusions 127

2. Future Work 129

References 131

List of Figures

Figure 1-Schematic representation of the different stages of the thesis. xxvi
Figure 2- Schematic representation of an artery. 4
Figure 3- Conventional angioplasty (a)) and angioplasty with stent (b)) 5
Figure 4- Conventional metallic stent (image adapted from:[7]). 6
Figure 5- Braided structure. 14
Figure 6- Scheme of work of braiding machine, with four gear wheels. 16
Figure 7- Biofilm formation (image adapted from [48]). 17
Figure 8-Layer-by-layer technique (figure adapted from [91]). 25
Figure 9- Schematic representation of the magnetron. 27
Figure 10- Example of a target used in magnetron sputtering. 27
Figure 11- Vertical braided machine used in the development of stents. 33
Figure 12- Scheme of resultant axial force in a stent when subjected to radial pressure. 35
Figure 13– Setup of radial compression test. 36
Figure 14-Setup of longitudinal compression test. 37
Figure 15- Measurement of unchanged bending diameter. 38
Figure 16-DSC analysis for PES fibers 40
Figure 17- DSC analysis for PA fibers. 41
Figure 18-DSC analysis for PP fibers. 41
Figure 19-Influence of fiber type and diameter on porosity [mandrel diameter: 6mm, braiding angle: 35º]. 45
Figure 20-Influence of mandrel diameter on cover factor of PA stents (a), PES stents (b) and PP stents (c) [braiding angle: 35º]. 46
Figure 21 - Influence of braiding angle on cover factor of PA stents (a), PES stents (b) and PP stents (c) [mandrel diameter:3.2 mm]. 48
Figure 22- Difference in PP260A35D6 (a)) and PES550A35D32 (b)) cover factor. 49
Figure 23 - Influence of fiber type and monofilament diameter on radial compression force for stents produced with 35° braiding angle and 3.2 mm mandrel diameter. 50
Figure 24 - Influence of mandrel diameter on radial force of PA stents (a), PES stents (b) and PP stents (c) [braiding angle:35º]. 52
Figure 25 - Influence of braiding angle on radial compression force of PA stents (a), PES stents (b) and PP stents (c) [mandrel diameter:3.2 mm]. 54
Figure 26 - Influence of fiber type and diameter on longitudinal compression force [braiding angle: 35º, mandrel diameter: 3.2 mm]. 57
Figure 27 - Influence of mandrel diameter on longitudinal force of PA stents (a), PES stents (b) and PP stents (c) [braiding angle: 35º]. 58
Figure 28 - Influence of braiding angle on longitudinal compressive force of PA stents (a), PES stents (b) and PP stents (c) produced using mandrel diameter of 3.2 mm. 60
Figure 29 - Comparison of unchanged diameter of PA stents (a), PES stents (b) and PP stents (c). 61
Figure 30- Summary of the production and mechanical behavior of developed fibrous stent. 65
Figure 31- Equipment of reactive magnetron sputtering and a schematic of the interior of the deposition chamber (not at scale). 69

Figure 32 - Variation of target potential as function of fO$_2$ for different applied density currents: a) 2.5 mA.cm^{-2} and b) 1 mA.cm^{-2}........ 72
Figure 33- Example of a sample without halo (a)) and a sample with halo (b))........ 76
Figure 34- Variation of Ag target voltage and total pressure in deposition chamber for different fO$_2$ (at a constant JAg of 1 mA.cm^{-2})........ 78
Figure 35 – XPS spectra of Ag3d core levels of Ag-300 and Ag$_x$O thin films and O1s spectra of Ag$_x$O thin film (inset)........ 79
Figure 36-XRD patterns of Ag-300 and Ag$_x$O coatings........ 81
Figure 37 - SEM top-view micrographs (recorded in BES mode at 5kX) of a) Ag and b) Ag$_x$O thin films and detailed view of c) Ag and d) Ag$_x$O thin film morphology (recorded in SE mode at 100kX). 82
Figure 38 - Results of antibacterial tests for SS316L (a)), Ag(b)) and Ag$_x$O (c)) regarding *Staphylococcus epidermidis* (I)) and *Staphylococcus aureus* (II))........ 85
Figure 39-Schematic illustrations of possible mechanisms of Ag dissolution, with and without Ag nanoparticles, when in contact with bacteria (adapted from [151])........ 86
Figure 40- Summary of production and characterization of developed silver and silver oxide thin films........ 88
Figure 41- Variation of Ag target voltage and total pressure in deposition chamber for different oxygen fractions in the discharge........ 95
Figure 42 -Variation of deposition rate for different oxygen fractions in the discharge........ 96
Figure 43-EDS composition for silver and silver oxide coatings........ 97
Figure 44 -SEM films cross section detailed view (recorded in SE mode at 100kX) and top-view micrographs (recorded in SE mode at 100kX) (a) to f) referent to Ag, AgO10, AgO20, AgO50, AgO80 and AgO100, respectively........ 99
Figure 45-XRD patterns of Ag and AgxO coatings, according to ratio of Ag/O composition estimated by EDS........ 100
Figure 46-AgO20 XRD pattern fitted using a monoclinic AgO structure, b) AgO20 XRD pattern fitted using a mixture of Ag$_2$O and AgO phases. The symbols correspond to the experimental results and the colour lines to the fitted lattice planes for the identified structures........ 102
Figure 47-XPS survey spectra and detailed regions of Ag3d (left) and Ag MNN (right) for Ag and AgOX thin films........ 104
Figure 48- XPS O1 (left) and C 1s (right) spectra for Ag and Ag$_x$O thin films........ 105
Figure 49-Results of antibacterial tests for: Ag (a)); AgO10 (b)); AgO20 (c)) and AgO100 (d))........ 107
Figure 50-Results of ICP-OES test. The data are expressed as mean ± standard deviations. One way ANOVA was used with significant level of 95% (* $p<0.05$)........ 108
Figure 51-Summary of the variation of the oxygen content and its influence on film's characterization and antibacterial properties........ 110
Figure 52-Braided PES stents uncoated, and coated with Ag and AgO100, by the same order. 116
Figure 53- SEM micrographs of uncoated and coated polyester stents and a more detailed view of surfaces........ 117
Figure 54- Rate of fibroblast cell viability, over time, for the different coatings........ 118
Figure 55- Logarithm of bacterial concentration after 24h of contact between stents and *Staphylococcus epidermidis* and SEM images of biofilm's formation. Concentrations that are significantly different (* $p<0.05$) of each compound compared to control........ 119

Figure 56-Logarithm of bacterial concentration in bacterial suspension after 24h of contact between stents and *Staphylococcus epidermidis*. Concentrations that are significantly different (*p<0.05) of each compound compared to control. 120
Figure 57-Relationship between force and extension for longitudinal (a)) and radial (b)) compression. 122
Figure 58-SEM micrographs of silver and silver oxide coated stents before (a) and b)) and after (a') and b')) mechanical tests, respectively. 123
Figure 59-Summary of the mechanical and biological behavior of polyester coated stent with silver oxide. 124

List of Tables

Table 1-Number and percentage of deaths from cardiovascular diseases and coronary heart diseases in Europe (adapted from:[1]) 4

Table 2- Advantages and disadvantages of conventional and pharmacological stents (adapted from [2]) 7

Table 3- Properties of nitinol and stainless steel (adapted from: [20]) 8

Table 4- Correlation of typical yield strength values with strut thickness for some stents 9

Table 5- Summary of clinical trial data with inorganic coated stents 10

Table 6-Summary and schematic representation of mechanisms of silver antibacterial action... 23

Table 7- Properties of fibrous materials 32

Table 8- Characterization of raw materials 39

Table 9- Coding and producing parameters of samples for PES fiber 42

Table 10-Coding and producing parameters of samples for PA fiber 43

Table 11-Coding and producing parameters of samples for PP fiber 44

Table 12- Diameter recovery and longitudinal extension of stents after radial compression 55

Table 13- Comparison of properties between produced fibrous stents and commercial Nitinol stent 64

Table 14-Surface energy components for tested liquids 75

Table 15- Conditions of coating's depositions and thickness 77

Table 16-Water (θ_w), formamide (θ_F) and α-bromonaphtalene ($\theta_{\alpha\text{-}B}$) contact angles, surface energy components (apolar Lifshitz-van der Waals surface free energy component, Y^{lw} ; electron acceptor surface free energy component, Y^{+}; electron donor surface free energy Y^{-}; and hydrophobicity (ΔG_{mwm}) of SS316L, silver and silver oxide coatings 84

Table 17-Thickness and of Ag/O ratio composition of silver oxide coatings 98

Table 18-XPS analysis of different coatings [137,159–161] 104

Table 19-Water (θ_w), formamide (θ_F) and α-bromonaphtalene ($\theta_{\alpha\text{-}B}$) contact angles, surface energy components (apolar Lifshitz-van der Walls surface free energy component, Y^{lw} ; electron acceptor surface free energy component, Y_i^{+}; electron donor surface free energy component, Y_i^{-}.......... 106

Nomenclature

α	Braiding Angle
α_0	Initial Braiding Angle
$\boldsymbol{\beta}$	Half the Maximum Intensity (FWHM)
Δh	Total Length of Stent
ΔG	Variation of the Free Energy
Δm	Material's Surface
ΔG_{mwm}	Variation of the Free Energy of interaction between the material's surface immersed in water
θ	Angle made by a pair of adjacent horn gears at the machine center
Θ	Bragg angle
θ_w	Water Contact Angle
θ_F	Formamide
$\theta_{\alpha\text{-}B}$	α-bromonaphtalene Contact Angle
λ	Wavelength of X-rays
$\boldsymbol{\Phi}Ar$	Argon flow
$\boldsymbol{\Phi}O_2$	Oxygen flow
a.u.	Arbitrary unit
AFM	Atomic Force Microscopy
AP	Auger Parameter
Ar	Argon
Ag	Silver
Ag_xO	Silver Oxide
AgSD	Silver Sufadazine
BSE	Backscattering electron
CFUs	Colonies Forming Unities
CVD	Cardiovascular Diseases
CVD^*	Chemical Vapour Deposition
D	New Average Stent Diameter
D_a	Average Stent Diameter
D_b	Stent Diameter in Bent Condition
D_i	Initial Stent Diameter
d_{hkl}	Distance Between Atomic Planes
Dc	Direct Current
DES	Drug Eluting Stents
DLC	Diamond-like carbon
DMEM	Dulbecco Modified Eagle Medium
DNA	Deoxyribonucleic Acid
DSC	Differential Scanning Calorimetry
E	Young's Modulus
EDS	Energy-dispersive X-ray Spectroscopy
F	Radial Force
FBS	Fetal Bovine Serum
FCC	Face Cubic Centred
FDA	Food and Drug Administration
fO_2	Oxygen Fraction in the Discharge

FWHM	Full Width at Half Maximum
G	Shear Modulus
I	Moment of Inertia
I_p	Polar Moment of Inertia
ICDD	International Centre for Diffraction Data
ICP-OES	Inductively Coupled Plasma Optical Emission Spectrometry
J	Current Density
Jis Z 2801:2000	Japanese Industrial Standard Z 2801: 2000
K	Dimensionless Shape Factor
L	Length of Stent
L_f	Length of a Single Filament
LBL	Layer by Layer
LW	Lifshitz-van der Waals
MTS	3-(4,5-dimethylthiazol-2-yl)-5-(3-carboxymethoxyphenyl)-2-(4-sulfophenyl)-2H-tetrazolium inner salt
N	Diffraction order
n_c	Number of Bobbins
N_h	Number of horn gears
NaCl	Sodium chloride
NP	Nanoparticle
P	Radial Pressure
PA	Polyamide
PBS	Phosphate Buffer Saline
PBMA	Poly(nbutyl methacrylate)
PDLA	Poly (D-lactic acid)
PE	Polyethylene
PES	Polyester
PET	Polyethylene terephthalate
PEVA	Poly(ethylene-co-vinyl acetate)
PLD	Pulsed Laser Deposition
PLGA	Poly(lactic-co-glycolic acid)
PLLA	Poly(L-lactic acid)
$pO_{2,in}$	Input oxygen partial pressure
PP	Polypropylene
PS	Penincilin Steptomycin
PTFE	Polytetrafluoroethylene
PVD	Physical Vapour Deposition
QACs	Quaternary Ammonium Compounds
R	Mandrel Radius
Rf	Radio Frequency
ROS	Reactive Oxygen Species
SAMs	Self-assembled Monolayers
SE	Secondary Electron
SEEY	Secondary electron Emission Yield
SEM	Scanning Electron Microscopy
SIBS	Poly(styreneb-isobutylene-b-styrene)
SS 316L	316L Stainless Steel

T	Time taken by the horn gear to make one revolution
T	Mean Size of the Ordered (Crystalline) Domains
TSA	Tryptic Soy Agar
TSB	Tryptic Soy Broth
V	Take up speed
XPS	X-ray Photon Spectroscopy
XRD	X-ray Diffraction
ω	Angular Speed of Bobbins
$\omega 2$	Take out Speed
W_h	Angular velocity of the horn gears around their own centers
W_y	Monofilament width
Y_l^{Tot}	Surface Free Energy
Y_l^{LW}	Apolar Lifshitz-van der Waals Surface Free Energy Component
Y_l^{+}	Electron Acceptor Surface Free Energy Component
Y_l^{-}	Electron Donor Surface Free Energy Component
Z_1, Z_2, Z_3	Number of Teeth of gear wheel 1, 2 and 3, respectively;

Scope of the thesis

Metallic stents, commonly used nowadays, have several disadvantages, such as corrosion, infection and restenosis, leading to health complications for the patient, or even to his death.

Although there are different kinds of stents, like pharmacological stents, that can deliver drugs, there is not an “ideal” stent being able to overcome the disadvantages of commercial ones.

Thereby, the main purpose of this work is to develop a multifunctional fibrous stent, able to eliminate corrosion and minimize the disadvantages of metallic stents, increasing the useful life of the stent and well-being of the patient.

In addition, the innovation of the present study is the incorporation of silver and silver oxide nanocoatings, on the stent’s surface, so that silver can be released, providing an antibacterial effect and thus, preventing infections. The developed coating should not be cytotoxic, once it will be in contact with human body and no harm should be observed, as well as the delamination of the coating should not be observed.

The innovative stent will be different from the available stents, because there is no 100% fibrous stent, with mechanical performance similar to metallic ones, with a coated surface, that provides an antibacterial behavior.

Therefore, the main motivation of this research work is to develop a fibrous based stent (and, this way, eliminate the corrosion problem) and understand the behavior of silver-based coatings on the antibacterial properties of stents and solve the disadvantages associated with current stents.

Structure of the Thesis

This thesis is divided in six chapters.

Chapter I concerns a general introduction about stents and the main problems associated to them. Due to the need to continue studying and developing new materials and techniques to avoid the major problems of current stents, fibrous materials have begun to be used. Although the innovation in materials reduces and eliminates some problems, like corrosion, infection is an important issue that need to be controlled. Thus, an explanation about possible functionalization techniques and antibacterial agents is added in this chapter.

Globally, this first chapter describes the disadvantages of metallic stents, currently available in the market, and explain how to reduce their utilization through the use of fibrous materials, associated with functionalization techniques, in order to provide antibacterial properties to stents.

Chapter II encloses the production and mechanical characterization of fibrous stents, outlining the fundamentals about the methodologies, as well as the influence of production technique parameters in final mechanical behavior. Taking in account all the mechanical tests performed, and after the comparison between the results for fibrous stents with the results of nitinol stents, described in literature, the fibrous stent with the best performance was chosen. This stent is in the further research experiments related to the functionalization with antibacterial properties.

Chapter III describes silver and silver oxide coatings production by non-reactive and reactive pulsed dc magnetron sputtering, respectively. These coatings were produced in order to evaluate if they can be suitable candidates to functionalize the fibrous stent and provide it antibacterial behavior. Thus, silver and silver oxide coatings were chemical, morphological and physical characterized.

With the study presented in this chapter it was possible to observe that silver oxide coating was a potential coating with antibacterial properties, however, the main reason for that behavior was not clear. So, the influence of the oxygen in the antibacterial properties should be studied.

Chapter IV presents the production of silver and silver oxide coatings, by non-reactive and reactive pulsed dc magnetron sputtering, with the variation of the oxygen content, in order to understand the influence of oxygen in the coating's properties, which was not clear in previous chapter.

In **Chapter V,** and after study and chose the best coatings in Chapter IV, the fibrous stent produced in Chapter II was functionalized with silver and silver oxide coatings. The result stents were biological characterized, where, cytotoxicity and antibacterial performance was evaluated in further detail. Additionally, and in order to evaluate the coating's behavior when subjected to mechanical forces, coated stents were, again, mechanically tested.

Finally, in **Chapter VI**, the major conclusions of this thesis are presented and future work is suggested.

Figure 1 shows a diagram representing the different stages of this research project, which will be described, along the thesis.

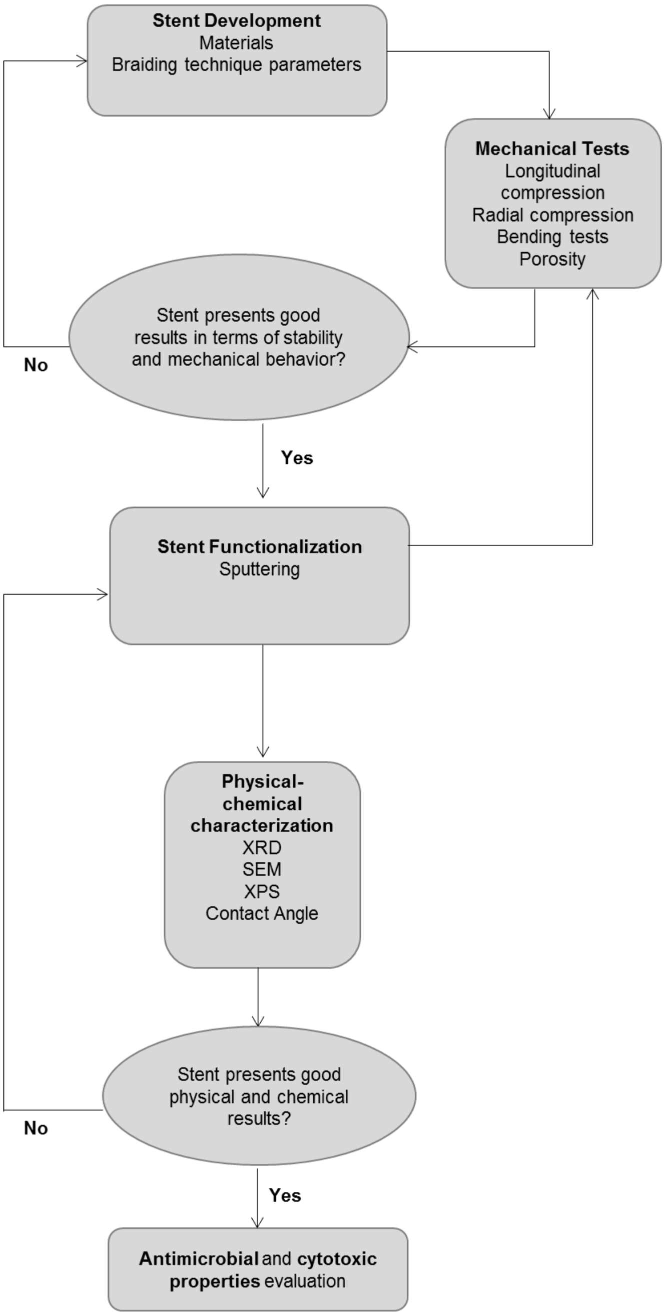
Stent Development
Materials
Braiding technique parameters
Mechanical Tests
Longitudinal compression
Radial compression
Bending tests
Porosity
Stent presents good results in terms of stability and mechanical behavior?
No
Yes
Stent Functionalization
Sputtering
Physical-chemical characterization
XRD
SEM
XPS
Contact Angle
Stent presents good physical and chemical results?
No
Yes
Antimicrobial and **cytotoxic properties** evaluation

Figure 1-Schematic representation of the different stages of the thesis.

CHAPTER I

State of the Art

The following papers published within this research work have been taken into consideration for this part of the work:

R. Rebelo, R. Fangueiro, S. Carvalho, M. Henriques, and S. Rana, "Methods of incorporation antimicrobial agents in stents," Int. J. Eng. Sci. Innov. Technol., vol. 3, no. 2, pp. 409–422, 2014.

R. Rebelo, N. Vila, S. Rana and R. Fangueiro, "Poly Lactic Acid Fiber Based Biodegradable Stents and Their Functionalization Techniques," in Natural Fibers: Advances in Science and Technology Towards Industrial Applications : From Science to Market, vol. 12, R. Fangueiro and S. Rana, Eds. RILEM Bookseries, 2016, pp. 331–342.

1. Introduction

Metallic stents used nowadays, have several disadvantages, like corrosion, low radiopacity, restenosis and can cause infection. Thus, it is important to study new materials, in order to eliminate or minimize those disadvantages and proportionate a long durability to stents and a better well-being to the patient.

1.1. Coronary diseases

Cardiovascular diseases (CVD) are a tremendous problem for public health, since they are a major cause of death among Europeans and worldwide in both sexes, and have high health care costs. The Global Burden of Disease study estimated that in 2010 CVD caused more deaths than all communicable, maternal, neonatal and nutritional disorders combined, and double the number of deaths caused by cancers, reaching 15616.1 million deaths, corresponding to 29.6% of all deaths worldwide [1].

Coronary heart disease, namely, atherosclerosis of the coronary arteries is one of the most principal CVD and manifests itself when there is clustering of cholesterol (fat produced by the body) in the arterial walls, obstructing blood flow. Additionally, the accumulated cholesterol can cause a clot, leading to severe circulatory problems [2]. In Table 1 is represented the number and correspondent percentage of deaths from CVD and, in particular, coronary hearth diseases in Europe, in the last available year (2014).

Table 1-Number and percentage of deaths from cardiovascular diseases and coronary heart diseases in Europe (adapted from:[1])

	Cardiovascular Diseases (total)		**Coronary Heart Diseases**	
Males				
Total deaths	1 862 774	42%	876 017	20%
Deaths before age 75	939 698	36%	473 501	18%
Deaths before age 65	508 132	31%	253 432	16%
Females				
Total deaths	2 219 326	51%	903 330	21%
Deaths before age 75	536 712	37%	232 683	16%
Deaths before age 65	201 492	27%	77 166	10%
Total				
Total deaths	4 082 100	46%	1 779 347	20%
Deaths before age 75	1 476 410	37%	706 184	18%
Deaths before age 65	709 624	30%	330 598	14%

Arteries are blood vessels, whose main functions are myocardial irrigation and oxygen and nutrients transportation, carrying blood from the heart to all parts of the body. These vessels are composed by different layers (Figure 2). The outer layer is composed of connective tissue, the intermediate layer is based in smooth muscle tissue and elastic tissue and the inner layer is comprised of endothelial cells. Atherosclerosis occurs when there is a damage in the innermost layer of arterial tissue [2].

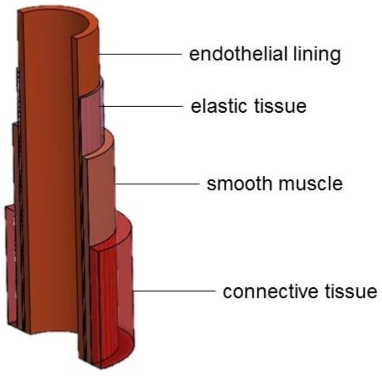

Figure 2- Schematic representation of an artery.

Atherosclerosis of the coronary arteries can be treated by drugs, such as anticoagulants or antiplatelet agents, or by surgical procedures. Initially, this disease was treated by coronary angioplasty [3], which is a surgical procedure, whose goal is the extension of the coronary arteries, to restore normal blood flow. In this procedure, a catheter, which has a small balloon at its end, is inserted at patient's blocked artery. The balloon catheter is positioned at the obstruction and it is inflated, in order to cause a dilation of the artery [4]. However, although angioplasty is a very innovative technique, it has some disadvantages, including high rates of restenosis or reocclusion of arteries [5]. Thus, stents have emerged as a mean of solution to this problem (Figure 3).

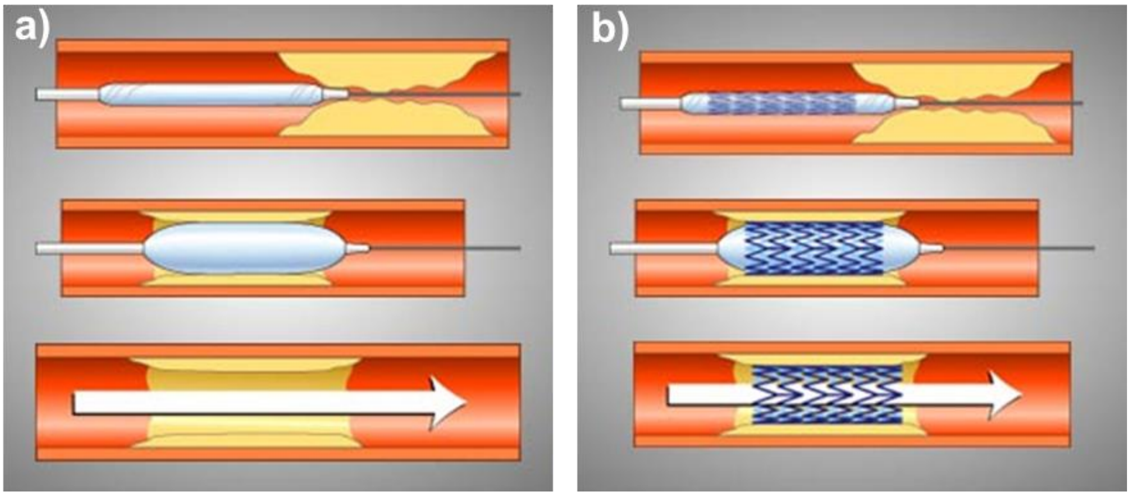

Figure 3- Conventional angioplasty (a)) and angioplasty with stent (b))
(image adapted from:[2]).

1.2. Stents

Stents are rigid and perforated tubular structures, which are inserted into blood vessels (Figure 3b) in order to prevent or inhibit the constriction of blood flow, restoring the normal blood flow, when blood vessels are clogged, and are nowadays used in 70% of angioplasties [2,6]. The use of cardiovascular stents has become one of the most important achievements of the last century in the area of surgical cardiology in heart diseases [7]. Cardiovascular stents were first used in 1986 in Toulouse, France, but its approval by the FDA (Food and Drug Administration) only occurred in 1994. First coronary stents used were bare-metal. Since then, stents have been evolved, in terms of implantation mechanism, materials, methods of manufacture and coatings. These devices can be divided into conventional or pharmacologic stents. The first ones are endovascular fasteners, typically in metal (Figure 4), whose function is to maintain dilated artery. Pharmacologic stents belong to the second generation of stents and are available commercially since 2002. These stents are also metallic stents; however, they have the incorporation of drugs [2].

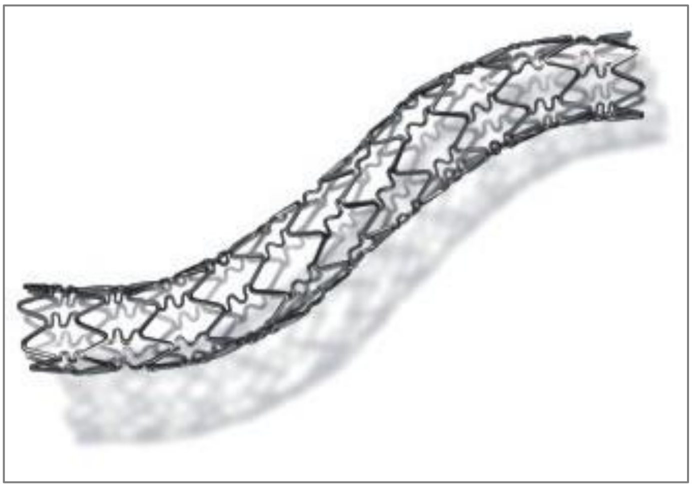

Figure 4- Conventional metallic stent (image adapted from:[8]).

Nevertheless, although pharmacologic stents reduced rates of restenosis, when compared with balloon angioplasty, restenosis continued to develop in 20% - 30% of lesions. Even though stent insertion stabilizes vascular dissections and prevents arterial recoil, restenosis still occur because of physiological processes that induce the cells' growth in stents, leading to arterial reclusion. In addition to act as a vascular scaffold, stents soon evolved to become drug delivery systems in the form of Drug Eluting Stents (DES). These devices aim to minimize vascular inflammation and cellular proliferation, which leads to restenosis [9].

Despite the first generation of DES had be considered revolutionary, by today's standards they are rudimentary. First DES were comprised by a metallic stent, usually stainless steel, coated with a polymer that elutes drugs as antiproliferative or anti-inflammatory agents [9]. There are two drug-eluting stents approved by FDA: poly(ethylene-co-vinyl acetate) (PEVA) and poly(nbutyl methacrylate) (PBMA), and poly(styreneb-isobutylene-b-styrene) (SIBS). The first one is made of 316L stainless steel and coated with a mixture of PEVA and PBMA, which contains sirolimus, to combat restenosis. In order to control drug release, a drug-free top coat of PBMA is applied. The second one is, equally, made of 316L stainless steel, but it is coated with SIBS mixed with paclitaxel [10]. Besides the good results showed by these stents, polymer coatings may lead to thrombosis and, in this way, polymer-free coatings/surfaces appeared. This approach uses nanoporous and microporous surface stents, as well as nanoparticles on stents surface [11]. Although nanoparticles have been extensively studied and applied as drug delivery system, the results of stent surface coated with them have few reports [12].

Sousa *et al.* [13] compared the performance between conventional and pharmacological stents (sirolimus coated stent), and their study showed that the use of pharmacological stents leads to a reduction of, approximately, 80% of restenosis. Table 2 presents the advantages and disadvantages associated to both types of stents.

Table 2- Advantages and disadvantages of conventional and pharmacological stents (adapted from [2])

Stents	Advantages	Disadvantages
Conventional	Low price, Reduced chance of late clots forming.	Higher rates of restenosis; Induction of trauma during deployment; Corrosion and the consequent release of ions to the body.
Pharmacological	Lower rates of restenosis.	Delay healing and increase endothelial inflammation; Higher rates of thrombosis; Price.

Stents must possess certain requirements, in order to, adequately, perform its function, such as biocompatibility (so that its use does not cause damage on the health of its user), longitudinal mechanical strength ([0.16-5.28] N), radiopacity (so that it is easy to see), longitudinal flexibility, ease of handling, corrosion resistance and having high radial strength ([1.13-2.9] N) and ability to recover [2,14].

1.3. Metallic Stents

Stents can be made of different materials, but metals, particularly stainless steel, are the most common, due to its high tensile strength and corrosion resistance. However, metallic stents have low radiopacity. There are, also, some metal alloys used in stents production, such as cobalt chromium alloy, once they are radiopaque and biocompatible with high radial strength, and nickel-titanium, or nitinol [2].

Nitinol is a nickel and titanium alloy, which has properties suitable for stent applications, such as: shape memory properties, which enables this material to be easily compressed, but when in contact with blood flow it reacquires the size, i.e., it assumes the original shape after exposure to body temperature; high elasticity and resistance to fracture [15–17]. Moreover, although the human body is a very complex electrochemical system, which provides extremely aggressive and corrosive environment, nitinol implants show no signs of corrosion. This advantage is due to the fact that when inserted into human body, the implant is covered with a thin layer of oxide, which reacts with titanium to form titanium oxide that stabilizes the surface and prevent the reaction between the medium and nickel ions [18,19]. Although there are some researches testing nitinol biocompatibility and showing that no significant negative effects are found in nitinol implants, it is theoretically possible that nickel may dissolve from the material and cause adverse effects [20].

In Table 3, a comparison between main mechanical properties of nitinol and stainless steel is presented.

Table 3- Properties of nitinol and stainless steel (adapted from: [21])

	Strength	**Stiffness**	**Fatigue**	**Corrosion Resistance**
Stainless Steel	300-560 MPa	200 GPa	Good in load control	Good- Cr_2O_3
Nitinol	500- 1400 MPa	25 - 80 GPa	Good in strain control	Excellent- TiO_2

Nevertheless, the use of most metallic stents presents some disadvantages, such as: corrosion, restenosis and bleeding complications. Restenosis occurs in approximately 30% of patients in the period of 9 months after the procedure and it is associated with a high mortality rate, as well as the costs of health care [2]. One of the main factors associated with restenosis is the damage of the arteries caused by stents metal rods, which causes an immune and inflammatory response by the body [6]. With the intention of minimize the disadvantages of metallic stents, some studies were carried out, namely to improve high-strength and radiopacity, and minimize metal ion release and restenosis [22]. One of the most important properties of stents is their thickness, once this characteristic affects the ability of track the stent through the blood vessel and then cross through lesions. Stents with thinner struts are more flexible, reduce cross section profiles and, hypothetically, reduce restenosis rates [23,24]. Despite the effect of thickness in restenosis, the long-term effect leads to developments to higher-strength materials, able to be design with reduction in strut thickness. Thus, the introduction of cobalt-chromium alloys that have the advantage of having a good corrosion resistance, in stents production began to be studied and developed. In Table 4 are summarized some coronary stents that use this trend of reducing thickness by the use of higher-strength materials and composite structures [22].

Table 4- Correlation of typical yield strength values with strut thickness for some stents

Stent name/ manufacturer	**Material**	**0.2% Yield strength (MPa)**	**Strut thickness (μm)**
BX Velocity®/Johnson & Johnson	316L	340	140
Express®/Boston scientific	316L	340	132
Driver®/Medtronic	CoCr MP35N	415	91
Vision™/Abbott	CoCr L605	510	81
TriMaxx™/ Abbott	316L/Ta/316L	Not applicable	74

Furthermore, biocompatibility issues have been increasing attention, once it was believed that the increase in surface biocompatibility could reduce restenosis rate for bare metal stents below the typical levels of 20% - 30%. Regardless of the effort and novel approaches, these coatings seems not to play a significant result in the restenosis reduction, in their existing configuration, as demonstrated in Table 5.

Table 5- Summary of clinical trial data with inorganic coated stents

Study description	**Restenosis rates**
DLC vs stainless steel [25]	31.8% for Diamond Flex AS stent 35.9% for bare Flex AS stent
DLC vs stainless steel [26]	24.3% for Phytis™ Diamond 21.8% for Penta™ stainless steel
Ion-implanted carbon vs. stainless steel [27]	11.0% for Arthos^{Inert} carbon implanted stent 16.1% for Arthos stainless steel stent (NS)
TenaxTM SiC vs.NIR 316L [28]	30.0% for SiC-coated stainless steel stent 26.7% for NIR™ stainless steel stent
TiNOX trial [29]	15.0% for titanium-nitride-oxide coated stent 33.0% for same design stainless steel stent

In order to minimize the drawbacks associated with metallic stents, new materials, like fibrous materials, have begun to be used. As the surface of fibrous materials can be easily functionalized to enhance their compatibility with human tissues, they present high potential for application in stents [30].

1.4. Fibrous Stents

Fibrous materials used in medical applications include: fibers, yarn (monofilament or multifilament), textile structures (braided, knitted, woven and non-woven) and composites. These materials, applied in medicine, can be natural or synthetic, biodegradable or non-biodegradable. Currently, there are fibrous stents or stents with fibrous components: stents with fibrous structure combined with metals, stents coated with polytetrafluoroethylene (PTFE), polyester (PES) stents, polyamide (PA) stents, polyethylene (PE) stents, PTFE stents and poly (L-lactic acid) (PLLA) stents [2,22].

The idea of using implantable fibrous structures is not new and the use of these materials in stents have been studied, because they eliminate the problem of corrosion and can minimize the occurrence of restenosis associated with metallic stents. Furthermore, the use of monofilaments has a high potential for stents development because, in addition to being biocompatible, these materials allow the application of various surface treatments, such as drug delivery [2,30]. Furthermore, monofilament exhibit excellent mechanical properties, like greater stiffness and good results when subject to compression, tensile and bending forces, since these forces will be directly borne by the yarn [31].

Freitas *et al.* [31] developed polypropylene stents through two distinct methods: knitting and braiding technologies. Better results were obtained for braided structures, such as dimensional stability, mechanical strength and high recovery of the original shape, and concluded that this technique is the most suitable for stents development.

Braiding technique consists in the interlacing of two or more thread systems, in the diagonal directions, forming an integrated structure. This method is an advantage, since it provides greater visibility of the stent, flexibility and rate of collection up to 87% of the stent on the device, in addition to be a simple process, versatile and provide a high level of compliance, torsional stability and wear resistance [6].

The use of polypropylene monofilaments showed some advantages, such as low cost, high stiffness and resistance to rupture. However, stents were not sufficiently flexible for blood vessel contours.

Further studies were carried out in order to find the ideal fibrous material for stents and other implantable devices. França and Pereira [6] showed that the polyester fiber is the most commonly used for vascular grafts because of its biocompatibility and availability in the market, besides being an inert, flexible and resilient material. On the other hand, Avino *et al.* [32] evaluated the placement of nitinol stents coated with polyester in dog's aortas, and concluded that although there is an increased proliferation of cells in the stent surface, the lumen area was not changed. Furthermore, Marty *et al.* [33] found that polyester stent, when inserted in smaller vessels; induced a cellular response that can lead to thrombosis.

More recently, hybrid braided stents of polyamide and nitinol were developed, showing excellent dimensional stability and mechanical performance and the use of based nitinol stents exhibit a shortening in less than 3% [2,6]. Thereby, it was found that the braiding technique is very efficient and the stent performance is, directly, related to the braiding angle [2].

Some of natural based stents were also studied and they are already marketable. Tamai *et al.* [34] used PLLA stents in human applications (Igaki-Tamai stent). This stent presents a thickness of 0.17 mm and a zigzag helical coil pattern, and was implanted in 15 patients. During 30 days no thrombosis or major cardiac events were observed, and follow-ups with angiography and intravascular ultrasounds were realized 1 day, 3 months and 6 months after stent implementation. No major cardiac event, except for repeated angioplasty, developed within 6 months [34].

Nishio *et al.* [35] evaluated the long-term safety of the Igaki-Tamai stent over 10 years, where 50 patients with 63 lesions were treated electively with Igaki-Tamai stents. Generally, clinical follow-up for cardiac events and rates of scaffold thrombosis was analyzed with the results of angiography and intravascular ultrasound. At the end of the study, authors conclude that the rate of major cardiac events were similar to those of metallic stents, and no stent recoil was observed, suggesting a long-term safety of Igaki-Tamai stent [35].

Absorb® (VHL) is a fully bioresorbable stent made of PLLA, coated with poly (D-lactic acid) (PDLA) that uses the everolimus drug, and it was approved in 2011 for use in Europe. The second generation of this stent (BVS 1.1) uses PLLA, as well, however, has some modifications in polymer processing and scaffold design that leads to a higher radial strength and mechanical integrity [36,37].

Despite the promising results for biodegradable stents these structures have a lower radial force when compared with metallic and should be compensated for thicker structures [36].

1.4.1. Methods of stent's production

Fibrous stents may be produced using woven, knitting and braiding technologies. The woven type, in addition to provide a low elasticity, tends to wrinkle and fold easily, with high difficulties in assuming the sinuous contours of the blood vessels [6]. Braiding technique is the most suitable technique for stent development as the produced structures exhibit good dimensional stability, mechanical strength, high shape recovery and flexibility [6]. Moreover, braiding technique is a simple and versatile process, providing the structures high compliance level and torsional stability [6]. Braided structures have been well studied for application in medical implantable devices like sutures, artificial ligaments, etc [38,39]. A few studies have demonstrated the possibility of using braided structures for producing self-expanding stents. For example, Zhao *et al.* [40] fabricated braided stents using shape memory Nitinol wires. The developed braided stents, however, showed lower radial strength as compared to the welded stents, owing to relative sliding of Nitinol wires within the braided structures and therefore, found less effective to restore the patency of the stenotic artery. Further studies on Nitinol braided stents revealed that due to the slippage between the wires and superelastic behavior of Nitinol, they showed a hysteresis between loading and unloading cycles under the compressive tests [41].

Braiding angle was observed to be the main design parameter deciding the mechanical performance of Nitinol braided stents. Braided stents have also been fabricated using shape memory polymers such as polyurethane and their mechanical performance has been characterized and simulated using finite element analysis [42]. It was observed that the design parameters like fiber diameter and braiding angle can be carefully selected to match the performance of polyurethane stents to that of metallic stents. However, shape memory polyurethane shows viscous phenomena such as stress relaxation and creep, which should be minimized. Also, due to much inferior mechanical properties of this polymer to Nitinol, it should be used as thicker fibers, reducing blood flow through the vessels. The strong influence of number of filaments and stent diameter on the mechanical performance of stents was also noticed in the case of braided stents produced with polyester fibers [42].

The possibility of producing bioabsorbable braided stents has been explored using PLLA fibers [38] and the produced stents showed similar radial pressure stiffness to metallic stents and maintained, at least, half of their radial pressure stiffness for more than 22 weeks. These initial research studies on braided stents investigated separately the influence of some of the design parameters on selected properties of stents such as radial compression.

1.4.1.1. Braiding technique

Braided fibrous structures result from the interlacing of two or more systems of yarns in the diagonal directions, forming an integrated structure. This type of processing is simple and versatile and differs from woven and knits in the method of insertion of the wires and the way the threads are interlaced [43,44]. Production of braided structure is relatively simple and no complex yarn preparation process is required. Therefore, this technique is one of the most cost - effective textile manufacturing processes. Additionally, braiding technique can work even with the most difficult and least flexible yarns once yarn’s path in braiding structure is simple and straight [45].

Braiding machines are used for the production of braided structures, which can be vertical or horizontal, depending on the take out direction of the structure, and can produce 2D or 3D structures. Circular braiding process is used to produce hollow and circular shapes. A circular braiding machine is composed by a circular platform where carriers are placed, to hold the spools of yarn. The number of spools can be controlled and depends on the desired density of yarn in the final braided structure. A mandrel, which, usually, is a solid and removable component, can be added during the production in order to provide the final shape and give longitudinal reinforcement. The shape and thickness of the mandrel is another parameter that can be controlled. The yarns are held together, during the braiding process, in the mandrel's surface, forming a braided self-supported structure [45]. Two of the most important controlled parameters are the rotation speed of carriers and mandrel's take out velocity. In Figure 5 is represented a typical braided structure.

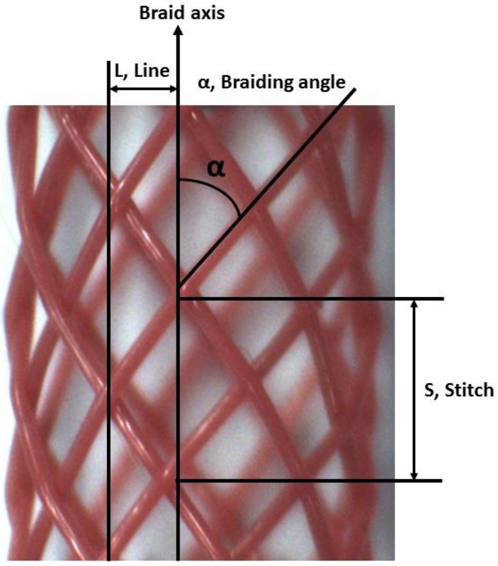

Figure 5- Braided structure.

Braiding axis consists in the direction of braiding formation. Line can be described as one repeat of braiding structure perpendicular to braiding axis while stich is one repeat of braiding structure along the braid axis. Regarding braiding angle, it is the most important parameter of braiding process and it determines the mechanical performance of braiding structure [45]. This parameter depends on the number of braiding yarns and the take up speed. The braiding angle (α) represents the angle between the monofilaments and the longitudinal axis of braided structure (Figure 5). Braiding angle can be calculated using equation (1) [14,46]:

$$\alpha = \tan^{-1}\left(\frac{\omega R}{V}\right) \tag{1}$$

where,

α= braiding angle (rad);

ω= angular speed of bobbins (rad/s);

R= mandrel radius (cm);

v= take up speed (cm/s).

Angular velocity (ω) and angle made by horn gears can be calculated using the following equations:

$$\omega = \frac{\theta}{T} \tag{2}$$

where,

θ= angle made by a pair of adjacent horn gears at the machine center (rad);

T = time taken by the horn gear to make one revolution (s).

$$\theta = \frac{2\pi}{(\frac{N_h}{2})} = \frac{4\pi}{N_h} \tag{3}$$

$$T = \frac{2\pi}{N_h} \tag{4}$$

$$\omega = \frac{2\omega_h}{N_h} \tag{5}$$

Therefore,

$$\alpha = \tan^{-1}(\frac{2\omega_h R}{N_h V}) \tag{6}$$

Take out velocity can be controlled varying the teeth of gear wheels in a braiding machine, as observed in Figure 6.

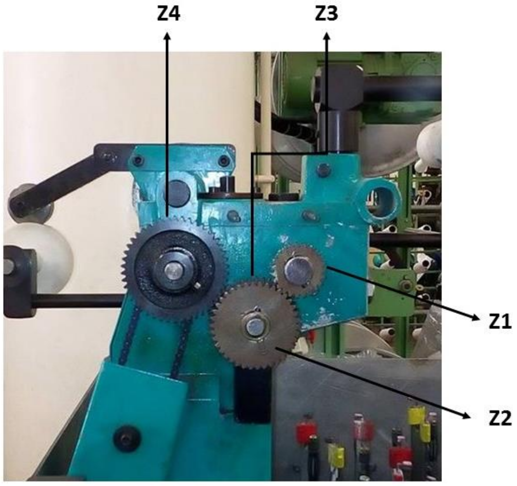

Figure 6- Scheme of work of braiding machine, with four gear wheels.

(Z1 - 1st gear wheel, Z2 – 2nd gear wheel, Z3- 3rd gear wheel and Z4- 4th gear wheel)

A braiding machine works with four gear wheels that can be varied, increasing or decreasing the take out speed. The first gear wheel receives the rotation caused by the motor and gives it for the others gear wheels. This gear wheel is in contact with the reduction zone which comprises two gear wheels on the same axis. These two are in contact with the last gear wheel, which provides rotation to the axis of the calender. Varying the position and the teeth of gear wheel is possible to control the take out speed, through equation 7 [2].

$$\omega_2 = \frac{Z_3}{46} * \frac{Z_1}{Z_2} * \omega \tag{7}$$

Where,

Z_1, Z_2, Z_3= number of teeth of gear wheel 1, 2 and 3, respectively;

ω= angular speed of bobbins (rpm);

ω_2= take out speed (rpm).

2. Infection

Despite the innovation on stents, its use also has some disadvantages, namely bacterial infection. Usually, this infection results in prolonged hospitalization and, therefore, a higher cost associated with medical services, and in extreme cases, death of the patient [6].

After stent implantation, proteins, from the blood or tissue, directly adsorb onto the surface. The layer formed by adsorbed proteins has a very important role in bacterial adhesion [47,48]. The free swimming bacteria, in the so - called planktonic state, will *in vivo* adsorb to this surface coated with proteins (Figure 7 (A)). These bacteria will proliferate and recruit another bacterium from the neighbor environment (Figure 7 (B)), forming a colony in surface, and change their gene expression pattern (Figure 7 (C)). This gene modification will be responsible for the production of extracellular polymeric substances, which are essential in the formation of biofilm along with nucleic acids and other substances (Figure 7 (D)). [49]. The biofilm slowly grows and small parts of it can break off and planktonic bacteria escape from the biofilm and can invade new, clean surfaces at distant sites (Figure 7 (E)).

Thus, a biofilm is an accumulation of microorganisms embedded in a matrix of polysaccharides difficult to eradicate. Biofilms are medically important, since they are responsible for over 80% of microbial infections in the body, and they may be form on biological or non-biological surfaces [50].

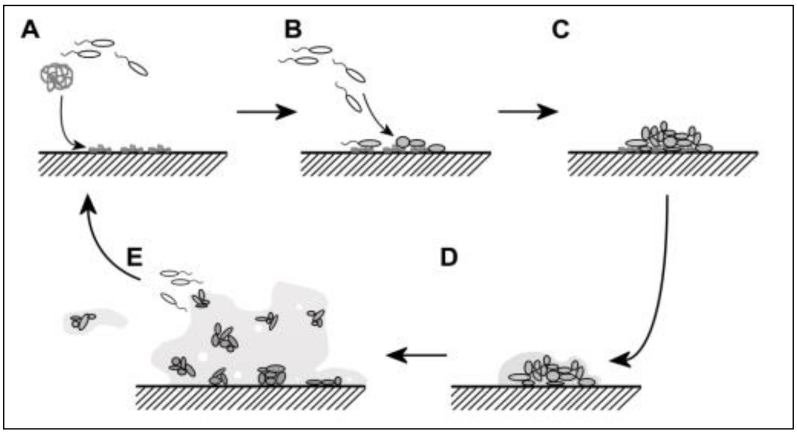

Figure 7- Biofilm formation (image adapted from [49]).

Therefore, the stent surface characteristics, such as, hydrophobicity, roughness, porosity and chemical composition, have a direct influence in proteins adsorption and, consequently, in a biofilm formation and infection.

Even though coronary artery stent infections are associated with a high mortality rate only few cases of stents infection have been reported, however the percentage of hospital infection, in Portugal is 10.6%, a value that is above the European prevalence, which is 6.1% [51,52]. Nevertheless, infection of medical devices can arise due to several reasons and from different sources; some of the most common sources of infection are: contaminated device surfaces, hands of medical staff and patients own skin or mucus membrane, among others. Many of these risk factors can be easily avoided, but, infections are impossible to evade completely [53]. The infection of these devices is due to the colonization caused by gram-positive or gram-negative bacteria or yeasts [54,55]. Gram-positive *Staphylococcus* species, like *Staphylococcus epidermis and Staphylococcus aureus* are reported as the major isolated species from medical devices [54,56].

Staphylococcus epidermis is a gram-positive, coagulase-negative Staphylococcus (it does not produce the enzyme coagulase responsible by the blood plasma coagulation) that is a part of our normal flora and colonizes the skin and mucous membranes of the human body [57–59]. This bacterium is characterized for about 1 µm round cells, and it can be found in single cells, in pairs or in clusters [60]. Another bacterium associated with coronary diseases is *Staphylococcus aureus*, which is a gram-positive bacterium that can be found in the human respiratory tract and skin [61,62].

One way to prevent infection is trough surface modification of the implantable device, in such a way that no bacterial adhesion can occur. Characteristics like, hydrophobicity, roughness and chemical composition have an important influence on bacterial adhesion. Overall, higher hydrophobicity provokes greater bacterial adhesion [57,63].

Thus, in order to minimize the reaction of the human body and fight the adhesion of microorganisms to stent surface, some stent coatings have been developed, including: PTFE, polyethylene terephthalate (PET), polyurethane, carbon films and the incorporation of anti-thrombotic, anti-proliferative and antimicrobial agents, as well as incorporation and delivery of antibiotics and the use of novel metals and other compounds with antimicrobial properties [6,49].

3. Functionalization of stents

In order to minimize the limitations of available stents, many studies have tried to solve these problems by stent modification. With modification or coating of the stent's surface, it is intended to improve the stent's biocompatibility, modifying their surfaces with less thrombogenic and inflammatory materials, reducing the infection and the occurrence of thrombosis and restenosis, by coating the stent with therapeutic agents, which are released, over time, after stent implantation [64].

The main methods of coating include layer by layer (LBL) technique, thiol chemistry, chemical vapor deposition (CVD) and physical vapor deposition (PVD) methods.

3.1. Antibacterial Coatings

There are, mainly, three different types of stent's coating: biocompatible coatings, drug-delivery coatings and polymer-free coatings/surfaces [11].

Biocompatible coatings comprehend, mostly, inorganic materials, like silver, gold or carbon. These coatings have as main function, to increase the stent biocompatibility and to serve as a barrier to ion release by metallic stents. Usually, biocompatible coatings have no capacity to carry drugs. To avoid this disadvantage, biocompatible polymer coatings were developed, which can release therapeutic agents. These coatings can be nonbiodegradable polymers or biodegradable polymers like: poly(lactic acid) (PLA), poly(glycolic acid) and their copolymer, poly(lactic-co-glycolic acid) (PLGA). As previously mentioned, there are two drug-eluting stents approved by FDA: PEVA and PBMA. Even though the good results showed by these stents, polymer coatings may lead to thrombosis and, in this way, polymer-free coatings/surfaces appeared. [11,65].

Following, it will be described some therapeutic agents (antibiotics, quaternary ammonium compounds and silver based agents) with antimicrobial properties, which can be used, as coatings, in order to minimize infection and adverse reactions in the human body.

The use of antibiotics has increased considerably after the discovery of penicillin and they can be divided in two different types: bactericidal, when cell death is induced, or bacteriostatic, if just cell growth is inhibited. Antibiotics can inhibit deoxyribonucleic acid (DNA) synthesis, bacterial protein synthesis or bacterial cell walls synthesis [66]. Although the use of antibiotics is associated with implanted medical devices, it shows some disadvantages. Antibiotics, normally, cannot reach the bacteria, since it is quite difficult for them to penetrate the formed biofilm in the implanted devices. Therefore, the concentration of antibiotics presented in the biofilm becomes very low, and this led to the development of bacteria´s resistance to antibiotics [12,67].

To increase the effectiveness of antibiotics, they can be applied locally on the implant surface, because bacteria are then killed directly before the biofilm formation. Some biodegradable coatings containing antibiotics can be used [64]. In that case, antibiotics are released at the time when these coatings get degraded. This approach is not viable for long term implants, once the concentration of antibiotics is finite. Therefore, after some time, the implantable device is again subjected to biofilm formation and consequent infection [12]. Furthermore, there is a serious concerning by World Health Organization with the use of antibiotics and the antibiotic resistance caused, and consequently, the advertising of the reducing use of antibiotics [68].

Quaternary ammonium compounds (QACs) are used as antimicrobial agents and are very popular since it is very easy to manufacture these compounds in large scale as well as to modify their surface area. These compounds are used as antimicrobial compounds since 1935 and can be used as disinfectants also. The antibacterial effect showed by QACs can be explained by two different mechanisms. In the first one, the presence of positive charge on a surface can release cations to the bacteria wall, and in this way, break the external membrane of bacterium. In the second suggested mechanism, the cationic surface can change its configuration and, in this way, lead to the bacteria's lysis. In respect to the mechanism, the presence of a positive charge on QACs has a negative effect on cell survival in general [69,70]. On the other hand, when QACs are in contact with bacteria they will reduce their viability and cells will die. Moreover, QACs can cause antimicrobial resistance, which decrease their efficiency. Thus, the application of QACs is still very limited as antimicrobial surface coatings for medical implants [49].

The use of novel metals, as for example silver, is one of the most used strategies to prevent the adhesion of microorganisms to medical implantable devices. Silver has been used for centuries as an antimicrobial agent. From the medical point of view, silver was used by ancient Egyptians, Greeks and Romans to clean wounds. The use of silver in medical applications has grown until 1940, when penicillin was introduced for infection treatment. However, in 1968, silver nitrate was combined with sulphonamide to form silver sulfadazine (AgSD). This compound became the best known use of silver as an antibacterial agent and for treatment of burns. AgSD is like a reservoir of silver that slowly releases silver ions, causing membrane bacterial damage [71].

Despite silver being a well-known antimicrobial agent and having a broad-spectrum of activity, its mechanism of action is not fully understood [72,73]. However, it is suggested that the antimicrobial behavior of silver can be achieved by: i) the release of Ag^+ ions, ii) the interaction of bacteria with silver nanoparticles and iii) the formation of reactive oxygen species (ROS) [53,57,61,74].

In metallic state, silver is inert but it reacts with moisture and fluids from the wounds and gets ionized. In the case of silver ions, the antimicrobial properties are due to structural and morphological changes. Silver ions can penetrate inside the bacterial cells impeding the DNA replication and, consequently, leading to the cell lysis. Moreover, silver ions have a far lower propensity than classic antibiotics to induce antimicrobial resistance [75].

Besides the antibacterial properties exhibited by silver, it can be toxic to organisms after a prolonged contact with silver ions [22]. Despite all medical applications of silver and silver ions, the information about its toxicity is limited. However, some studies demonstrated that some forms of silver, especially silver ions (Ag^+), are more toxic than other forms [49].

The toxicity of silver can be observed in the form of argyria, which is an irreversible disease that discolours the skin. The ophthalmologic system can also suffer from prolonged exposure to silver resulting in a condition called argyosis [49,71,75].

Among all strategies for providing antimicrobial properties to implantable devices, like stents, the use of silver is one of the most common and effective techniques, nevertheless when silver is directly incorporated into implantable devices' surface can be released very quickly, limiting the time period of antibacterial protection [49,76–78]. Furthermore, metallic silver cannot provide enough antimicrobial activity and deteriorate fast [49,71,79] and the addition of silver salts into surface coatings is not a good solution because of the poor solubility of most silver salts [49].

Thus, the need arises for the incorporation of silver nanoparticles (NP) which may coat the implantable device surface and, dependent on the way the NP are fixed to the surface, increase the time period of silver's antimicrobial activity [31].

Silver nanoparticles can reduce colonization, infection rate, hospitalization days, and present economic benefits and are more efficient in antimicrobial aspects than silver salts due to their enormously large surface area, which provide better contact with the microorganisms [49]. In metallic state, silver interacts with thiol groups present in the bacterial cells and inhibits the respiratory process, leading to the cell death. In some specific bacterium, such as *Escherichia coli*, the antimicrobial effect is provided by the inhibition of the uptake of phosphate and release of phosphate, mannitol, succinate, proline and glutamine [71].

As mentioned previously, the mechanism of antibacterial action of silver is not absolutely clear. The silver nanoparticle's efficacy depends on the size and shape of particles. Small silver particles (< 10 nm) and triangular shaped particles demonstrate higher antibacterial activity as compared to big and spherical particles. Small silver nanoparticles produce electronic effects through the interaction with bacteria, and this intensifies the reactivity of nanoparticles [80]. According to Seil *et al.* [81], triangular shaped nanoparticles are a better option since they need less amount of silver to show bacterial inhibition. While triangular nanoparticles need 1 µg of silver, the spherical nanoparticles need 12.5 µg and rod shaped nanoparticles need 50 to 100 µg [71]. Silver nanoparticles activity against common bacteria, like *Staphylococcus aureus*, have been investigated and a concentration of 50 µg.mL^{-1} was reported as the need concentration to cause the death of bacteria [82,83]. Stents and other implantable medical devices with silver nanoparticles incorporated on a matrix on their surface slowly release silver ions into the matrix and, subsequently, into the solution. When in contact with bacteria and chemical compounds of their metabolism, the Ag dissolution increases and, consequently, bacterial inhibition is more effective.

The concentration of silver ions required for optimal antibacterial effect is observed between 10 nM and 10 µM [49].

Nakato *et al.* [84] deposited NP's on metallic stents surface and drug release kinetics was evaluated and they conclude that NP - eluting stent is a potential innovative method.

Several synthesis techniques were developed to obtain silver nanoparticles with different shapes and sizes, such as laser ablation, gamma irradiation, electron irradiation, chemical reduction by inorganic and organic agents, photochemical methods, microwave processing and thermal decomposition of silver oxalate in water and in ethylene glycol. The efficiency of antimicrobial properties is also dependent on synthesis technique.

Regarding the formation of ROS, they can be generated inside or outside the cell and are byproducts of respiring organisms' metabolism. Induction of ROS formation leads to the synthesis of highly reactive radicals that can cause the mitochondrial damage of the microorganism, accelerating the cell death or dysfunction. It is reported that silver can generate ROS, potentially including superoxide ($O_2^{\cdot -}$), hydroxyl radicals ($^{\cdot}OH_{\cdot}$), singlet oxygen ($^1O_2$) and the most stable ROS (H_2O_2) [85]. Therefore, it should be also possible to improve silver antimicrobial characteristics by forming reactive oxygen species, which leads to a most effective antibacterial behavior of silver, due to the toxic character of these species to bacterial cells. For example, Ferreri *et al.* [72] used oxidized nano-silver to achieve antibacterial behavior.

Silver oxides systems have not been well studied, since silver is, generally, consider as a non-reactive material [86]. The Ag-O system presents several defined compounds, such as Ag_2O, Ag_3O_4, AgO and Ag_4O_3, being the Ag_2O and AgO the most stable at high oxygen pressure and low temperature [87–89]. Regarding their synthesis, the most popular method is evaporation of metallic silver following by an oxidation, in a reactive environment (normally, a reactive plasma excited by dc (direct current) magnetron or microwave), or sputtering [86].

The different mechanisms of silver actuation are summarized in Table 6 .

Table 6-Summary and schematic representation of mechanisms of silver antibacterial action

Silver ions can penetrate inside bacteria and induce morphological and structural damage, promoting their lysis, by the inhibition of DNA replication.	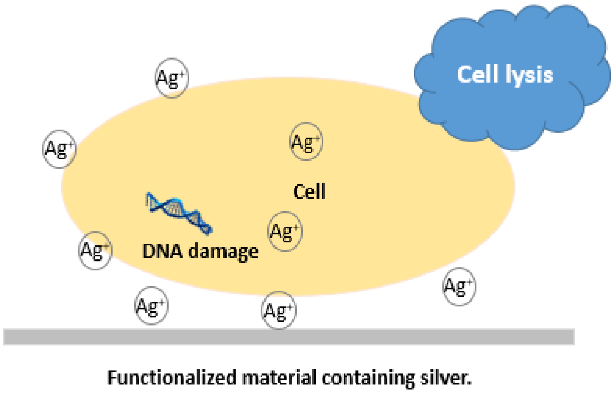 Cell lysis Ag^+ Cell DNA damage Functionalized material containing silver.
Silver nanoparticles (NP's) interact directly with bacteria, and are claimed to be more effective, once present a high surface to volume ratio, tending to be more easily ionized.	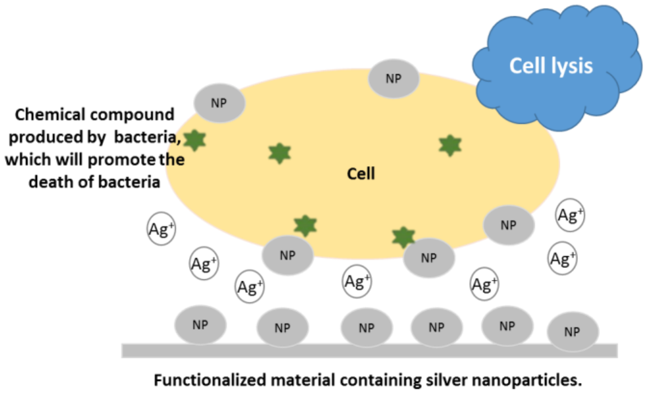 Cell lysis NP Chemical compound produced by bacteria, which will promote the death of bacteria Cell Ag^+ Functionalized material containing silver nanoparticles.
ROS lead to the synthesis of highly reactive radicals that can cause the mitochondrial damage, accelerating the cell death or dysfunction.	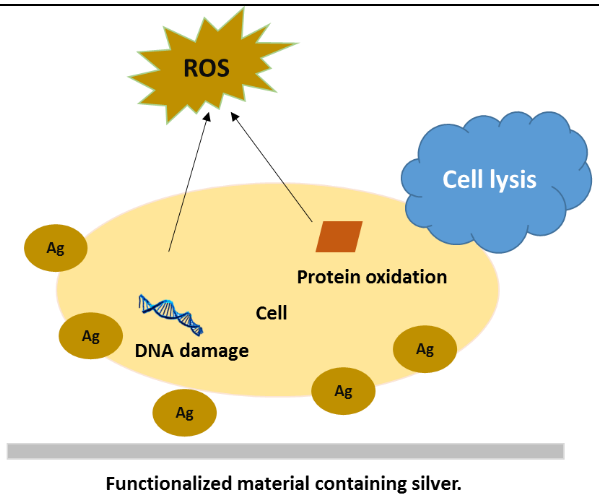 ROS Cell lysis Ag Protein oxidation Cell DNA damage Functionalized material containing silver.

In last few years the applications of silver nanoparticles and nanocoatings in medicine field have been rising [80].

3.2. Functionalization techniques

Generally, silver nanoparticles and nanocoatings are deposited, impregnated or coated onto medical devices for controlling infections. With the advance of nanotechnology, new techniques are used to coat the medical devices with thin layers of silver.

Impregnation is one of the oldest and simple methods of incorporating antimicrobial agents into textile fabrics. For example, it has been used for application of silver nanoparticles on to cotton fabrics. This technique is extremely simple and can be used in clinical situations, since it only requires $AgNO_3$, butylamine and absolute ethanol. The antimicrobial activity is controlled by the concentration of reactants used. Impregnation can be applied in fibrous materials. For example, dried cotton fabrics have cellulosic walls containing OH^- groups on the surface of cotton. Therefore, cotton can be functionalized through its immersion in the solution described above. The bonding with OH groups will reduce silver and provide an antimicrobial activity [90].

However, using the impregnation technique, the rate of the deposition of nanoparticles on the substrates is low and nanoparticles can be released due to weakness of interactions between nanoparticles and fibers [91].

Layer by layer is another technique of functionalization that was introduced in 1991 and since then it became one of the most popular techniques for preparation of nanoscale films with tailored properties. The principle of layer by layer technique is based on the alternating adsorption of materials containing complementary charged or functional groups to form integrated thin films. Normally, this technique begins with the adsorption of a species having opposite charge of the substrate and this reverses the charge of the substrate. This process is repeated forming several layers, until the desired thickness is achieved, as demonstrated in Figure 8 [92–94].

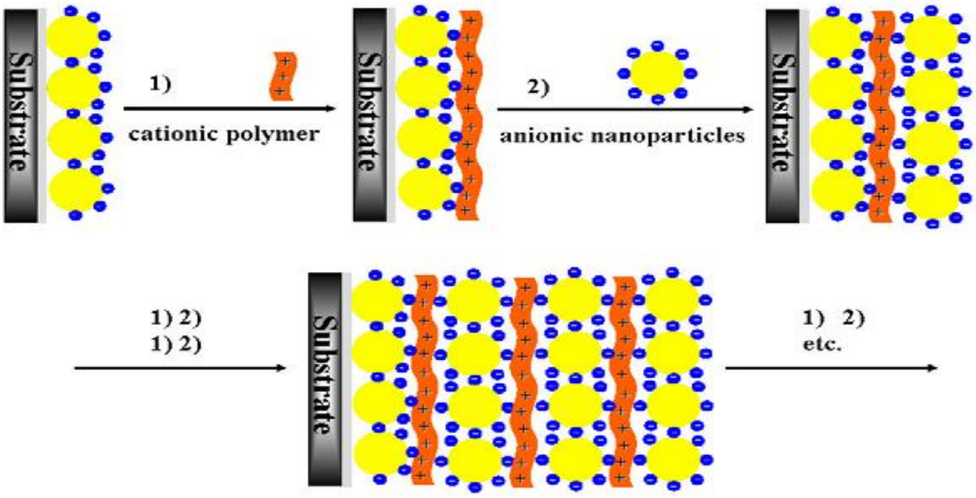

Figure 8-Layer-by-layer technique (figure adapted from [92]).

The film properties can be controlled by varying the type of species adsorbed, the number, and, consequently, the thickness of layers and the conditions employed during the assembly process.

The great advantage of this technique is that it allows a variety of materials, such as polymers, nanoparticles, proteins, among others; to be assembled on different substrates and the attachment can be through electrostatic interactions but also through hydrogen bonding, hydrophobic interactions, covalent bonding, and complementary base pairing [92].

This technique has been studied and employed on stents [95], by deposition of a thin film. For example, LBL assembly on nitinol surfaces facilitates the incorporation of nitric oxide donor and, this way, the bacterial adhesion is reduced [96].

Mahapatro *et al.* [97] used self-assembled monolayers (SAMs) to incorporate and deliver therapeutic drugs (prednisolone as model drug) from stent surface into human body. SAMs are ordered nanosized molecular coatings, which add 1 to 10 nm thickness to a surface. The study showed that monolayers with a few monometers thick can preserve the chemical groups on the surface and can persist on surface of stainless steel stents for 14 to 21 days, before oxidation and desorption of the thin film.

In the last few years, the deposition of metallic nanoparticles, onto polymeric substrates is being practiced increasingly due to their strong antimicrobial activity [91]. In order to modify surface properties or to fabricate self- assembled monolayers, the adsorption of thiol molecules, especially on noble metals, like silver and gold, are being studied. The adsorption of thiol occurs in several steps, starting with physical adsorption, then sulfur-metal bonding reaction, followed by the orientation of adsorbed molecules and, finally, the formation of a compact self –assembled layer [98].

One of the most widely used techniques for the functionalization of biomaterials is PVD. This technique is used in stents, due to its ability of deposition of a thin film onto non-uniform geometry. PVD provides strongly adherent films and optimal adhesion and integrity upon stent expansion [99]. PVD comprises a number of deposition techniques all of which allow transport of materials in the solid state between the target and the substrate (the material to be coated), through evaporation or sputtering, forming a thin film, due to nucleation and coalescence. This process begins with the nucleation of small clusters, which grows and coalesces, forming a thin film on substrate surface [96].

This entire process must occur under vacuum, to prevent material contamination, and to increase the distance between collisions among atoms, allowing the majority of atoms leaving the material to migrate to the substrate surface [100].

In the sputtering technique, the target is bombarded with very energetic ions gas (with previous plasma formation) which will lead to the ejection of particles of target material to be transported and deposited on the substrate. Ejected particles are, essential, atoms in fundamental state and ions [101]. Sputtering yield depends on the mean number of ejected atoms from target by incident particle, allowing quantification of technique's efficiency. This parameter depends on several factors as: energy of the incident particles, type of target, incidence angle, and type of incident particle (mass and reactivity) [101]. Reactive gases can be used, in order to obtain a reactive atmosphere. In this case, the sputtering process is denominated reactive sputtering and interactions between sputtered atoms and reactive gases occurs in target and substrate surfaces [102].

Sputtering presents some advantages such as: i) sputtering target provides a stable and extended lifetime source; ii) it is possible to use reactive gases, such as nitrogen, oxygen and acetylene and iii) it is an ecological process. In this technique there are different configurations like magnetron, radio frequency or pulsed source sputtering. The magnetron sputtering is used in 90% of PVD techniques [103].

Magnetron sputtering uses a magnetic field, along with a direct current (dc) or radio frequency (rf) source, formed by the introduction of magnets, which is placed in parallel to the target and perpendicularly to the electric field, causing an increased flow of electrons around the target (Figure 9). The magnetic field induces a circular movement in electrons, and, in this way, increases the probability of collision between electrons and ions of the gas, typically argon. With the increase of ion density, due to the increased number of collisions between the electrons and gas atoms, the deposition rate increases, due to the higher sputtering yield [101,104].

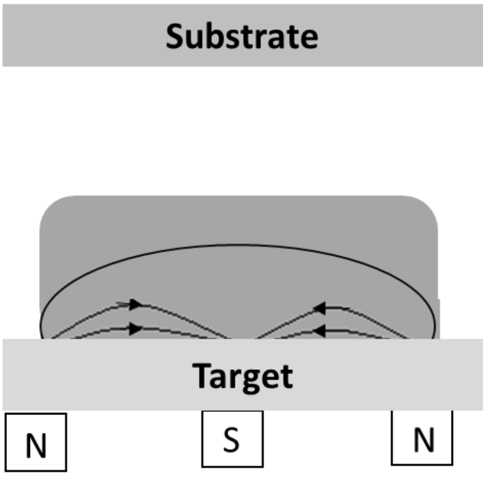

Figure 9- Schematic representation of the magnetron.

The major disadvantage of this process lies in the fact that only 20-30% of the target material is used, as observed in Figure 10 .

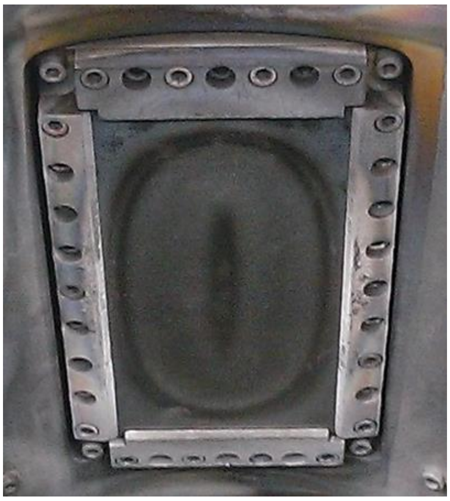

Figure 10- Example of a target used in magnetron sputtering.

In contrast, the magnetron sputtering allows controlling effectively the deposition parameters and the quality of coatings and reduces the impurities in the film [101,103].

Reactive magnetron sputtering occurs when a gas is introduced in deposition chamber with the intuit of making part of the final film, allowing the formation of complex compounds from a simple metallic target, as for example, the formation of silver oxides, through the introduction of oxygen in the deposition chamber. The main disadvantage of this process is its complexity, due to the unpredictability of where the reactions can occur: in the substrate, during the atoms transportation or in the target. If the reactions take place in the target, it is poisoned and sputtering yield decreases, as well as the deposition rate [101].

Diamond-like carbon films (DLC films) for cardiovascular implants have successfully been prepared by dual-target unbalanced magnetron sputtering and Rapid Photothermal Processing, achieving a biocompatible coating of a Ti/DLC nanolayers, suitable for medical implants [105].

Furthermore, PTFE and 316L stainless steel, as potential materials to be applied in stents, have been co-deposited by radiofrequency magnetron sputtering to produce a gradient surface coating that progresses from a metal base to PTFE at the surface [106].

More recently, Elmrabet *et al.* [107] used PVD magnetron sputtering to coat minitubes with magnesium for Mg - biodegradable stent applications. As main conclusions, authors referred magnesium minitubes as a candidate system for a biodegradable stent with a good corrosion resistance in phosphate buffer saline (PBS).

Taking in account all the improvement and developments in materials, design and production of stents, and antibacterial agents and functionalization techniques, it is extremely important to compromise all the factors in order to produce a new stent. This stent should have good mechanical and antibacterial properties but, at the same time, with a biomaterial behavior, i.e., with no adverse reaction with human body. Thus, the main innovation of this work was the development of a 100% fibrous stent, able to compete with the mechanical properties of those available in the market, with the advantaged of being coated, through magnetron sputtering, with a silver-based antibacterial agent, able to avoid infections and, this way, minimize the advantages of currently used stents.

CHAPTER II

Development and Mechanical Behavior of Fibrous Stents

This chapter is based on the publications:

R. Rebelo, N. Vila, R. Fangueiro, S. Carvalho, and S. Rana, "Influence of design parameters on the mechanical behavior and porosity of braided fibrous stents," Mater. Des, vol. 86, pp. 237–247, 2015.
R. Rebelo, N. Vila, R. Fangueiro, S. Carvalho, and M. Henriques, "Development of Braided Fiber-Based Stents," in Studies in Health Technology and Informatics, M. Graña, C. Toro, R. J. Howlett, and L. C. Jain, Eds. IOS Press, 2014, pp. 135–144.

1. Introduction

According to studies conducted over the applicability of fibrous materials on medicine, polyamide, polyester and polypropylene fibers appear to be the most suitable for implantable devices [2,30]. Polypropylene fibers were slowly inserted in the market, not only due to economic reasons, but also technical. The main technical reasons for this delay were the material's sensitivity to heat, limitations of dyeing and requirements of the manufacture process. Currently, polypropylene is used in steam sterilization because it presents a high melting point, 170 °C, low moisture absorption and high impact strength [108].

Polyester is a synthetic thermoplastic fiber widely used, i.e., deformable with heat, but not with cooling. The most important commercial polyester fiber is obtained through polyethylene terephthalate (PET). Polyester is widely used in fibrous prosthetic, being relatively inert, flexible and resilient, resistant to wear and tear and can be sterilized by all methods [109]. This fiber has also high mechanical strength and high dimensional stability, as well as biocompatibility [2,108].

The main polyamide fibers used are polyamide 6 and polyamide 6.6. Polyamide 6.6. was the first to appear in the world market, produced by DuPont®, while the polyamide 6 appeared only about two years later. Polyamides (polyamide 6 and polyamide 6.6) have a high capacity to absorb moisture, are resistant to very low temperatures, have high term oxidative stability, have high mechanical strength and abrasion resistance and are resistant to organic solvents and hydrocarbons [108]. Table 7 shows the main properties of the fibers to be used in this research.

Table 7- Properties of fibrous materials

Fibers	Characteristics
Polypropylene	Steam sterilization, low moisture absorption, good impact resistance.
Polyester	Good mechanical strength, good dimensional stability, inert, flexible, resilient, it can be sterilized by all methods.
Polyamides	High moisture absorption capacity, resistance to very low temperatures, high mechanical strength, high term oxidative stability, high abrasion resistance, resistance to organic solvents and hydrocarbons.

Fibrous stents may be produced using woven, knitting and braiding technologies, being the braiding technology the most suitable.

Research studies on braided stents investigated separately the influence of some of the design parameters on selected properties of stents. However, effective designing of braided stents should consider the influence of all important design factors related to material (such as fiber type and diameter), structure (such as braiding angle) and process (mandrel diameter) on the required characteristics such as porosity and cover factor, radial and axial compression, bending behavior, etc. As no existing study investigated all these factors together, a systematic investigation is highly essential to study and understand all these factors and properties, in order to produce suitable fibrous stents for replacing commercial metallic stents. To address this, the present study investigates the influence of different design parameters such as monofilament type and diameter, braiding angle, and mandrel diameter on the porosity and various mechanical properties (longitudinal and radial compression and bending properties) of braided fibrous stents and suitable parameters have been selected to design fibrous stents with characteristics matching with the commercial Nitinol stents.[1]

---

[1] The production and mechanical characterization of fibrous stents, corresponding to this chapter of the work, was developed in partnership with other researcher from Fibernamics group, at University of Minho.

2. Materials and Methods

2.1. Characterization of raw materials

Polyester (PES), polyamide 6.6 (PA) and polypropylene (PP) monofilaments were used to produce braided stents. Linear density, mechanical and friction properties of these monofilaments with three different diameters were evaluated. For the determination of monofilament breaking force and elongation at break, ISO2062 standard [110] was used. Linear density was measured following NP2060 standard [111] while friction coefficient was evaluated using the method described in ASTM 3108 [112] which reports the procedure for friction coefficient measures between fibers and solid materials. The result of the measurement assumes a value between 0 and 1.

2.2. Braiding Conditions

In order to produce the braided stents, a vertical braiding machine (Trenz Export 16/100), shown in Figure 11, with 16 yarn bobbins, was used. All stents were produced using 16 filaments. Stents with different characteristics were produced by varying the monofilament type (polyester, polyamide and polypropylene) and diameter (300 µm, 400 µm and 500 µm for PA; 270 µm, 350 µm and 550 µm for PES and 260 µm, 300 µm and 370 µm for PP), mandrel diameter (3.2, 5 and 6 mm) and braiding angle (20°, 30° and 35°). These combinations of braiding angles were accomplished taken in account previously calculation, using equation 1.

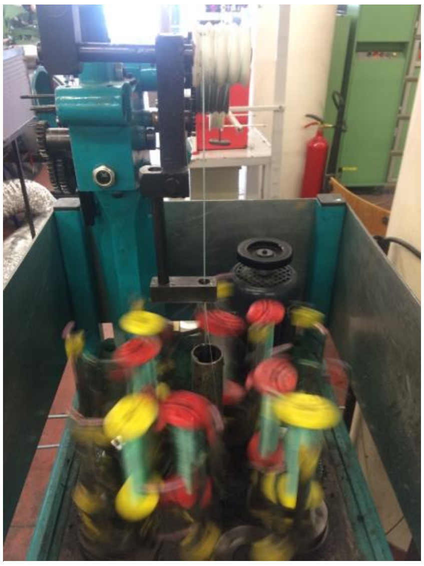

Figure 11- Vertical braided machine used in the development of stents.

After production, stents were thermofixed in order to maintain the integrity of the braided structure. The temperature of thermofixation for each type of fiber was set after differential scanning calorimetry (DSC) analysis. DSC is a thermal analysis which allows the measuring of material's physical properties as function of time and temperature. DSC is used to measure melting point temperature, heat of fusion, latent heat of melting, reaction energy and temperature, glass transition temperature, crystalline phase transition temperature and energy, among other properties [113].

2.3. Cover Factor and Porosity Evaluations

The amount of fibrous materials deposited on the mandrel surface during the braiding process depends on the braiding process parameters and it can be estimated using cover factor. Cover factor is defined as the percentage of mandrel surface covered by monofilaments. This is a good indicator of braid's structural uniformity [46]. Porosity is another important parameter for stents and should range between 70 and 80% [41]. Cover factor and porosity were calculated using equation 8 and equation 9, respectively.

$$CoverFactor = 1 - \left(1 - \frac{W_Y n_c}{4\pi R \cos\alpha}\right)^2 \tag{8}$$

Where,

Wy=monofilament diameter (mm);

nc= number of bobbins;

R= mandrel radius (mm);

α= braiding angle (rad).

$$Porosity = 1 - Cover\ Factor \tag{9}$$

2.4. Measurement of Radial Compression

It is highly essential to characterize the radial compression, as stents with insufficient radial force can lead to revision surgeries. When a radial pressure is applied, stents undergo a structural deformation leading to an expansion in the longitudinal direction and shrinkage in the transversal direction (Figure 12). This deformation results in change of stent diameter and braiding angle [114].

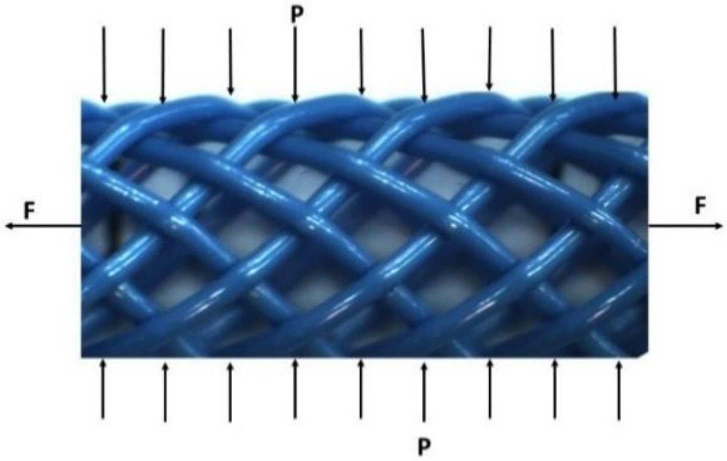

Figure 12- Scheme of resultant axial force in a stent when subjected to radial pressure.

Due to radial compression, stents decrease in diameter and increase in length. Therefore, the relationship between the length (L_f) of a single filament per turn and the stent diameter (D) becomes:

$$L_f = \frac{\pi D}{\sin \alpha} \tag{10}$$

$$D = D_a \frac{\sin \alpha}{\sin \alpha_0} \tag{11}$$

Where:

D= new average stent diameter (mm);

D_a= average stent diameter (mm);

α_0= Initial braiding angle (rad);

α= new braiding angle (rad).

The extension in the total length of stent (Δh) can be obtained by equation 12.

$$\Delta h = \frac{\pi D_a}{\sin \alpha_0} (\cos \alpha - \cos \alpha_0) \tag{12}$$

For the radial compression test, stents were held between two flat plates in a universal testing machine and 15 samples with 8 cm in length were compressed up to 25% of their original diameter, as shown in Figure 13. The average force of compression was then calculated.

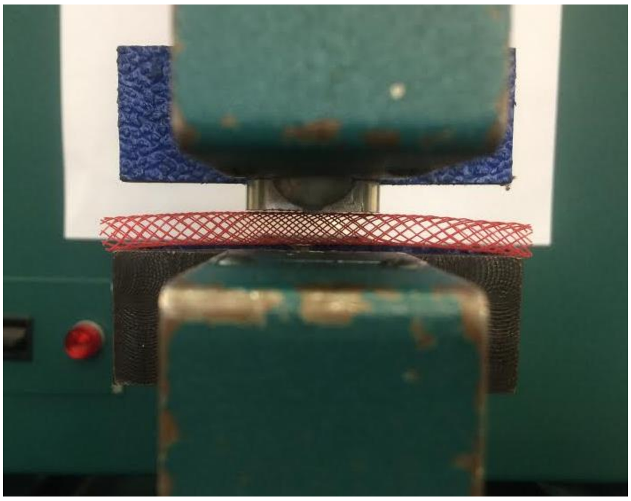

Figure 13– Setup of radial compression test.

Radial and longitudinal compression tests were performed at Laboratório de Física Têxtil da Universidade do Minho, in a universal tensile machine (Hounsfield HK100) with a load cell of 50 N, with a speed of 25 mm.min^{-1} and a pre-load of 0.01 N.

2.5. Determination of Longitudinal Compression

Stents should have good axial compression resistance; otherwise they will be easily compressed at their ends due to a slight trauma while exchanging different catheters [115]. Developed stents were compressed to 15% of their original lengths and the required force for this compression was measured [116]. For longitudinal compression tests, 15 samples of 8 cm length were compressed to 1.2 cm, in a universal testing machine (Figure 14), with the same conditions described for radial compression, and the average force was calculated.

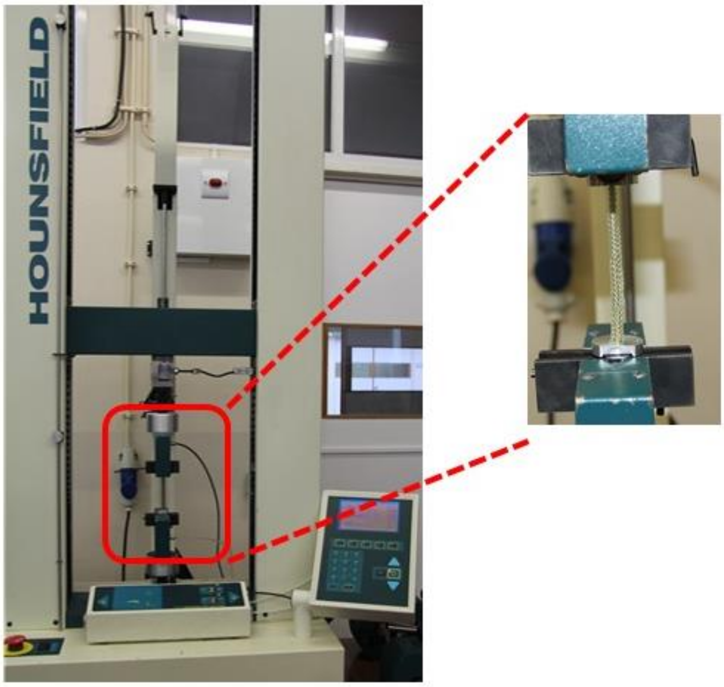

Figure 14-Setup of longitudinal compression test.

2.6. Determination of Bending Properties

Bending behavior plays a vital role in deciding the stent performance. After stents are implanted in to the human body, they should maintain at least, 75 % of its original diameter, in order to allow blood flow and avoid stent collapse. The diameter of a bent stent was measured at the midpoint of the bent section of the stent (shown in Figure 15 by arrow) according to the method proposed by Kim *et al.* [3]. By this method, 3 samples with 8 cm length were bent until their ends were separated by 2 cm (Figure 15). The ratio of the stent diameter in the bent condition and the initial diameter (expressed in percentage) was obtained and this parameter represents the percentage of original diameter which remained unchanged during the bending test. Unchanged diameter can be calculated using equation 13.

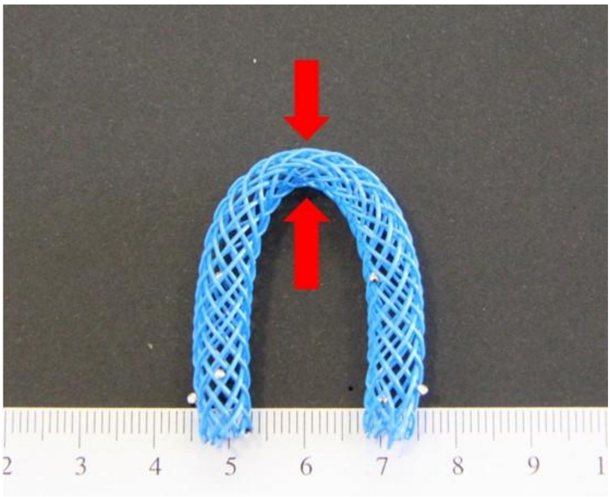

Figure 15- Measurement of unchanged bending diameter.

$$Unchanged\ diameter = \left(\frac{D_b}{D_i}\right) * 100 \tag{13}$$

Where:

D_b= stent diameter in bent condition (mm);

D_i= initial stent diameter (mm).

3. Results and Discussion

3.1. Development of braided fibrous stents

The results of fibrous materials characterization (monofilaments) are provided in Table 8.

Table 8- Characterization of raw materials

	PA			**PES**			**PP**		
Diameter (μm)	300	400	500	270	350	550	260	300	370
Linear density (Tex)	73.49 (0.04)	126.00 (0.04)	214.49 (0.03)	82.79 (0.03)	133.38 (0.02)	341.45 (0.13)	67.09 (0.03)	71.10 (0.02)	101.30 (0.02)
Tensile strength (N)	40.52 (0.66)	72.20 (1.56)	107.80 (4.45)	39.07 (1.11)	58.30 (1.26)	142.66 (1.93)	28.86 (0.33)	43.65 (2.02)	47.74 (0.32)
Initial Modulus (N/Tex)	2.03 (0.11)	1.75 (0.14)	1.72 (0.15)	5.79 (0.12)	1.10 (0.03)	4.65 (0.09)	2.57 (0.06)	5.51 (0.10)	2.88 (0.18)
Tenacity (N/Tex)	0.56 (0.01)	0.57 (0.01)	0.50 (0.02)	0.47 (0.01)	0.44 (0.01)	0.42 (0.01)	0.43 (0.01)	0.61 (0.03)	0.47 (0.01)
Elongation (%)	30.48 (2.36)	30.01 (1.67)	30.59 (4.20)	16.15 (1.58)	33.44 (1.64)	19.07 (1.29)	27.36 (5.76)	15.24 (1.31)	21.12 (1.13)
Friction coefficient	0.35-0.45	0.3-0.35	0.3-0.4	0.40-0.45	0.40-0.45	0.25-0.3	0.15-0.20	0.25-0.3	0.12-0.15
Density (g/cm^3)	1.14			1.38			0.9		

*The values within the brackets are S.D.

According to the type of fiber, stents were thermofixed at different temperatures. Along with the results of DSC, presented in Figure 16, Figure 17 and Figure 18 it is possible to observe that the melting point of PES, PA and PP is around 257.8 ^{0}C, 221.2 ^{0}C and 138.5 ^{0}C, respectively. Thus, polyester and polyamide stents were thermofixed at 182 ^{0}C and 186 ^{0}C during 1h, respectively. Regarding polypropylene, stents were thermofixed at 130 ^{0}C, during 10 min. These results are in agreement with those reported in literature [2,31].

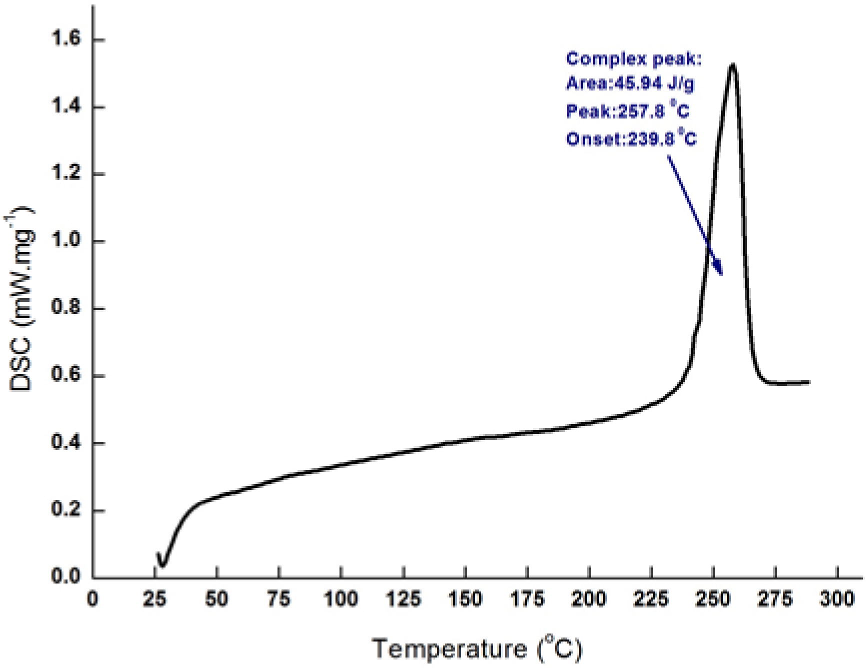

Figure 16-DSC analysis for PES fibers

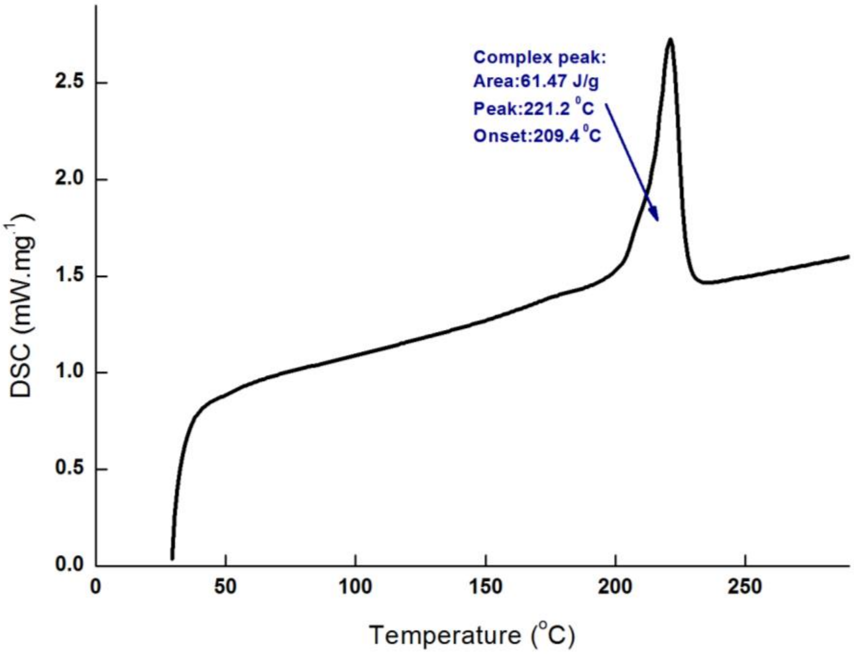

Figure 17- DSC analysis for PA fibers.

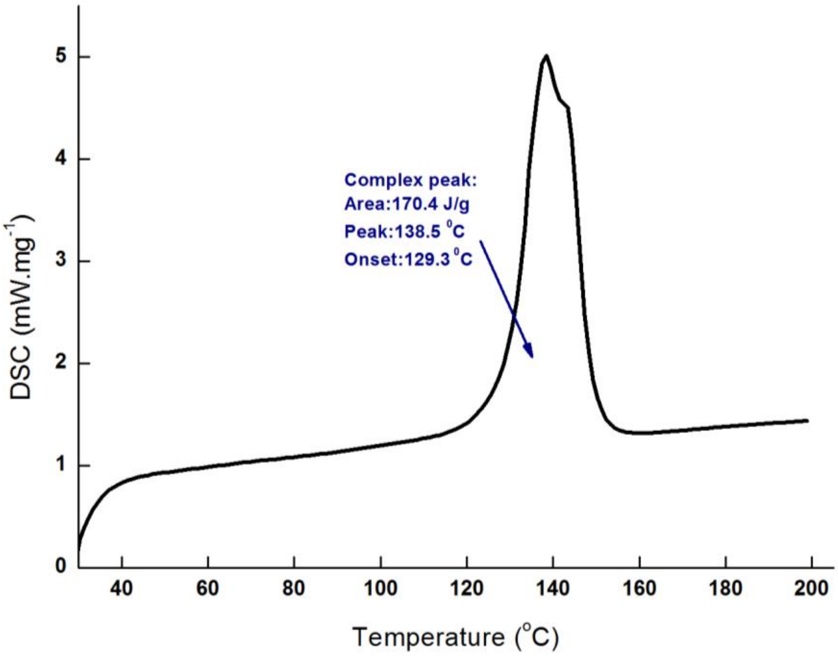

Figure 18-DSC analysis for PP fibers.

For easier understanding, samples were coded according to material type, monofilament diameter, braiding angle and mandrel's diameter, as shown in Table 9, Table 10 and Table 11. Thus, the sample code PES270A20D32 corresponds to a polyester sample with 270 µm monofilament diameter, braiding angle of 20° and mandrel diameter of 3.2 mm.

Table 9- Coding and producing parameters of samples for PES fiber

Sample Code	Fiber	Diameter of monofilament (µm)	Braiding angle (^{0})	Diameter of mandrel (mm)
PES270A20D32	PES	270	20	3.2
PES270A30D32			30	3.2
PES270A35D32			35	3.2
PES270A35D5			35	5
PES270A35D6			35	6
PES350A20D32		350	20	3.2
PES350A30D32			30	3.2
PES350A35D32			35	3.2
PES350A35D5			35	5
PES350A35D6			35	6
PES550A20D32		550	20	3.2
PES550A30D32			30	3.2
PES550A35D32			35	3.2
PES550A35D5			35	5
PES550A35D6			35	6

Table 10-Coding and producing parameters of samples for PA fiber

Sample Code	Fiber	Diameter of monofilament (µm)	Braiding angle (^{0})	Diameter of mandrel (mm)
PA300A20D32	PA	300	20	3.2
PA300A30D32			30	3.2
PA300A35D32			35	3.2
PA300A35D5			35	5
PA300A35D6			35	6
PA400A20D32		400	20	3.2
PA400A30D32			30	3.2
PA400A35D32			35	3.2
PA400A35D5			35	5
PA400A35D6			35	6
PA500A20D32		500	20	3.2
PA500A30D32			30	3.2
PA500A35D32			35	3.2
PA500A35D5			35	5
PA500A35D6			35	6

Table 11-Coding and producing parameters of samples for PP fiber

Sample Code	Fiber	Diameter of monofilament (µm)	Braiding angle (^{0})	Diameter of mandrel (mm)
PP260A20D32	PP	260	20	3.2
PP260A30D32			30	3.2
PP260A35D32			35	3.2
PP260A35D5			35	5
PP260A35D6			35	6
PP300A20D32		300	20	3.2
PP300A30D32			30	3.2
PP300A35D32			35	3.2
PP300A35D5			35	5
PP300A35D6			35	6
PP370A20D32		370	20	3.2
PP370A30D32			30	3.2
PP370A35D32			35	3.2
PP370A35D5			35	5
PP370A35D6			35	6

3.2. Mechanical behavior of fibrous stents

3.2.1. Cover Factor and Porosity

3.2.1.1. Influence of fiber type and diameter

Monofilament diameter strongly influences the cover factor and therefore, the stent porosity. As per equation 8, for the same production parameters, samples with lower monofilament diameter should show a lower cover factor and, consequently, higher porosity. This is attributed to the fact that the filaments with lower diameter (i.e. lower width) can cover less area on the mandrel surface for a particular mandrel diameter and braiding angle. Consequently, samples with higher monofilament diameter should present high cover factor and lower porosity. The influence of monofilament diameter and type on stent's porosity is shown in Figure 19. It can be noticed that the experimental results are in good agreement with equation 8. For all materials, an increase in monofilament diameter reduced the porosity due to better cover factors, as observed in Figure 19.

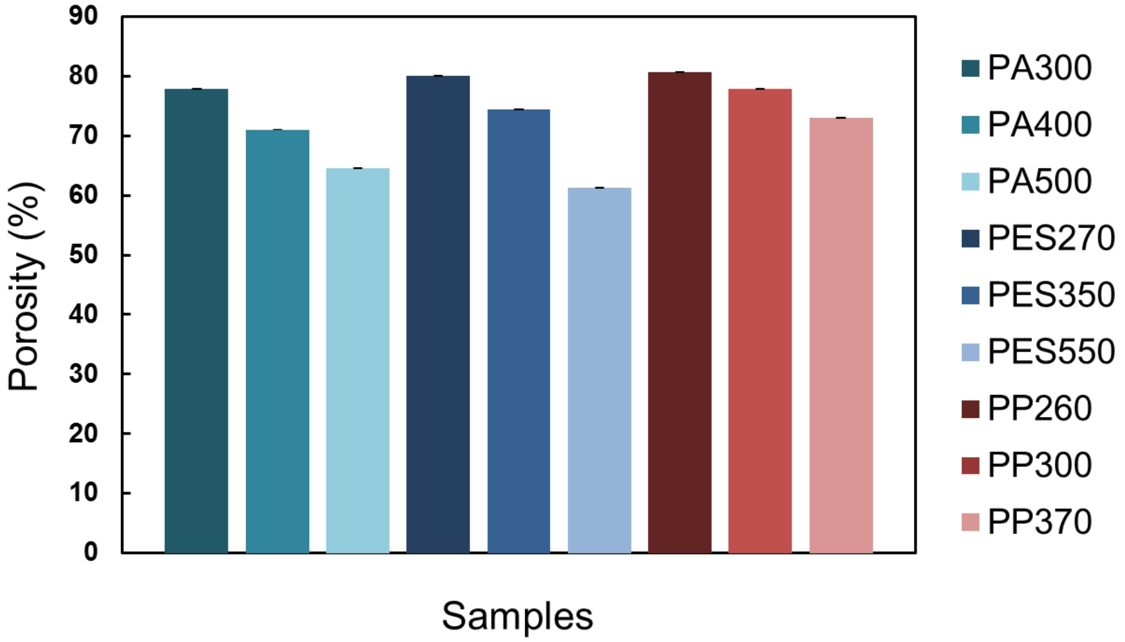

Figure 19-Influence of fiber type and diameter on porosity [mandrel diameter: 6mm, braiding angle: 35º].

The influence of material in porosity of produced stents depends mainly on their diameters. Overall, due to lower monofilament diameter, polypropylene stents presented lower cover factor and higher porosity (reaching maximum porosity of 81%) as compared to polyamide and polyester stents with maximum porosity of 78% and 76%, respectively.

3.2.1.2. Influence of mandrel diameter

The influence of mandrel diameter on cover factor of produced stents is shown in Figure 20. It is clear that the cover factor decreased with the increase in mandrel diameter. This is in agreement with the trend predicted using equation 8. If all other parameters are kept constant, an increase in mandrel diameter places less number of yarn coils on the mandrel and thereby reduces the area of mandrel covered by yarns. Therefore, an increase in mandrel diameter decreases its cover factor and consequently, increases the porosity.

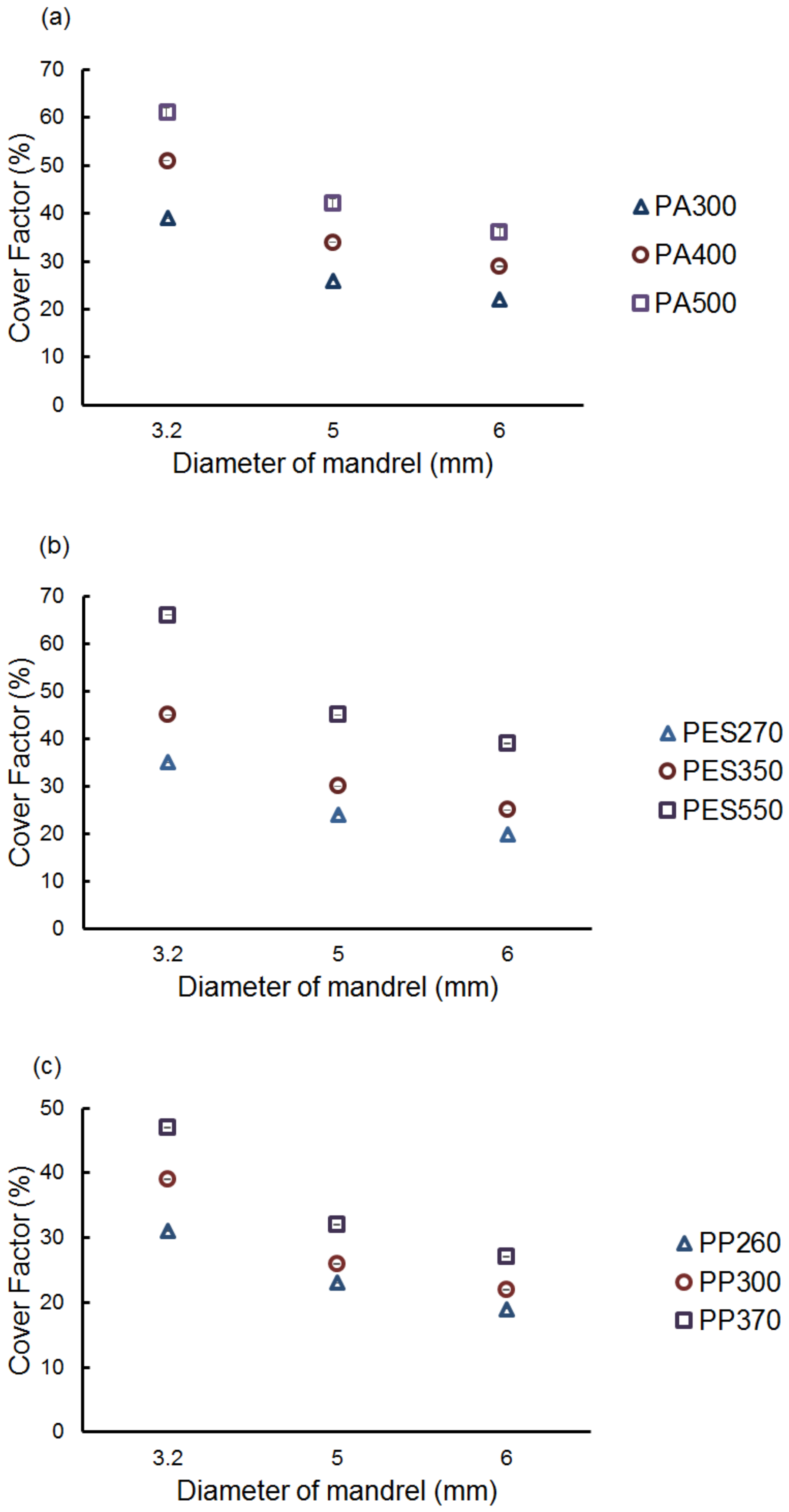

Figure 20-Influence of mandrel diameter on cover factor of PA stents (a), PES stents (b) and PP stents (c) [braiding angle: 35º].

3.2.1.3. Influence of Braiding Angle

Figure 21 presents the influence of braiding angle on cover factor of produced stents. An increase in the braiding angle led to an increase in the cover factor. This trend is also in agreement with equation 8. As shown in Figure 21, braiding angle is the angle between the yarn and the longitudinal axis of braids and therefore, in increase in the braiding angle leads to deposition of braiding yarns more towards the transverse axis. As a result, if a certain length and volume of mandrel is considered, higher braiding angle resulted in deposition of higher number of yarn coils and therefore, increased the cover factor. Consequently, porosity of the braided stents decreased with the increase in braiding angle.

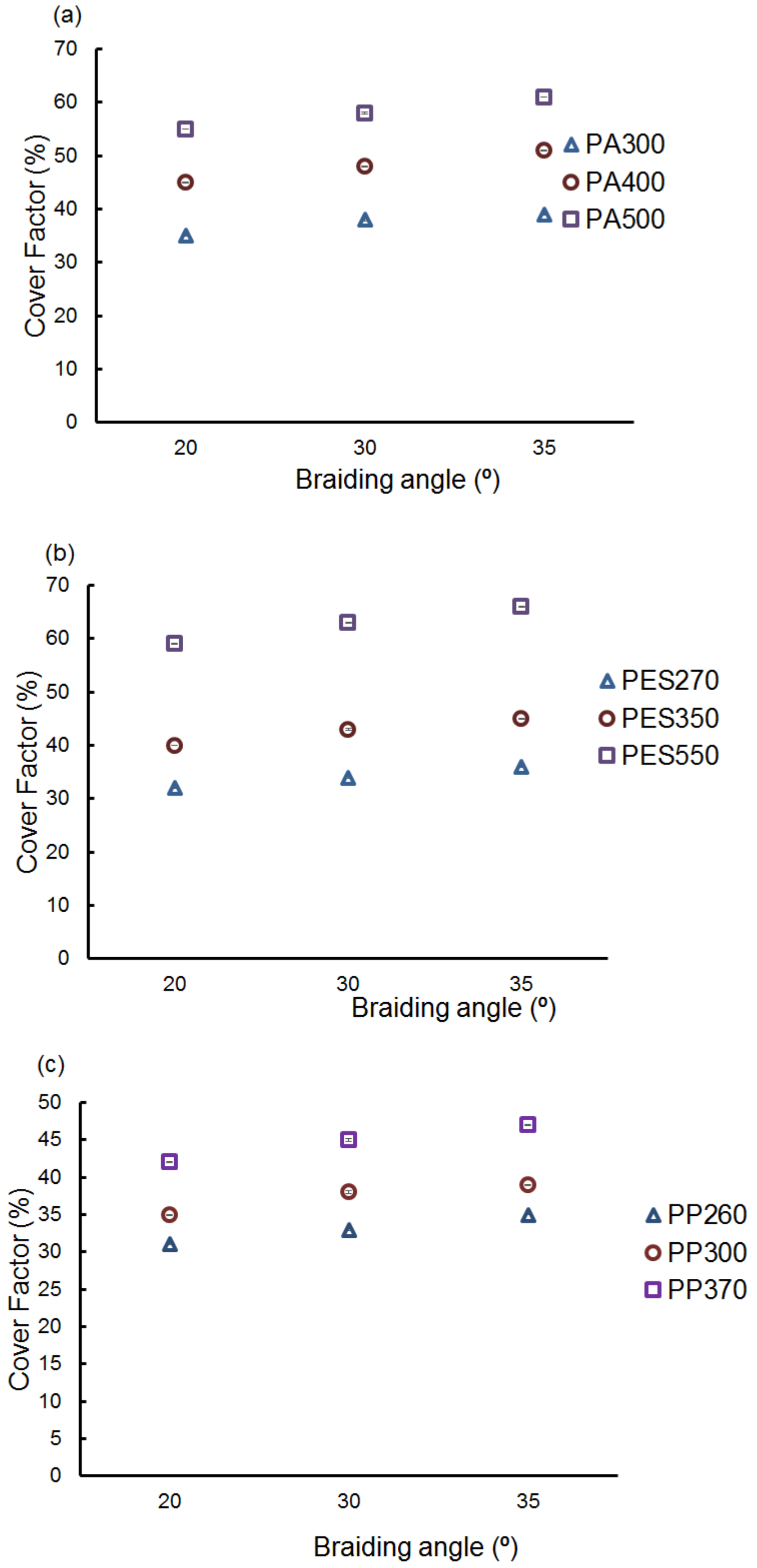

Figure 21 - Influence of braiding angle on cover factor of PA stents (a), PES stents (b) and PP stents (c) [mandrel diameter:3.2 mm].

In Figure 22 it is possible to observe the difference between the stent with lower cover factor (PP260A35D6 - 19%) and the stent with higher cover factor (PES550A35D32 - 66%).

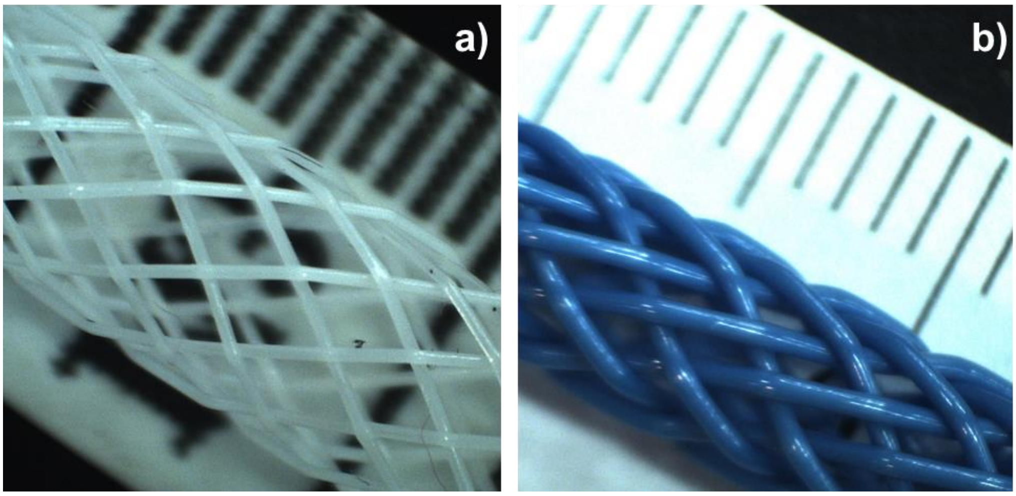

Figure 22- Difference in PP260A35D6 (a)) and PES550A35D32 (b)) cover factor.

3.2.2. Radial Compression

Theoretically, the radial compression pressure of stents can be expressed as:

$$P = -\frac{2Fn_c}{DL}\tan\alpha \tag{14}$$

Where,

P= radial pressure (MPa);

F= radial force (N);

n_c= number of bobbins;

D= average stent diameter (mm);

L= length of stent (mm);

α= braiding angle (rad).

Therefore, theoretically, radial compression force is dependent on the applied force, number of filaments, stent diameter and length as well as braiding angle.

3.2.2.1. Influence of fiber type and diameter

The influence of fiber type and diameter on radial compression force is shown in Figure 23. The force for radial compression is highly dependent on the monofilament type and their diameter. As the diameter of different monofilaments was not the same, it was quite difficult to understand the independent effect of monofilament type on radial compression. But overall, polyester stents required higher force than polyamide stents and the lowest resistance to radial compression was shown by the polypropylene stents. Also, the force for radial compression strongly increased with the monofilament diameter. This was attributed to several reasons: (a) higher monofilament diameter led to a higher stent wall thickness, resulting in higher radial compression resistance, (b) higher monofilament diameter also improved the cover factor, thereby improving the structural integrity and compactness of stents and this resulted in higher compression resistance, (c) radial compression led to bending and buckling of the monofilaments and therefore, higher bending or buckling resistance at higher diameters also increased the force for radial compression. The radial compression force for all polyester samples varied between 16.19 N and 1.06 N; for all polyamide varied from 15.55N to 0.31N and for all polypropylene varied from 3.66 N to 0.31 N. In case of PP stents, the differences observed in radial compression force were very small, as the diameter difference was smaller.

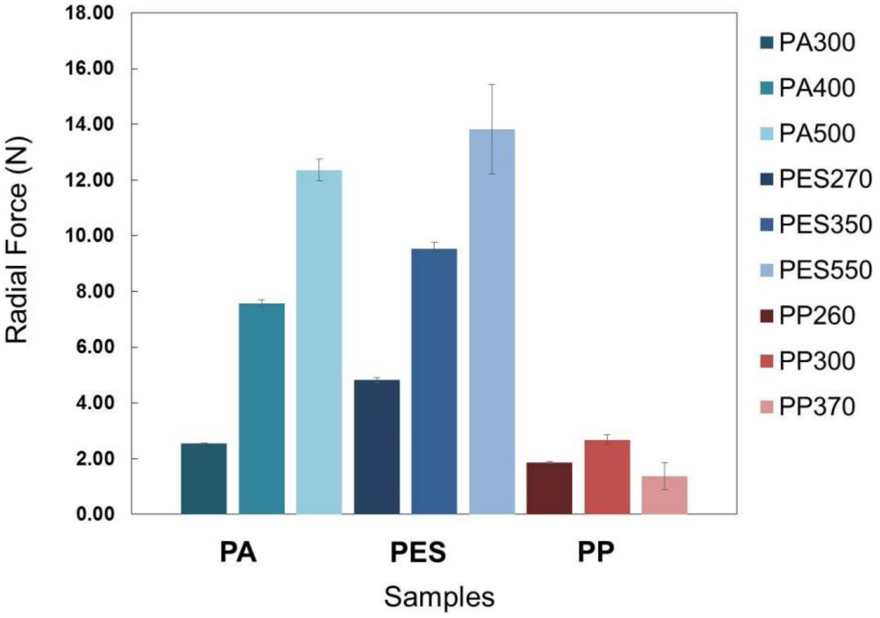

Figure 23 - Influence of fiber type and monofilament diameter on radial compression force for stents produced with 35° braiding angle and 3.2 mm mandrel diameter.

3.2.2.2. Influence of mandrel diameter

The influence of mandrel diameter on radial compression force is presented in Figure 24. It can be observed that, except PES550 stent, an increase in mandrel diameter resulted in a decrease in the force required for radial compression. As the stents were compressed between two flat parallel plates during radial compression, bending and buckling of the monofilaments occurred, besides some structural rearrangements which increased the length of stents. An increase in mandrel diameter also increased the diameter of stents and the length of the monofilaments under the buckling force. Since the buckling force is inversely proportional to the length of monofilaments, an increase in mandrel diameter reduced the compression resistance of the stents. However, the specimen PES550 did not follow the trend as shown by the other specimens. This exception was perhaps due to the higher monofilament diameter with the low frictional coefficient of these monofilaments, which could cause monofilament sliding during the compression test and therefore, behaved differently from other samples.

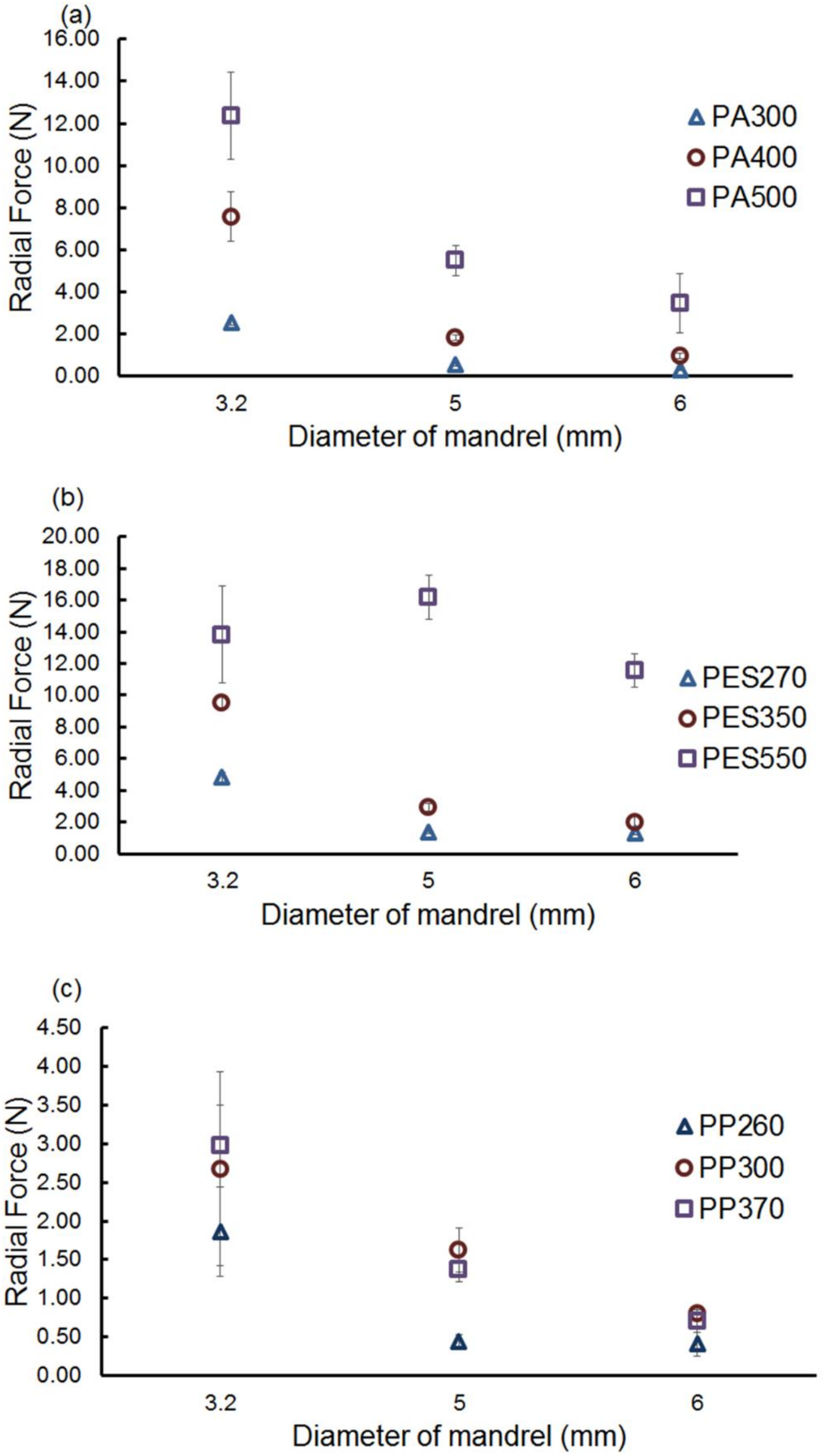

Figure 24 - Influence of mandrel diameter on radial force of PA stents (a), PES stents (b) and PP stents (c) [braiding angle:35^{0}].

3.2.2.3. Influence of braiding angle

The influence of braiding angle on radial compression force is presented in Figure 25. It can be noticed that for most of the stents an increase in the initial braiding angle increased the radial compression force. This trend is in agreement with equation 14. The primary reason behind this was the deposition of yarns more towards the transverse axis of the stents at higher braiding angles, leading to more resistance towards transverse forces acting during radial compression. Moreover, higher braiding angle also improved the cover factor and compactness of the stent structure resulting in higher resistance towards radial forces. However, too high braiding angle may also reduce the interlocking of the filaments (as they are arranged more parallel to each other) and increase the chance of slippage during compression. As a result, a decrease in the radial force (i.e. variation from regular trend) was also observed for some samples at high braiding angles and with samples presenting low friction coefficient and high monofilament diameter, such as PES550, PA500 and PP300.

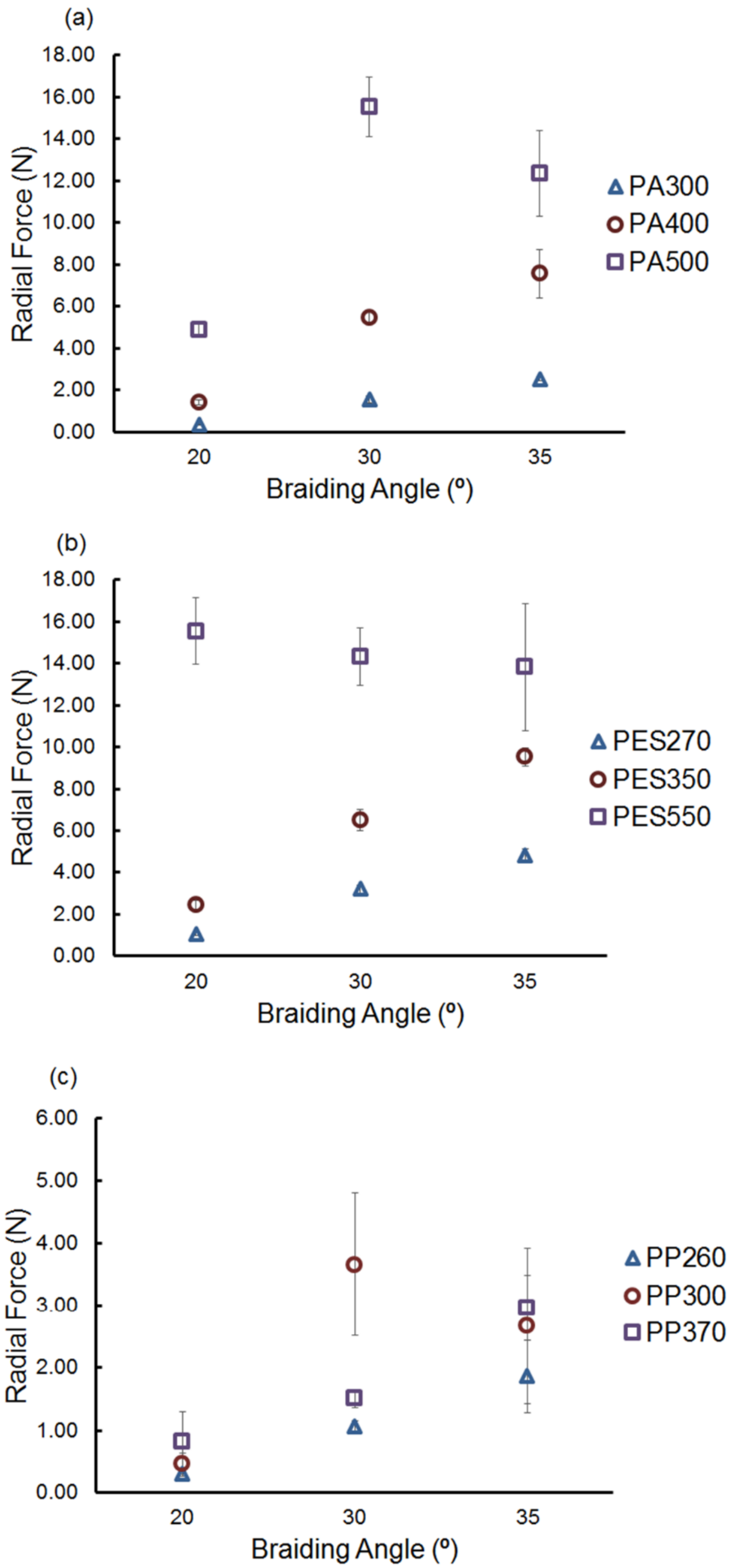

Figure 25 - Influence of braiding angle on radial compression force of PA stents (a), PES stents (b) and PP stents (c) [mandrel diameter:3.2 mm].

As mentioned in Section 3.2.2., radial compression leads to increase in the length of stents and this can be calculated using equation 12. After the compression test and relaxation, the stents showed some change in the diameter and length, indicating unrecoverable deformation. Table 12 lists the diameter recovery and longitudinal extension for selected PA and PES samples produced with high monofilament diameter and lower mandrel diameter, once these samples shown more exceptions in trends presented in section 3.2.2.. PP samples were not analyzed due to the lower friction coefficient and similar monofilament diameters, which avoids to correctly study the influence of the monofilament diameter.

It can be noticed that after compression test and relaxation, braiding angles (α) changed to some extent from the original ones (α_0), indicating structural rearrangement. Some increase in stent's length can also be noticed. Although, stent diameter could not recover completely back to the original values, the diameter recovery was more than 80% (Table 12), which is comparable with the value obtained with previously reported polypropylene stents [38].

Table 12- Diameter recovery and longitudinal extension of stents after radial compression

Sample	**α_0 (^{0})**	**α(^{0})**	**Da (mm)**	**D (mm)**	**Diameter recovery (%)**	**Δh (mm)**
PA500A20D32	35	28.48	4.2	3.49	83.10	1.38
PA500A30D32	31.02	27.95	4.3	3.82	88.84	0.68
PA500A35D32	32.64	29.44	4.2	3.83	91.19	0.7
PES550A20D32	34.29	29.2	4.3	3.72	86.51	1.12
PES550A30D32	30.35	28.94	4.3	4.12	95.81	0.33
PES550A35D32	31.84	25.16	4.3	3.47	80.70	1.42

3.2.3. Longitudinal Compression

The axial force on tubular stents can be expressed by the following equation [117].

$$F = 2n_c * [\frac{GI_p}{K_3} * \left(\frac{2\sin\alpha}{k_3} - k_1\right) - \frac{EI\tan\alpha}{K_3} * \left(\frac{2\cos\alpha}{K_3} - K_2\right)] \tag{15}$$

Where:

$K_1 = \frac{\sin\alpha_0}{D_0},\ k_2 = \frac{2cos^2\alpha_0}{D_0},\ K_3 = \frac{D_a}{\cos\alpha_0};$

Where,

n_c= number of bobbins;

E= Young's modulus (Pa);

G= Shear modulus (Pa);

I= Moment of inertia (kg.m^2);

I_p= Polar moment of inertia (m^4)

α_0= Initial braiding angle (rad);

α= new braiding angle (rad).

D_a= average stent diameter (mm).

It can be noticed from equation 15 that, theoretically, the axial force depends on several parameters such as number of yarns, modulus of rigidity and elasticity of braided tubes, moment of inertia of the fibers, braiding angle and stent diameter. However, this relationship is quite complex to understand the independent effect of each parameter on axial force.

3.2.3.1. Influence of fiber type and diameter

Figure 26 presents the longitudinal compression force for samples with braiding angle of 35° and mandrel diameter of 3.2 mm. It can be noticed that PES stents showed higher axial compression force as compared to PA stents, which exhibited significantly higher axial compression force than PP stents. The higher axial compression resistance of PES stents was attributed to the higher modulus of polyester filaments as compared to polyamide filaments. The main reasons for much lower axial compression force of PP stents were the lower diameter of PP monofilaments as well as their lower modulus. Stents containing higher diameter monofilaments exhibited higher longitudinal compression force due to their higher bending rigidity, as during longitudinal compression stents are also subjected to bending and buckling forces. Similar to the case of radial compression, PP stents developed with different monofilament diameters presented very small difference in longitudinal compression behavior, mainly due to small difference in their diameters.

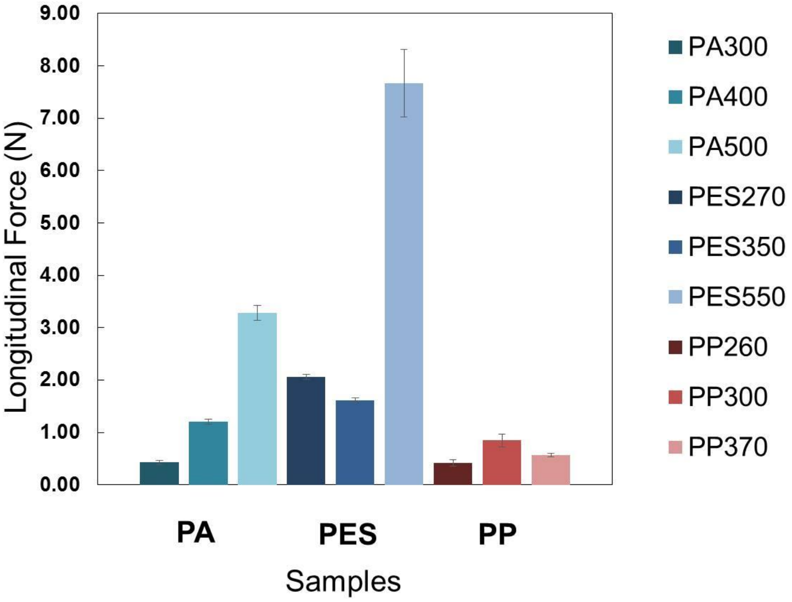

Figure 26 - Influence of fiber type and diameter on longitudinal compression force [braiding angle: 35^0, mandrel diameter: 3.2 mm].

3.2.3.2. Influence of mandrel diameter

The relationship between longitudinal compression force and mandrel diameter can be observed in Figure 27. Similar to radial compression, an increase in the mandrel diameter led to a decrease in the longitudinal compression force. Higher mandrel diameter resulted in lower cover and inferior structural integrity of the stents, resulting in lower resistance towards axial compression force.

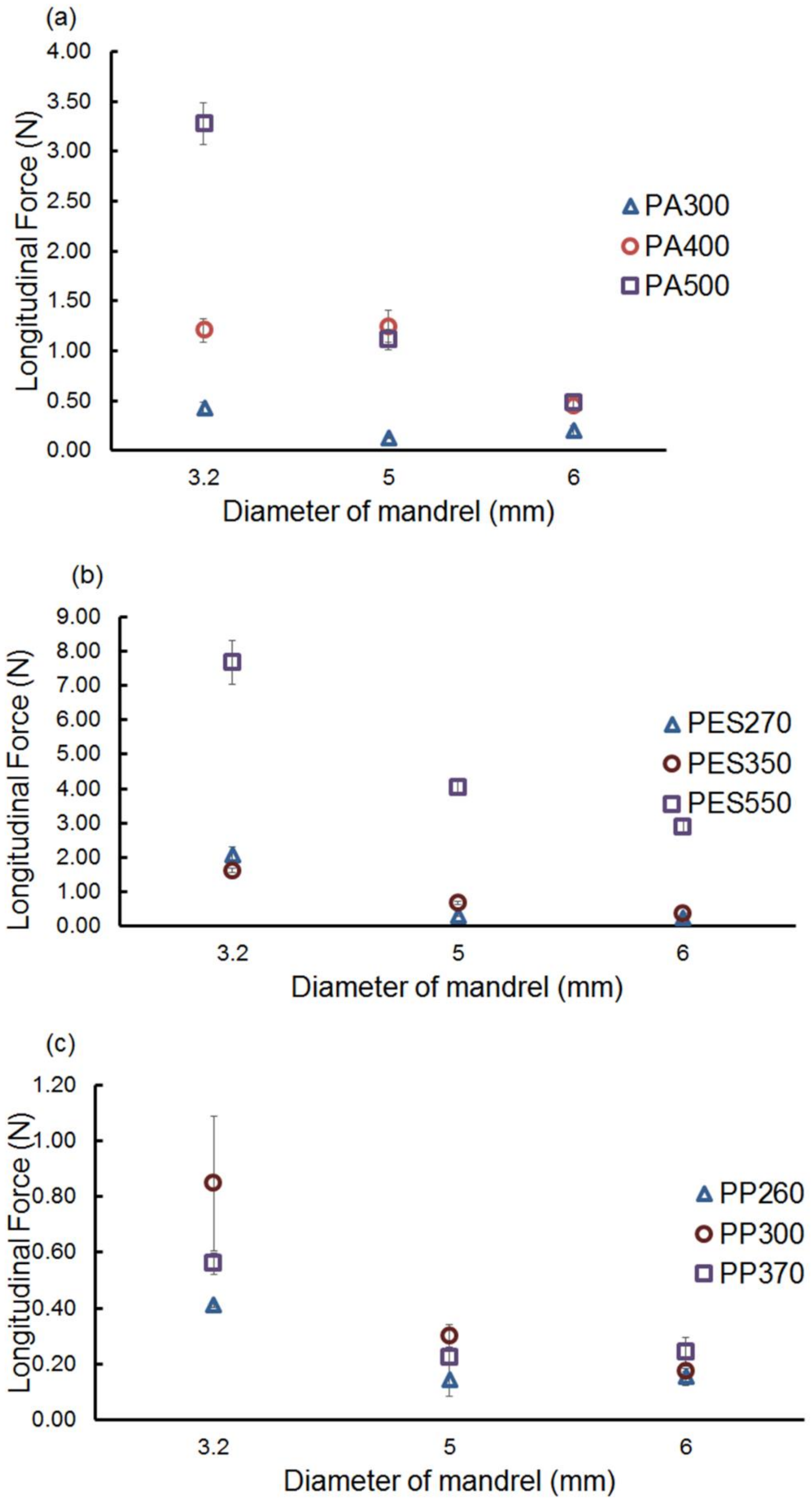

Figure 27 - Influence of mandrel diameter on longitudinal force of PA stents (a), PES stents (b) and PP stents (c) [braiding angle: 35^0].

3.2.3.3. Influence of braiding angle

Figure 28 presents the influence of braiding angle on the longitudinal compression force. An increase in longitudinal compression force with braiding angle can be clearly observed for most of the stents. This was attributed to the better cover of the stent structures at higher braiding angles, resulting in better structural integrity and higher compressive load bearing capability. However, at higher braiding angles, yarns became more oriented towards the transverse axis, thereby reducing their resistance to axial compression. Due to these two opposing factors, for some of the stents there was almost no change in longitudinal compression force with braiding angle.

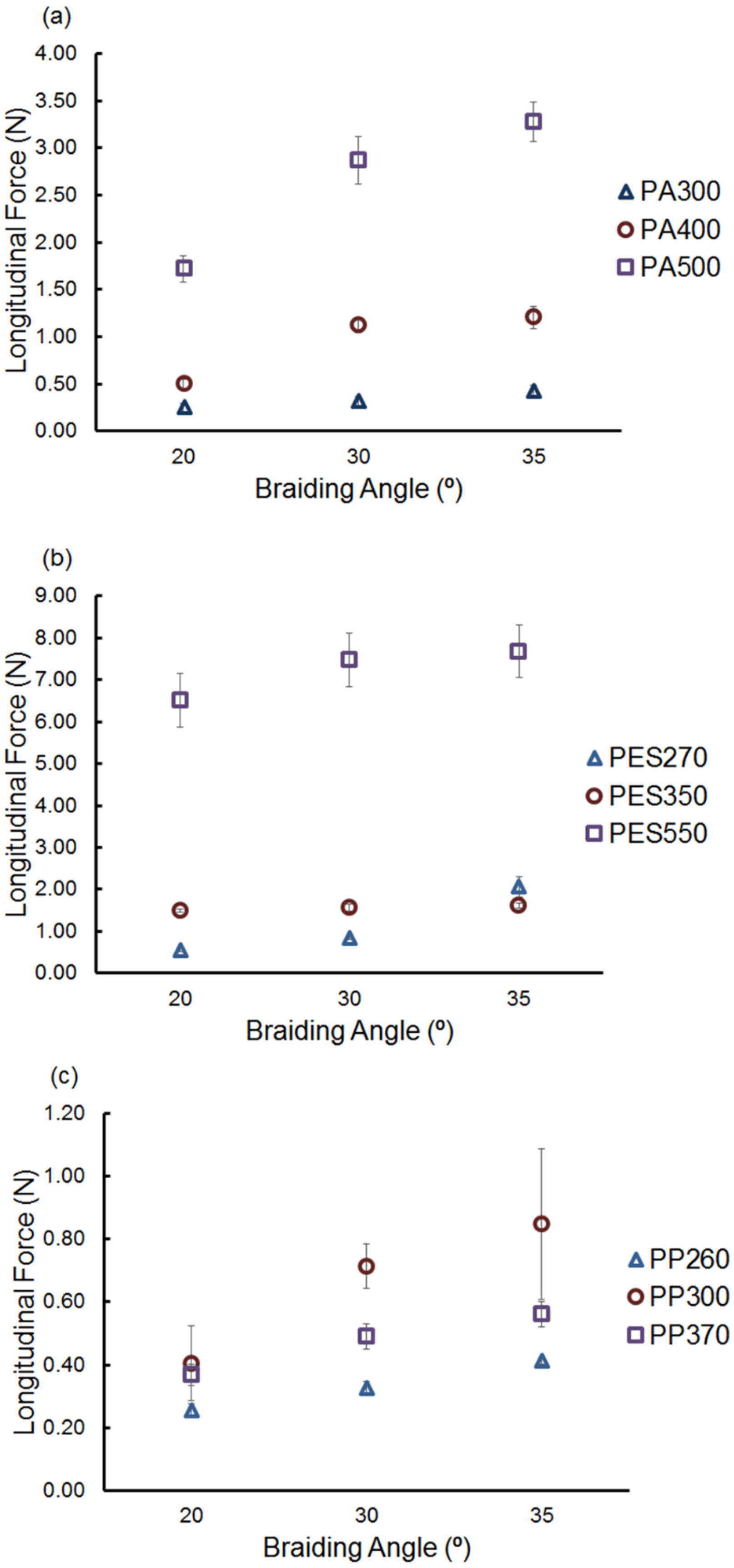

Figure 28 - Influence of braiding angle on longitudinal compressive force of PA stents (a), PES stents (b) and PP stents (c) produced using mandrel diameter of 3.2 mm.

3.2.4. Bending properties

Bending properties of developed stents were significantly influenced by all studied parameters, namely type of fiber, braiding angle, monofilaments diameter and diameter of mandrel and therefore, it was too difficult to find independent influence of each of these parameters on bending properties. However, for samples of PES and PA with lower monofilament diameters (270 µm, 350 µm and 300 µm, 400 µm) it was observed that an increase in the braiding angle resulted in better bending resistance and higher unchanged diameter. The comparison of bending behavior of various stents is presented in Figure 29. It is clear that most of the samples retained more than 75% of their original diameter during the bending test (indicated by the straight line).

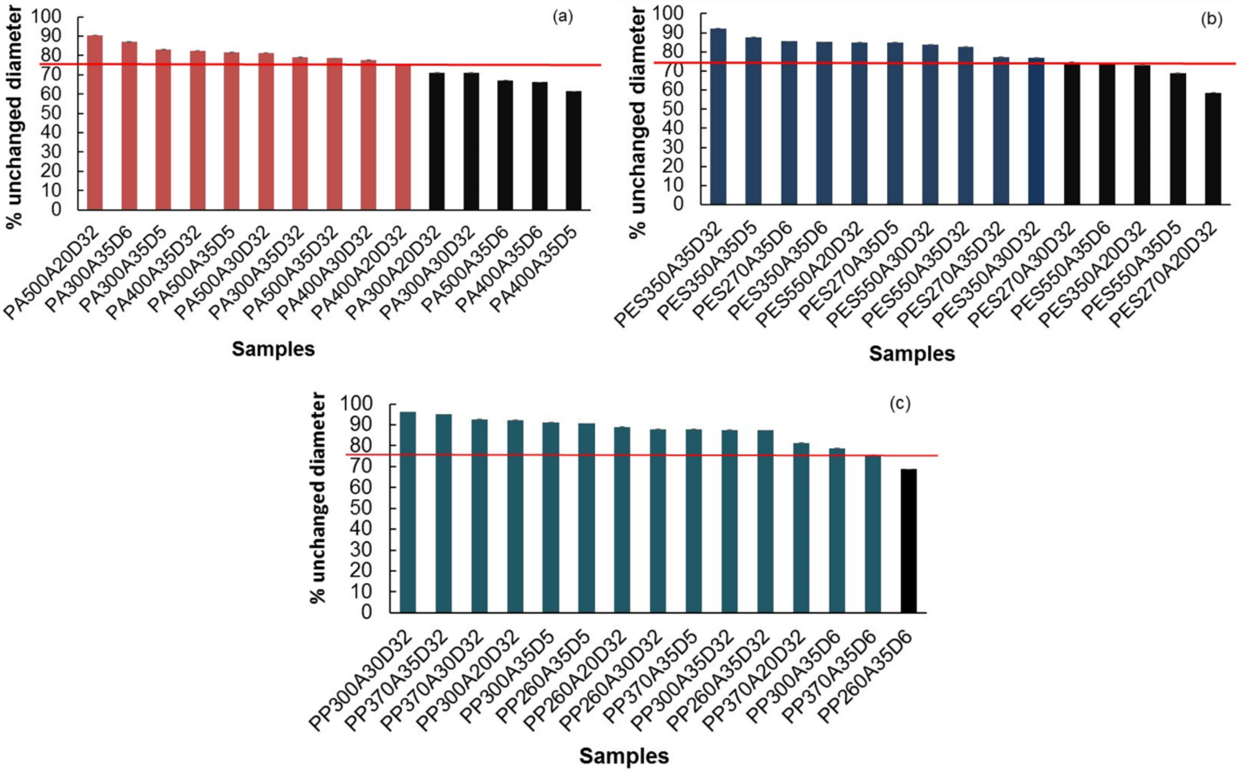

Figure 29 - Comparison of unchanged diameter of PA stents (a), PES stents (b) and PP stents (c).

3.3. Discussion

Different requirements have been reported in the literature for obtaining optimal stent design. Most of these properties are associated with the mechanical and physical properties of the stent's materials and structures [118]. An ideal stent should have biocompatibility and X-ray and magnetic resonance imaging visibility, radial strength, acute and chronic recoil, axial and radial flexibility, deliverability and long term integrity [118]. Most of the above properties are dependent on each other and their careful control is required to obtain an optimal design. For the commercial self-expandable Nitinol stents, the reported important physical and mechanical properties include radial compression, longitudinal compression, bending properties and porosity [116]. Therefore, in order to design a fibrous stent that can replace commercial Nitinol stents, the present research attempted to investigate important material and structural parameters of braided stents and to select suitable parameters to obtain above properties matching with those of Nitinol stents (force for longitudinal compression: [0.16-5.28] N and force for radial compression: [1.13- 2.90] N).

The experimental results presented in the previous sections show that the various properties of braided stents are highly dependent on different material and structural factors. Fiber diameter is an important material property which significantly influenced all the investigated properties. Higher fiber diameter led to higher radial and axial compression resistance, however, at the cost of reduced porosity. Similar effect was also observed in case of braiding angle. Higher braiding angle improved the mechanical performance, but reduced the porosity. In opposition, the influence of mandrel diameter (i.e. stent diameter) was exactly opposite, i.e. higher stent diameter improved the porosity and reduced the mechanical performance. The influence of fiber type was primarily associated with the fiber's inherent mechanical properties such as elastic modulus, bending rigidity, etc. Among the studied fibers, polyester fiber possesses better mechanical properties and therefore, improved the mechanical performance of the stents. Most of the produced stents could maintain more than 75% of their original diameters during bending test, fulfilling the requirement of commercial Nitinol stents. Besides these parameters, fractional properties of fibers also had significant influence. For braided stents, fibers should not have very low frictional coefficient as it results in relative sliding between the fibers and therefore, results in lower resistance towards axial or radial compression.

The fibers used in the present study, i.e. polyester, polyamide and polypropylene have been widely used in medical applications like sutures [39]. These fibers are suitable for these applications due to their good mechanical performance. Biocompatibility of implantable medical devices is also an important property and can be strongly influenced by the type of fibers. Overall, the fibers studied in this research have good biocompatibility as they lead to low tissue reactions and polypropylene is the best fiber in this aspect due to its highly inert nature.

3.3.1. Selection of fiber type and design parameters

The main objective of the present study was to develop 100% fibrous stents possessing similar physical and mechanical properties as commercial stents. Therefore, suitable design parameters have been selected in order to develop stents with properties matching with the commercial Nitinol stents. However, according to the requirements of specific applications, completely different set of parameters can also be selected. In the present case, samples with higher mandrel diameters (5 mm and 6 mm) and braiding angle (35°) can be selected to produce the best design. Although the increase in mandrel diameter reduced the mechanical performance, it increased the porosity and therefore, higher mandrel diameter was found favorable to obtain a good balance between mechanical performance and porosity. Similarly, polyester stents were found more advantageous due to higher mechanical performance as well as good porosity. Moreover, stents produced with lower monofilament diameters can be considered better due to higher porosity with sufficient mechanical performance. Considering all these factors, the best specimen produced in this research was PES270A35D6, as the properties offered by these stents closely matched with the Nitinol stents. Similar approach of selecting design parameters was also followed by Kim *et al.* [3] in case of shape memory polyurethane braided stents and in that case, fiber diameter and braiding angle were selected as the design parameters to obtain properties similar to Nitinol stents.

3.3.2. Comparison with commercial stents

Commercial Nitinol stents were tested elsewhere [116] and their mechanical properties have been compared with the selected fibrous stent produced within this study (PES270A35D6). From Table 13, it is possible to conclude that the developed fibrous stents fulfil the requirements of commercial stents, as far as the physical and mechanical properties are concerned and therefore, they can be good candidates for practical application.

Table 13- Comparison of properties between produced fibrous stents and commercial Nitinol stent

Properties	**Nitinol Stent** [3,116]	**PES270A35D6 Stent**
Force for Longitudinal compression	[0.16-5.28] N	0.23 N
Force for Radial compression	[1.13-2.90] N	1.29 N
Porosity	>70%	80%
Unchanged bending diameter	>75%	85.5%

4. Partial Conclusion

Within this work, 100% fibrous stents were developed using braiding technology and the influence of different materials, process and structural parameters such as fiber type, braiding angle and mandrel diameter on their performance was thoroughly investigated.

According to the experimental results, the best performance (i.e properties closely matched with those of commercial metallic stents) was achieved for polyester stents with 270 μm yarn diameter, braiding angle of 35^0 and mandrel diameter of 6 mm, providing the values of radial compression, longitudinal compression, porosity and unchanged bending diameter of 1.29 N, 0.23 N, 80% and 85.5%, respectively. The results obtained in the present study, as summarized in Figure 30, can be used to understand different parameters that influence the properties of braided stents and will help to design a 100% fibrous stent with targeted set of properties. As the properties of these 100% fibrous stents are in the range offered by commercial metallic stents, they have good potential for commercial use and this sample will be used for now on in the remaining work.

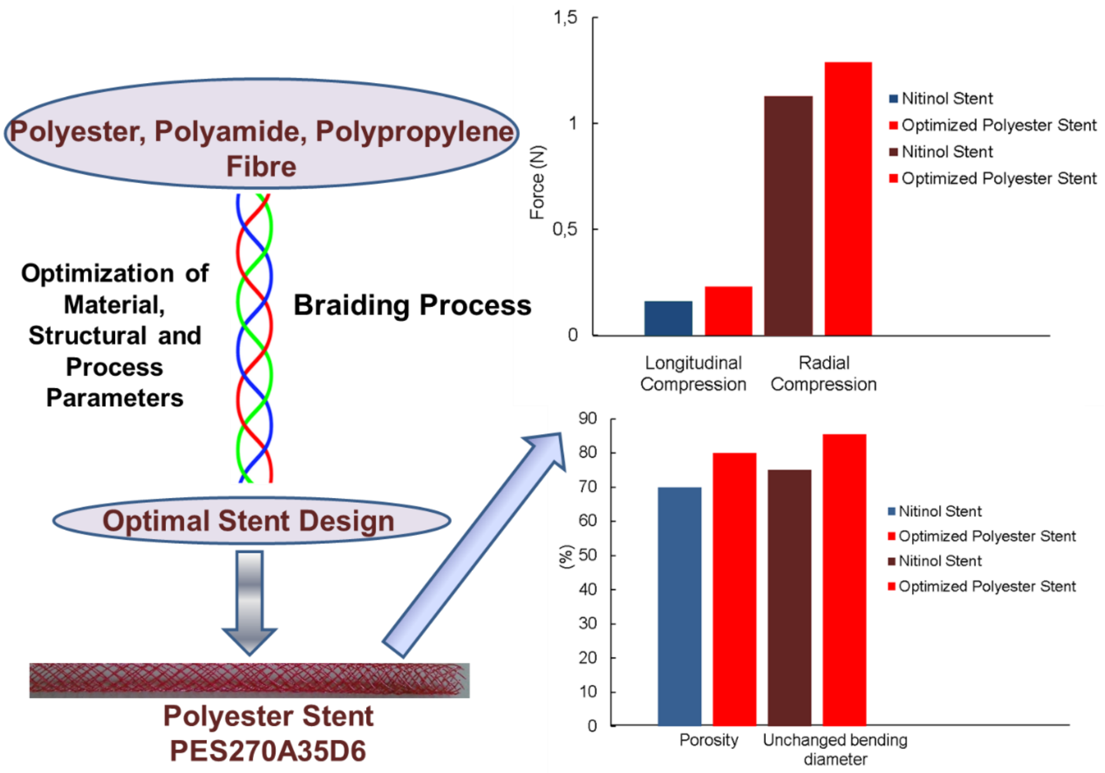

Figure 30- Summary of the production and mechanical behavior of developed fibrous stent.

CHAPTER III

Development and Characterization of Antibacterial Coatings

This chapter is based on the publication:

R. Rebelo, N. K. Manninen, L. Fialho, M. Henriques, and S. Carvalho, “Morphology and oxygen incorporation effect on antimicrobial activity of silver thin films,” Appl. Surf. Sci., vol. 371, pp. 1–8, 2016

---

1. Introduction

Despite the great innovations in the development of new stents with improved lifetime, namely the use of fibrous materials instead of metal, in order to avoid corrosion, stents, independently of the material, still present some disadvantages like bacterial colonization, which leads to the occurrence of infections [6]. Thus, in order to prolong the stent lifetime and patient´s safety the development of new stent materials with antibacterial properties is of great importance. With the advance of technology, new techniques are used to coat the medical devices with thin layers of antibacterial agent, such as physical vapor deposition (PVD), one of the most used techniques [91]. One of the principal techniques of PVD is sputtering whose purpose is the controlled transport of atoms between a target and a substrate on which will take place, at an atomic level, the formation and growth of a thin film, which will be the coat [103].

In this work, a reactive magnetron sputtering equipment, presented in Figure 31, was used to make depositions. This equipment is located at Laboratório de Revestimentos Funcionais II, in Departamento de Física, at Universidade do Minho.

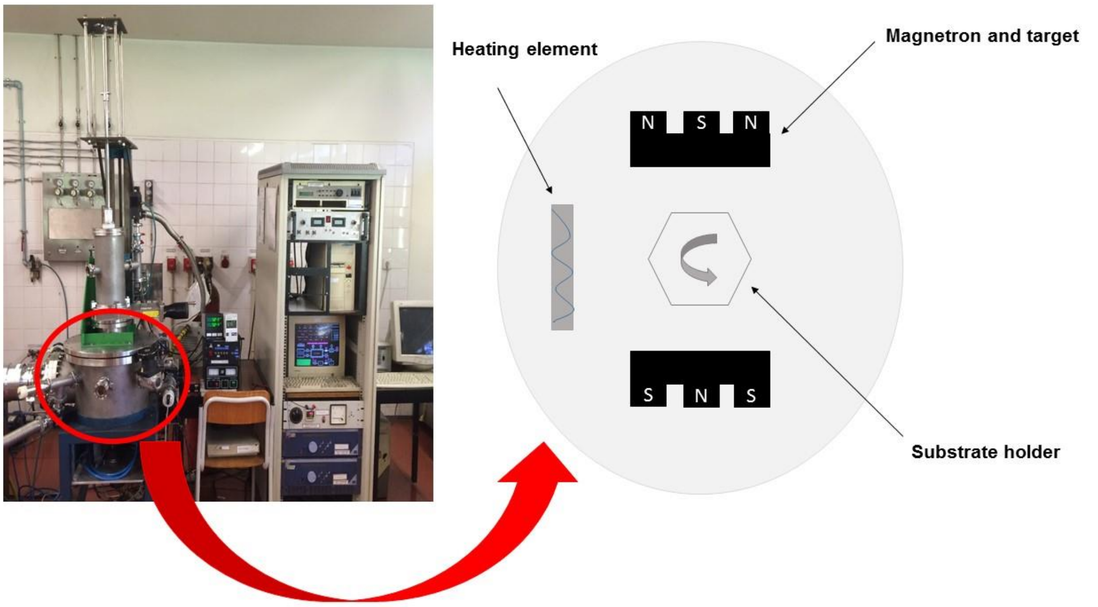

Figure 31- Equipment of reactive magnetron sputtering and a schematic of the interior of the deposition chamber (not at scale).

1.1. Silver-based Coatings

In the past years, silver has been studied as an antimicrobial agent [49,119,120]. The antimicrobial effect provided by silver depends on the amount of silver and the rate of Ag^+ released along time. Silver can exist in diverse forms: as metal, as a compound or as a free dissolved ion. The antibacterial efficiency of bulk Ag and Ag thin films is quite poor due to the high stability of Ag, which turns its ionization and solubility in water very low. In fact, any perfectly formed metallic surface in contact with an electrolyte will stabilize quickly; thus if a continuous release of Ag^+ ions is required, a driving force must exist to provide silver ionization. In order to achieve a continuous ion release, researchers have attempted many novel activation processes, such as: thermal, mechanical, chemical and electrical stimulation [121–124],still, in a practical point of view the application of these external driving forces are quite complex. One adopted approach is the incorporation of Ag nanoparticles in different matrix coatings or polymers, which are claimed to present an effective bactericidal effect, due to their higher reactivity, promoted by the high surface to volume ratio [125].

Another approach is demonstrated by Sant *et al.* [125] that claimed that the presence of heterogeneities in Ag based coatings enable to develop bioactive films. In fact, those authors found that the presence of fine grain size, incorporation of oxygen species and presence of lattice defects allowed to improve the Ag^+ dissolution rate, which is attributed to the high energy associated with these structural defects. Furthermore, the incorporation of oxygen species can lead to a higher productivity of ROS. These species induce oxidative stress in bacterial cells leading to their proteins, lipids and DNA damage and, consequently, the death of bacteria [72,126].

Thus, and with the ultimate intuit of functionalize a PES stents with antibacterial activity, stainless steel (SS316L) and silicon samples were coated with silver and silver oxide thin films. Silver coatings were chosen due to the known antibacterial properties of silver and silver oxide coatings were chosen as a way to promote the higher ionization of silver. These substrates were chosen in order to easily study and characterize the coating.

2. Materials and Methods

2.1. Production of silver and silver oxide coatings

Ag and Ag_xO coatings were deposited onto 316L stainless steel (20 x 20 mm^2) and silicon substrates (10 x 10 mm^2) by reactive pulsed dc magnetron sputtering. In this stage of the work, polyesters stents were only used as substrates, in order to verify the integrity of the stent after the deposition process. Once the main objective was the optimization of the coating, SS316L and silicon substrates were used to perform the coatings characterization. Before deposition the substrates were ultrasonically cleaned with distillate water, ethanol and acetone during 10 minutes in each solution. In order to minimize the contamination and remove impurities, before each deposition, the silver target and the substrates were etched in an argon atmosphere (Ar flow of 80 sccm) during 5 minutes. During the etching process a pulsed dc power supply (MKS, ENI RPG 50) with a current of 400 mA and a reverse time and frequency of 1536 ns and 200 kHz, respectively, was applied to the substrate holder. Simultaneously, the Ag target was connected to a dc power supply, and a current density (JAg) of 0.5 $mA.cm^{-2}$ was applied.

Two coatings were deposited: silver coating (Ag) and silver oxide coating (Ag_xO), with a deposition time of 300s and 3600s, respectively. The coatings were deposited from an Ag target (purity of 99.99%) with 200 x 100 mm^2. During deposition, the sputtering atmosphere consisted in a constant argon flow (60 sccm) for both coatings. For oxide coating, a reactive gas (oxygen) was introduced with a constant flow of 15 sccm (the maximum flow for the chamber), corresponding to a variation in the fraction of oxygen in the discharge [127] (fO_2 = $\boldsymbol{\Phi}O_2$ /($\boldsymbol{\Phi}O_2$ + $\boldsymbol{\Phi}$Ar) to 0.2, resultant in a input oxygen partial pressure ($pO_{2,\,in}=fO_2{*}p_{total}$) of $1.5{*}10^{-1}$ Pa. The silver coating was deposited with the 2.5 $mA.cm^{-2}$ as current density applied from a pulsed dc power supply to the Ag target.

Prior to the production of a complete set of samples, some tests were performed varying the current applied to the silver target from 2.5 and 1 $mA.cm^{-2}$. Figure 32 shows the Ag target potential as a function of the fraction of oxygen in discharge. The results demonstrated that only in the case of lower current density the poisoning mode could somehow be reached concomitantly, the possibility of silver oxides formation is improved.

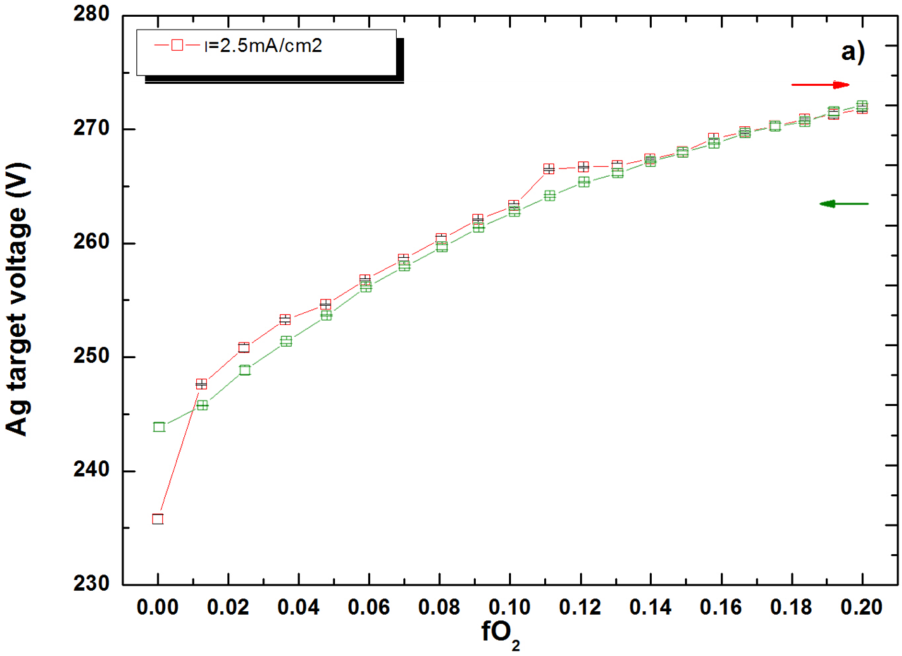

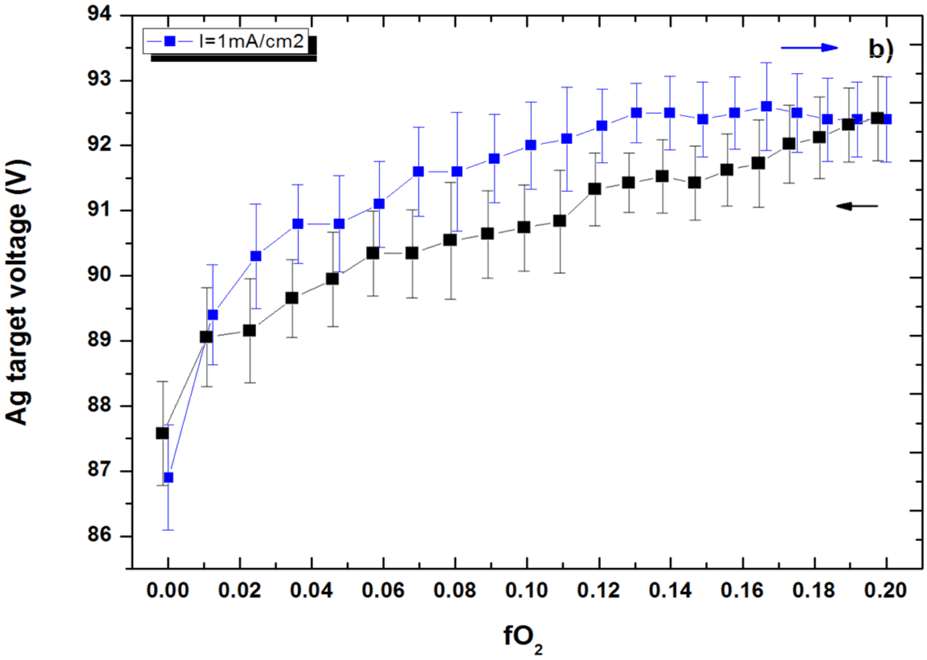

Figure 32 - Variation of target potential as function of fO_2 for different applied density currents: a) 2.5 mA.cm^{-2} and b) 1 mA.cm^{-2}.

Thus, for the deposition of the oxide coating 1 mA.cm^{-2} of current density on the Ag target was applied, in order to reach the reactive mode deposition. The reverse time and frequency were kept at 1536 ns and 200 kHz, respectively. Samples were placed in a substrate holder that rotated at a constant velocity of 7 rpm, 70 mm away from the target. These conditions were chosen based in other studies [128,129] and taking in account that the final purpose is to deposit in fibrous materials, and no structural damage should be observed in the substrate. In this sense, the depositions were performed without any external heating and no bias polarization was applied on the substrate holder.

2.2. Characterization of silver and silver oxide coatings

Stainless steel 316L substrates were used in all characterization techniques that evaluate the functional properties, while silicon substrates were used in characterization techniques that evaluate the coating´s morphology and structure. Thus, silicon substrates were used in in X-ray diffraction (XRD) analysis, once silicon avoids the appearance of substrate's peaks. In X-ray photoelectron spectroscopy (XPS), since silicon's surface is smoother than stainless steel 316L, the analysis is more reliable.

XPS analysis was performed in order to obtain information about the coatings binding state. This technique allows to identify the elements presented in a material's surface and allows obtaining information about their chemical bonds. This information is obtained after the incident of X-rays on the material surface (usually with a depth between 0.5 nm and 10 nm), once the X-rays energy leads to electron emission from the material surface. The elements are identified through the measurement of the electron energy, which allows the calculation of the binding energy and, consequent, identification of the element [130].

The XPS analysis was performed on silicon samples coated with Ag and Ag_xO in a Kratos AXIS Ultra HSA equipment, with VISION software for data acquisition and CASAXPS software for data analysis. The analysis was carried out with a monochromatic AlKα X-ray source (1486.7 eV), operating at 15kV (90 W), in FAT mode (Fixed Analyzer Transmission), with a pass energy of 40 eV and a pass of 0.1 eV for regions ROI and 80 eV of pass energy and 1.0 eV of step for survey. Data acquisition was performed with a pressure lower than $1*10^{-6}$ Pa, and a charge neutralization system was used. The effect of the electric charge was corrected by the reference of the carbon peak (285 eV). The samples were sputter-cleaned in situ using a broad 2 keV Ar^+ beam for 5 min. XPS measurements were performed at Laboratório de Análise de Superfícies in CEMUP (Centro de Materiais da Universidade do Porto).

The morphology of Ag and Ag_xO coatings deposited in SS316L and the thickness of coatings deposited on silicon substrates were evaluated by scanning electron microscopy (SEM) analysis in an EDAXNova nano-SEM200 equipment, being analyzed 3 different regions and presented a representative micrograph. In SEM analysis, an image is obtained by the interaction of an electron beam with the material. This interaction produces a several signals that can be detected, as secondary electrons (SE), backscattering electrons (BSE), X-ray and auger electrons, and information about material's morphology and composition (when linked with an energy-dispersive X-ray Spectroscopy (EDS) equipment) is obtained [101,131]. SEM top-view micrographs were recorded in BES mode at 5kX and thin films morphology were recorded in SE mode at 100kX.

XRD is one of the most used and powerful characterization technique. This technique allows to determinate the crystalline size and access information about the crystal structure. In this technique, a monochromatic X-ray radiation is incident on material and it is reflected or diffracted by the material crystal planes. This interference between radiation and material's crystal planes results in a diffraction peak, which is reported by the Bragg's law, as demonstrated in equation 16 [131].

$$n\lambda = 2d_{hkl} * \sin \Theta_{hkl} \tag{16}$$

Where:

n=Diffraction order;

λ= X-ray wavelength (nm);

d_{hkl}= Distance between atomic planes (nm);

Θ= Angle formed by the incident beam and Bragg considered diffraction plane (º).

XRD analysis was carried out in order to understand the structure and phase distribution of the coatings, in a PANalytical X´Pert PRO MPD system using CuK radiation (45 kV and 40 mA) with a parallel beam configuration. The analysis was performed in grazing incidence mode with an angle of incidence of 5°. The X-rays reach the entire sample area, thus only one sample was analyzed, which is the common procedure in this technique. The grain size was determined by Scherrer formula [132] (equation 17) using the (111) peak in case of Ag thin film. The XRD peak was fitted with pseudo-voigt function, which allowed us to calculate either the full-width at half-maximum (FWHM) and the peak position (2θ). Silicon substrates were used for XRD analysis.

$$T = \frac{K\lambda}{\beta \cos\theta} \tag{17}$$

Where:

T= Mean size of the ordered (crystalline) domains (nm);

K= Dimensionless shape factor (0.9)

λ= X-ray wavelength (nm);

$\boldsymbol{\beta}$= Half the maximum intensity (FWHM) (rad);

Θ= Bragg angle (^{0}).

SEM and XRD measurements were performed at SEMAT-UM (Serviço de Caracterização de Materiais at Universidade do Minho).

The coatings hydrophobicity was evaluated through contact angle measurements, using the van Oss approach [133] in coatings deposited onto SS316L substrate, using an automated contact angle measurement apparatus (OCA 15 Plus; Dataphysics, Germany) located in the Centro de Engenharia Biológica at Universidade do Minho. For the contact angle analysis, 8 measurements were made, with three different liquids: water, formamide and α-bromonaphtalene, with different and known values of surface free energy [59,134], Y_l^{Tot}; apolar Lifshitz–van der Waals surface free energy component, Y_l^{lw}; electron acceptor surface free energy component, Y_l^{+}; and electron donor surface free energy component, Y_l^{-} (Table 14). For statistical analysis t-tests were performed, using the software GraphPad Prism 6. Tests were performed with a confidence level of 95%.

Table 14- Surface energy components for tested liquids

	Y_l^{Tot} (mJ.m^{-2})	Y_l^{lw} (mJ.m^{-2})	Y_l^{+} (mJ.m^{-2})	Y_l^{-} (mJ.m^{-2})
Water	72.8	21.8	25.5	25.5
Formamide	44.4	44.4	0	0
α-Bromonaphtalene	58	39	2.28	39.6

2.3. Preliminary antibacterial evaluation

A preliminary evaluation of the antibacterial activity, against clinical isolated *S. epidermidis* (IE 186), and *S. aureus* (ATCC 6538) strains, was performed in Centro de Engenharia Biológica at

Universidade do Minho, through halo inhibition zone tests, which is a rapid and simple qualitative technique for evaluation of antibacterial activity. In this methodology the size of the growth inhibition halo around the sample is measured. A colony of each species was taken from a fresh solid bacteria culture medium (Tryptic Soy Agar, TSA, Merck) and was added to 20 ml of Tryptic Soy Broth (TSB, Merck). Then the resultant suspension was incubated overnight, at 37 °C and 120 rpm. A volume of 1 ml of $1*10^7$ CFU.ml^{-1} cell suspension was added to 14 ml of TSA (at 45 °C) and placed onto each petri plate. Then, square samples of stainless steel 316L coated with silver and silver oxide were placed in the plates and incubated for 24 h at 37°C. All experiments were run in triplicate per sample (technical replicates), on three independent assays (biological replicates), for each bacterium. The halo, corresponding to the zone of bacterial growth inhibition, formed around the sample (Figure 33) was measured.

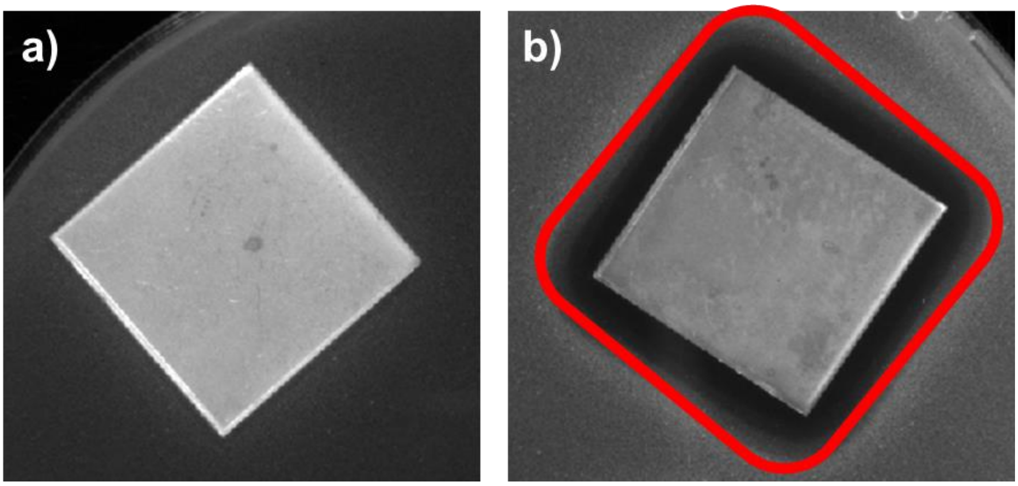

Figure 33- Example of a sample without halo (a)) and a sample with halo (b)).

3. Results and Discussion

3.1. Characterization of silver and silver oxide coatings

The coating´s deposition conditions and the oxygen fraction in the discharge (fO_2) and input oxygen partial pressure $pO_{2,in}$) are summarized in Table 15. The pure Ag coating was labelled as Ag while the Ag coating deposited in reactive sputtering mode was labelled as Ag_xO.

Table 15- Conditions of coating's depositions and thickness

Coating	Ar Flow (sccm)	O_2 Flow (sccm)	$fO_2=\frac{\Phi_{O2}}{\Phi_{Ar}+\Phi_{O2}}$	$p_{O2,\ in}$ (10^{-1} Pa)	J_{Ag} (mA.cm-^{2})	Time (s)	Thickness (nm ± S.D.)	Deposition Rate (nm.h^{-1})
Ag	60	0	-	-	2.5	300	55 ± 5	660
Ag_xO	60	15	0.2	33.3	1	3600	66 ± 2	66

The Ag coating was deposited with 0 sccm of O_2, in order to obtain a pure Ag coating, while for the silver oxide coating the oxygen flow was selected in order to perform a deposition in reactive mode, corresponding to 15 sccm of O_2. In Figure 34 it is possible to observe the variation of Ag target voltage (already present in section 2.1.) and total pressure in deposition chamber.

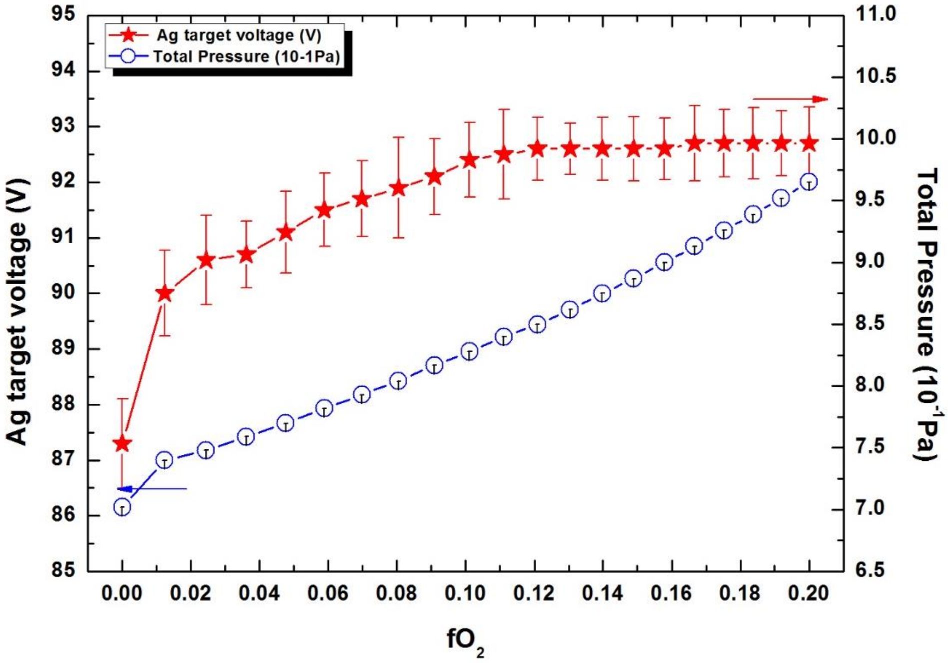

Figure 34- Variation of Ag target voltage and total pressure in deposition chamber for different fO_2 (at a constant JAg of 1 $mA.cm^{-2}$).

During reactive sputtering, a reactive gas was introduced to the discharge in order to deposit a compound material. For low reactive gas flows, all the gas atoms will react with the metal ejected from the target surface and no changes are observed either in the target voltage or in the reactive gas partial pressure, which corresponds to the deposition of compound materials in metallic mode. However, as the reactive gas flow is further increased, the reactive gas is not totally consumed by the growing thin film, which results in an increase in the gas partial pressure and also leads to the formation of a compound in the target surface. The variations in target surface condition are generally associated with a variation in effective secondary electron emission yield (SEEY), which for a constant current density, results in a significant variation on the target voltage [135]. The results presented in Figure 34 suggest that both target voltage and total pressure in deposition chamber increase at a higher rate when an oxygen flow of 1 sccm ($fO_2 \approx 0.02$) is introduced; afterwards the pressure increases linearly, while the target voltage increases up to 8 sccm ($fO_2 \approx 0.12$) showing almost constant value after this O_2 flow. It should be pointed out that the pressure inside the chamber varies from $7.4x10^{-1}$ Pa to $9.6x10^{-1}$ Pa with the introduction of oxygen, while the variations in Ag target voltage are small (varying from 87.3 V to 90 V with the introduction of 1 sccm of O_2 and up to 92.7 V for 15 sccm), which could turns the identification of reactive mode inaccurate. These small variations in Ag target surface condition were somehow expectable, since Depla *et al.* [136] reported previously that the presence of silver oxide in the target surface leads to an increase in the discharge voltage, still, the variation in relation to pure Ag is quite small, due to the low relative change of the effective emission coefficient by oxidation of Ag target. However, the variations of the target voltage combined with the observations in total chamber pressure allowed to predict that above 8 sccm of O_2 flow the deposition should be in reactive mode. The deposition rate of the thin films was calculated from the ratio of thickness (estimated by SEM) with the duration of deposition. Ag coating, deposited with 0 sccm of oxygen flow presented a higher deposition rate (0.66 $\mu m.h^{-1}$) in relation to the Ag_xO coating (0.06 $\mu m.h^{-1}$), deposited with an oxygen flow of 15 sccm. This reduction in coatings deposition rate might be related to the lower current density applied to the Ag target combined with the presence of oxygen, which forms Ag_xO on target´s surface, promoting a lower sputtering yield in relation to pure Ag [137].

The deposition time was adjusted in order to obtain a silver and silver oxide films with similar thickness (55 ± 5 nm for Ag coating and 66 ± 2 nm for Ag_xO coating – measured by SEM images). XPS analysis was carried out in order to evaluate the coatings chemical binding state. The results are shown in Figure 35 where the Ag3d and O1s (inset) spectra of Ag and Ag_xO thin films are depicted.

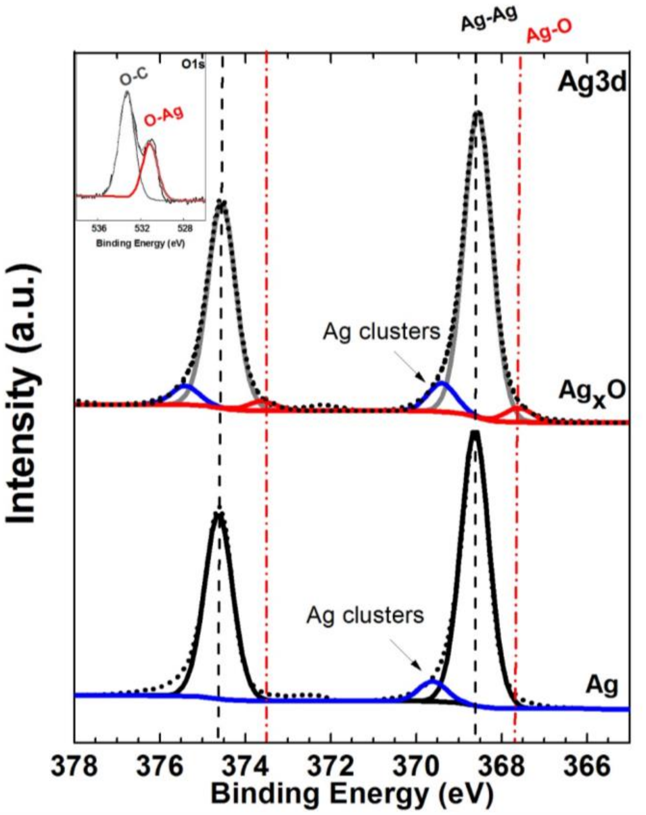

Figure 35 – XPS spectra of Ag3d core levels of Ag-300 and Ag_xO thin films and O1s spectra of Ag_xO thin film (inset).

The XPS spectra of Ag thin film suggested the presence of a doublet with the Ag 3d5/2 peak at 368.6 eV, which is reported to correspond to Ag-Ag bond, thus suggesting that Ag coating is in metallic state [138–140]. No evidence of Ag-O bonds is visible which was somehow expectable due to the low reactivity of silver with oxygen. Regarding the Ag_xO thin film the Ag3d spectra clearly revealed the presence of three distinct bonds: Ag-Ag, Ag clusters and Ag-O, being the third one located at 367.7 eV [141]. The XPS spectra of Ag_xO clearly show that Ag is the main phase and only a small contribution of both Ag clusters and Ag-O bonds are visible. The presence of Ag-O bond was also visible in the O1s spectra, with a peak at 531.0 (see inset in Figure 35), which revealed the presence of Ag-O [142] bond and C-O bond, which is found at higher binding energies, being the later associated with surface contamination. The surface contamination inevitably occurs when the material surface is exposed to atmospheric conditions, being very easily detected in XPS since the depth of analysis is of few nanometers. In fact, the presence of surface contamination turns the chemical composition analysis inaccurate; still, the results obtained by XPS revealed that the Ag_xO coating shows an Ag/O atomic ratio of 2.3, a value that could be overestimated, since the detected oxygen is a sum of the oxygen present in the coating combined with the oxygen coming from surface contamination. This excess of silver is concordant with XPS results, once the content of metallic silver is higher than silver oxide component.

XRD analysis was performed in order to obtain further information about the coatings structure. The XRD diffraction patterns of Ag and Ag_xO coatings are presented in Figure 36 , where the main identified crystalline phases are depicted, namely Ag (ICDD card no 00-004-0783), AgO (ICDD card no 00-043-1038) and Ag_2O (ICDD 00-065-6811).

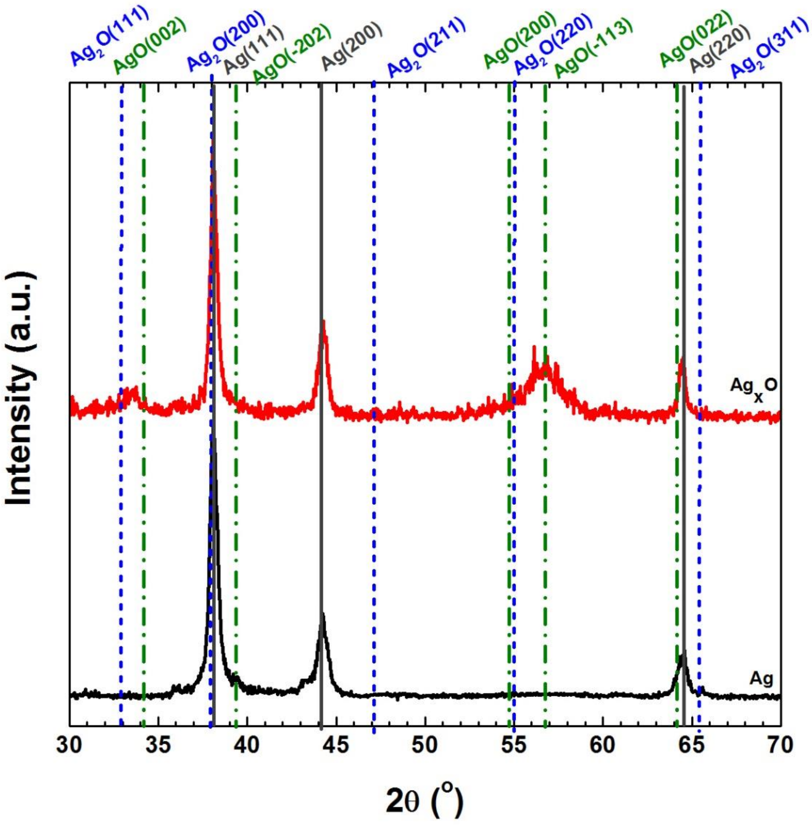

Figure 36-XRD patterns of Ag-300 and Ag$_x$O coatings.

The XRD pattern of Ag coating reveals that the coating crystallizes in a FCC-Ag crystal structure. According to the calculation obtained by the Scherrer method, for (111) peak, the grain size for Ag is about 40 nm. Regarding the Ag$_x$O thin film the presence of crystalline Ag phase is evident, however a second phase can also be detected, which can correspond to AgO or Ag$_2$O. The results obtained in XRD analysis are in good agreement with the XPS analysis, being clear in both techniques that the Ag$_x$O coating contains a phase mixture of Ag+Ag$_2$O or Ag+AgO. Moreover, the Ag/O atomic ratio obtained by XPS was above 2, which means that the amount of oxygen incorporated in the coating is not enough to obtain single phased Ag$_2$O or AgO thin films. Pierson *et al.* [87] have previously reported the formation of Ag and Ag$_2$O phases during reactive sputtering of silver in oxygen atmosphere. However, the presence of bi-phase coatings was only observed for low oxygen flows, being found that at higher oxygen flows the coatings are composed of a silver oxide single phase, being the Ag$_2$O the most common one due to the lower Gibbs free energy associated with its formation. In the present report the bi-phase coatings were obtained even in deposition in reactive mode, with high oxygen flows.

The coatings morphology was evaluated through SEM analysis. The SEM top-view micrographs (recorded in backscattered electron mode) of Ag and Ag$_x$O coatings are presented in Figure 37 (a) and (b), respectively. A more detailed view of Ag and Ag_xO thin films is shown in Figure 37 (c) and (d), respectively.

.

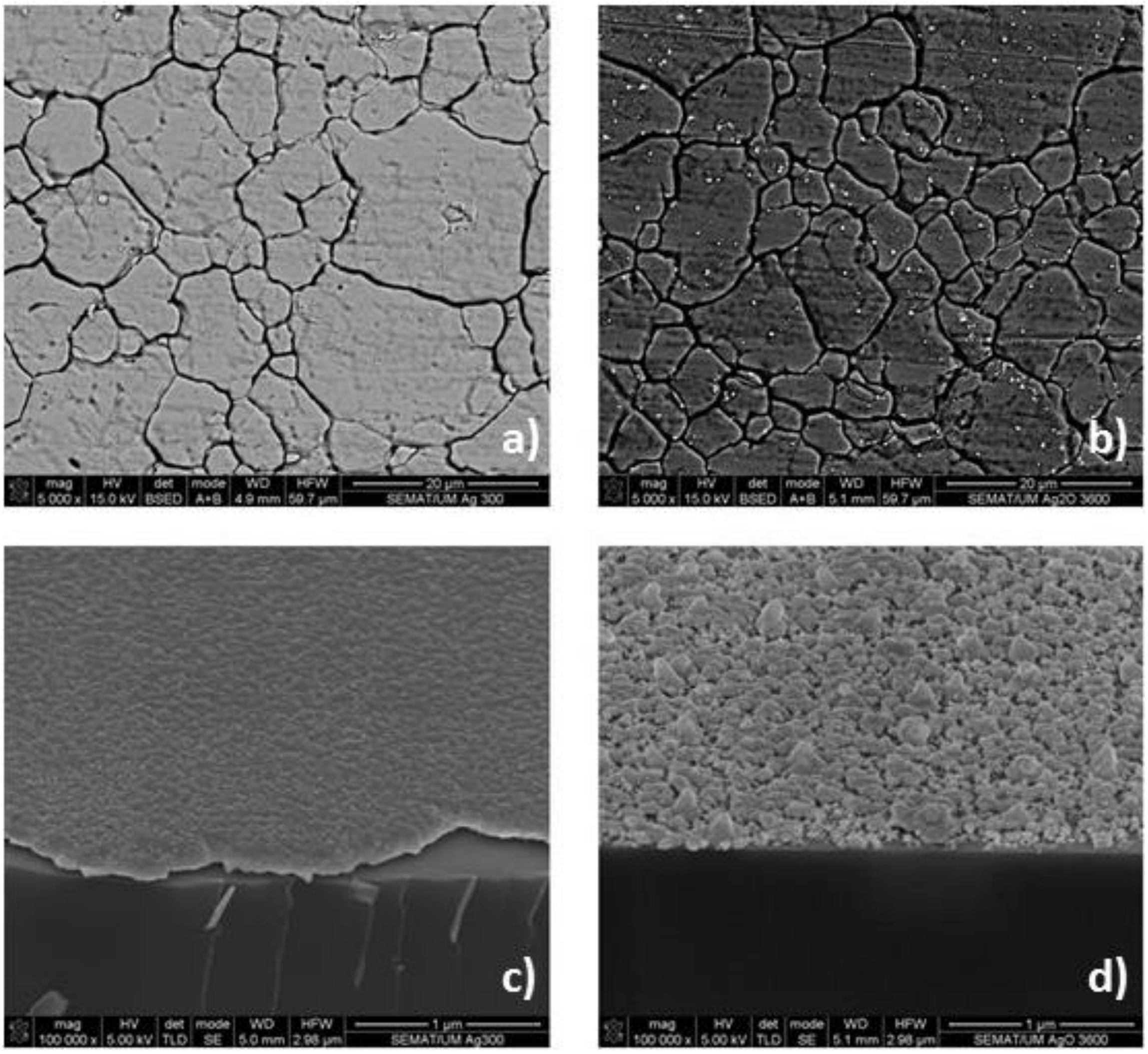

Figure 37 - SEM top-view micrographs (recorded in BES mode at 5kX) of a) Ag and b) Ag_xO thin films and detailed view of c) Ag and d) Ag_xO thin film morphology (recorded in SE mode at 100kX).

The SEM micrographs of both Ag and Ag_xO thin films recorded at low magnification suggest the presence of compact coatings surrounded by well-defined interface regions, which correspond to the intergranular regions of SS316L substrate. The SEM micrograph of Ag_xO thin film (see Figure 37 b)) suggests the presence of some circular features which appear brighter in the BSE micrograph, thus suggesting some mass contrast in relation to the matrix coating. These features might correspond to Ag agglomerates (showing sizes of several hundred nm) which should appear brighter in the BSE images, due to their higher mass in relation to the silver oxide phase, a result which is well correlated with the trends observed in XPS and XRD analysis which also suggests that

Ag_xO coatings are composed of two distinct phases: Ag + silver oxide. A more detailed view of Ag_xO thin film (see Figure 37 d)) indicates that the thin film is not continuous being composed by islands with hundreds of nanometers in size, surrounded by smaller islands with tens of nanometers. The thickness and deposition rate of Ag_xO thin film reported in Table 15 refer to the smaller islands. Conversely, the Ag thin film forms a continuous coating (see Figure 37 c)). Several mechanisms have been pointed out to explain the thin films growth from vapor phase, namely: (i) island (or Volmer-Weber), (ii) layer (or Frank –Van der Merwe), and (iii) Stranski-Krastanov, being the occurrence of each mechanism dependent on the interaction between the adatoms and the substrate. The occurrence of island growth mechanism observed in Ag_xO thin film occurs when the atoms or molecules in the deposit are more strongly bounded to each other than to the substrate, which promotes the clustering of metal atoms. As the amount of deposited metal is increased, the number of stable nuclei will grow up to a maximum and aftermost diminish due to coalescence phenomena, which eventually will lead to the formation of a continuous coating as observed in Ag thin film (see Figure 37 c)). Another interesting feature observed in Ag_xO thin film is the bimodal size distribution, being clearly found that the surface is covered by bigger islands with hundreds of nanometers surrounded by smaller islands with tens of nanometers. This bimodal size distribution suggests the presence of two different phases with different coalescence and growth rates. The bigger Ag islands with hundreds of nanometers should correspond to Ag, considering the results shown in Figure 37 b), still it is difficult to unequivocally identify to which phases the bigger and smaller islands correspond.

The surface characteristics such as interaction with water and surface free energy play a major role in biomedical devices, since numerous physiological events are determined by these surface properties. According to the van Oss approach the hydrophobicity of a material is defined by the variation of the free energy of interaction (ΔG) between the material's surface (Δm) immersed in water (w), ΔG_{mwm}. When this variation is negative, there is a greater interaction between material's molecules than with water, which leads to a hydrophobic surface. On the other hand when ΔG_{mwm} is positive the material's surface is hydrophilic [57]. In addition the water contact angle also allows the evaluation of the surface hydrophobic or hydrophilic character, since higher contact angles (above 90°[57] or 65^0 defended for some authors [143]) reveal the presence of hydrophobic surfaces, while lower water contact angles imply a more hydrophilic surface [57].

The hydrophobicity of a surface plays an important role in microorganism's adhesion since a higher density of apolar areas in material's surface promote an attachment of microorganism via the hydrophobic effect, due to the increment of hydrophobic interactions [144].

The contact angles, surface energy parameters and the degree of hydrophobicity of Ag and Ag_xO thin films are presented in Table 16.

Table 16- Water (θ_w), formamide (θ_F) and α-bromonaphtalene ($\theta_{\alpha\text{-}B}$) contact angles, surface energy components (apolar Lifshitz-van der Waals surface free energy component, Υ^{lw} ; electron acceptor surface free energy component, Υ^{+}; electron donor surface free energy Υ^{-}; and hydrophobicity (ΔG_{mwm}) of SS316L, silver and silver oxide coatings

Sample	Contact angle ±S.D.(°)			Surface energy components (mJ m^{-2})			ΔG_{mwm} (mJ m^{-2})
	θ_w	θ_F	$\theta_{\alpha\text{-}B}$	Υ^{lw}	Υ^{+}	Υ^{-}	
Ag-300	103±2	86±8	43±3	33	0	2	-79±9
Ag_xO	103±3	89±6	48±1	31	0	3	-72±10

The water contact angles obtained for Ag and Ag_xO samples revealed a value higher than 90°, thus indicating that all surfaces are hydrophobic, which is also confirmed by the negative ΔG_{mwm} values [57]. Moreover, the θ_w values are statistically similar (t-test, $p>0.05$) for all surfaces and no great variations in ΔG_{mwm} are observed, thus suggesting a very similar hydrophobic character for all surfaces. Additionally, coatings present a monopolar surface ($\Upsilon^{+}=0$ and $\Upsilon^{-}=2$ and $\Upsilon^{-}=3$ for Ag and Ag_xO, respectively).

The coatings' wettability is dependent on the incorporation of oxygen and films morphology [145]. Silver has been reported as present an hydrophobic behavior [59,146]. The incorporation of oxygen could lead to a decrease in the contact angle, which is not verified, probably, due to the difference morphologies presented by silver and silver oxide coatings [145,147].

3.2. Preliminary antibacterial evaluation: Halo Test

Halo inhibition zone tests were performed in order to assess the coatings antibacterial efficiency against *S. epidermidis* and *S. aureus.* The results obtained for three tested coatings against these two types of bacteria are presented in Figure 38.

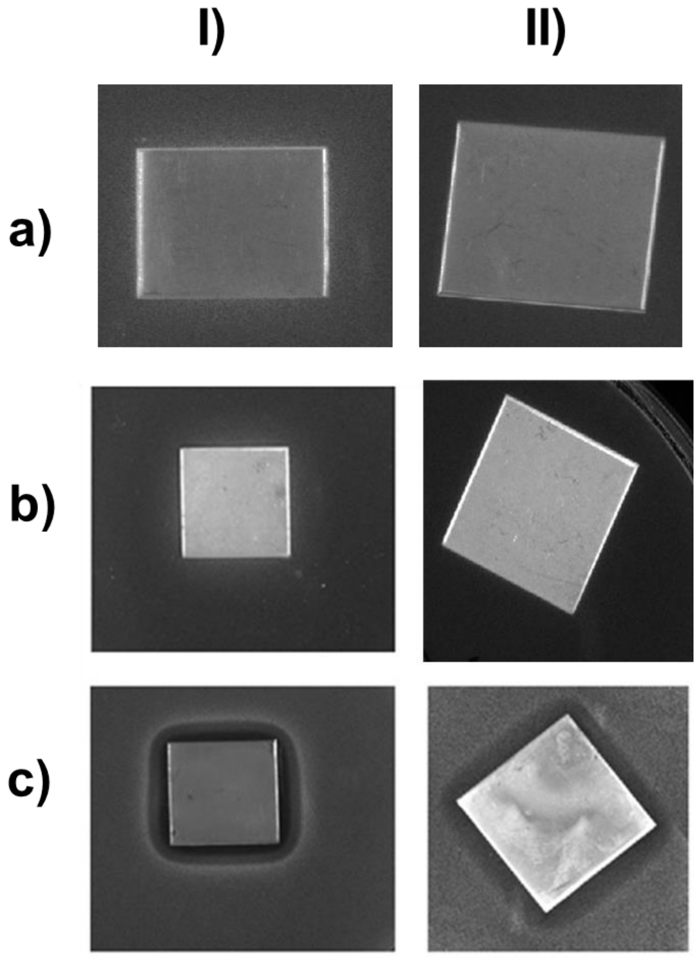

Figure 38 - Results of antibacterial tests for SS316L (a)), Ag(b)) and Ag_xO (c)) regarding *Staphylococcus epidermidis* (I)) and *Staphylococcus aureus* (II)).

Concerning the antibacterial tests, the results were similar for both bacteria. In Figure 38 a) and b) it is possible to observe that the bacteria grew all around the uncoated SS316L and Ag coating (no inhibition halo formation was observed). Nonetheless, coating Ag_xO (Figure 38 c)) presented halo around the sample, which means that there is an inhibition zone of bacteria growth. However, for *S. epidermidis* (Figure 38 c) I)) the halo presented for these samples is completely clear in the zone nearby the sample and became less clear when it moves away, which suggest that there is a zone of non-growth of bacteria (clear halo) and a zone of inhibition of bacteria growth (diffuse halo), which may be due to the silver released to the agar medium. For *S. aureus* there is not visible a clear halo, which indicates that there is a zone of inhibition of bacteria growth but there is not a complete death of bacteria. Similar results, where *S. epidermidis* presented more sensibility to silver than *S. aureus* has been previously reported [148–150]. Silver sensitivity of microorganisms depends on species- or even strain-specific mechanisms reflecting differences in metabolizing silver or repairing silver-related cell damages [149].

The contact angle measurements suggested that Ag and Ag$_x$O coated SS316L present very similar surface characteristics (surface energy parameters and the degree of hydrophobicity), in this sense, the differences in biological properties cannot be attributed to any changes in surface properties. Therefore, the different behaviors can only be attributed to the Ag antibacterial activity, which seems to be different in Ag and Ag$_x$O thin films. Recently, proteomic analysis revealed that even a short exposure of silver nanoparticles to bacterium cells resulted in alterations in the expression of a panel of envelope and heat shock proteins. Ag nanoparticles can penetrate and disrupt the membranes of bacteria, providing a loss of intracellular potassium. Furthermore, Ag nanoparticles decreased the ATP levels, which culminates with the death of bacteria [151,152]. Similar results can be observed with silver ions. Although pure metallic silver is stable in usual conditions and, consequently, has low solubility in water [125], when in contact with bacteria, some chemical compounds, that facilitate the release of Ag$^+$ ions, are formed and, therefore, increase the antibacterial activity [153,154]. Ag$^+$ ions penetrate the bacteria cell wall and bind to phospholipid layer of the cytoplasmic membrane and to bacteria DNA disrupting its replication [155]. Regarding the antibacterial results, it is clear that there is antibacterial activity only in Ag$_x$O sample. So, these results suggest that the form of silver (NP's; clusters; islands or continuous films) could have influence on the antibacterial efficacy; in addition, the presence of silver oxide matrix could promote the release of silver. In Figure 39 a possible mechanism of Ag dissolution when in contact with bacteria is represented, for both studied coatings: Ag$_x$O (which surface is composed of islands combined with smaller Ag particles) and Ag (which form a continuous thin film).

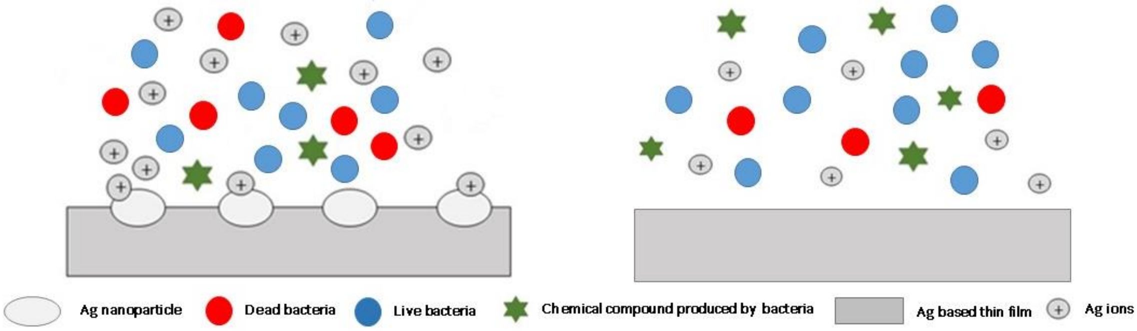

Figure 39-Schematic illustrations of possible mechanisms of Ag dissolution, with and without Ag nanoparticles, when in contact with bacteria (adapted from [154]).

Althgouth the mechanism of silver release from metallic surfaces is poorly understood [156], the silver form plays an extremely important role in antimicrobial behavior of silver based surfaces. In fact, the Ag thin film which formed a continuous layer based on crystalline Ag phase did not show any evidence of antibacterial activity, conversely the Ag_xO thin film which is composed of islands and small Ag particles, being mainly composed by a mixture of Ag and silver oxide crystalline phases, showed indication of antibacterial activity. As previously mentioned,the activity of nanosilver is predominantly associated with the presence of Ag^+ ions and also to small Ag nanoparticles, which tend to be more easily ionized [157], being also claimed that they are able to directly interact with bacteria promoting their destruction. The presence of silver clusters and silver agglomerates in Ag_xO sample (see Figure 37 d) results in a higher exposed surface area when compared with continuous Ag layer, consequently, a higher release of Ag^+ ions could be expected when the surface is exposed to the TSA and bateria medium.

4. Partial Conclusion

Silver and silver oxide thin films were deposited by non-reactive (for Ag thin film) and reactive (for Ag_xO thin film) pulsed dc magnetron sputtering in order to assess the coatings antibacterial activity against *S. epidermidis* and *S. aureus*, two of the most common bacteria associated with nosocomial infections found in cardiovascular stents. The structural and morphological characterizations revealed that Ag thin film forms a continuous layer, while the incorporation of oxygen in the deposition atmosphere lead to the formation of a thin film composed by a mixture of two crystalline phases: Ag and silver oxide. The latter thin film was characterized by the presence of islands with several hundreds of nanometers surrounded by smaller particles with tens of nanometers. The halo inhibition zone tests revealed the antibacterial behavior of Ag_xO thin films against both of the tested bacteria; conversely no antibacterial effect was found in Ag thin film, as summarize in Figure 40.

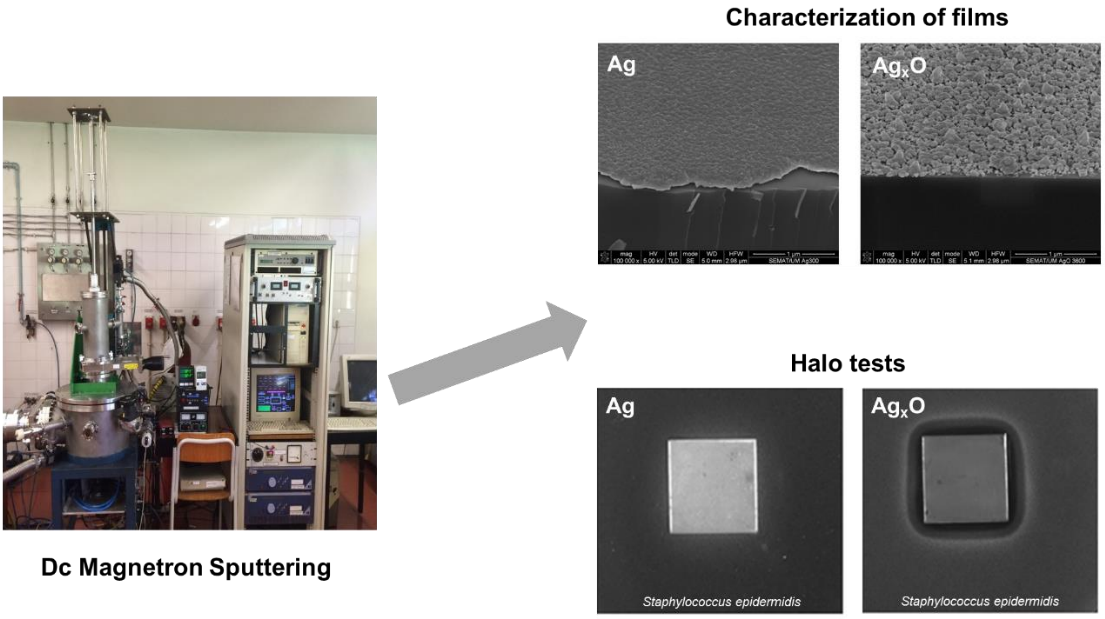
Characterization of films
Ag
Ag_xO
Halo tests
Ag
Ag_xO
Staphylococcus epidermidis
Staphylococcus epidermidis
Dc Magnetron Sputtering

Figure 40- Summary of production and characterization of developed silver and silver oxide thin films.

The differences between these two coatings might be related not only to the presence of silver oxide phase, but also to the differences found in coatings growth mode; with Ag coatings forming a continuous layer and Ag_xO forming islands surrounded by smaller nanoparticles. These differences might lead to better interaction between the thin film surface and bacteria, due to the higher surface to volume ratio, which can increase the Ag ionization rate or the direct interaction between Ag and bacteria. The obtained results suggest that Ag_xO coating, deposited by reactive dc magnetron sputtering, present antibacterial properties for both bacteria used and it has great potential to be applied in cardiovascular stents. However, it is still unclear if the chemical composition was responsible for the antibacterial activity or it was only the morphology on islands that promotes an antibacterial action. Thus, in order to evaluate, more accurately, what is in fact controlling the antibacterial efficacy of Ag_xO, a detailed study about Ag_xO thin films is necessary. Next chapter will be focus on the influence of the introduction of the oxygen on silver coatings on the structural and consequent antibacterial activity.

CHAPTER IV

Influence of Oxygen Content on the Antibacterial Coatings

This chapter is based on the publication:

R. Rebelo, S. Calderon, R. Fangueiro, M. Henriques, and S. Carvalho, “Influence of oxygen content on the antibacterial effect of Ag-O coatings deposited by magnetron sputtering,” Surf. Coatings Technol., vol. 305, pp. 1–10, 2016.

1. Introduction

Taking in account the results obtained for silver oxide coatings and keeping in mind that silver oxides systems have not been well studied, since silver is, generally, consider as a non-reactive material [86], it was important to study the influence of the oxygen content.

Regarding silver oxide synthesis, the most popular method is evaporation of metallic silver following by an oxidation, in a reactive environment (normally, a reactive plasma excited by dc magnetron or microwave), or sputtering [86]. Nevertheless, only few reports of the application of magnetron sputtering in the formation of silver oxides, and consequently combination of the advantages of magnetron sputtering technique and reactive processes [73], especially the controlling in the reactive gas and, consequently, film's composition, have been published. The formation of these oxides in form of thin films, depends on the availability of oxygen in the deposition chamber and the energy required for the oxidation, i.e., growth conditions/reaction kinetics [158]. The synthesis of metal oxide films, by reactive magnetron sputtering, can be achieve by two distinct mechanisms: i) sputtering of the material from the target and its condensation on the substrate or ii) chemical reaction between the condensing material and reactive gas species. In the second mechanism, the target is sputtered in metallic mode, an higher yiel is promoted and an higher deposition rate is achieved [127].

Barik *et al.* [159], for instance, studied silver oxides prepared by reactive dc magnetron sputtering, operating in constant power mode at 25 W observing that at oxygen flow of 1.71 sccm and 2.01 sccm a stoichiometric Ag_2O (FCC) was formed. Additionally, Raju *et al.* [158] also evaluated the influence of oxygen partial pressure changes during films growth, by pulsed laser deposition (PLD), revealing that with the increase of the oxygen pressure from 9 to 50 Pa, in the deposition chamber, an Ag_2O phase transforms into AgO. In their study, only oxygen pressure was varied, maintained the others growth parameters constant: temperature (300K), fluence (1.006 $J.cm^{-2}$), substrate-target distance (3 cm) and deposition time (90 min). For an oxygen pressure of 9 Pa, a pure Ag_2O hexagonal crystal system was formed. As chamber pressure increases, an AgO monoclinic crystal system began to appear. For 10 Pa it was observed a mixture of AgO and Ag_2O and for pressures higher than 20 Pa only AgO was formed. Dellasega *et al.* [160] obtained pure AgO (at higher fluence: 1.6 $J.cm^{-2}$) and conclude the threshold pressure to obtain AgO was 4 Pa. Furthermore, Kumar *et al.* [88] deposited AgO thin films by RF reactive magnetron sputtering, with a sputtering power of 50W, at room temperature, with oxygen flow rates from 10 sccm to 30 sccm. The results showed an uniform and stoichiometric AgO (monoclinic crystal system), oriented along the (-111). Silver oxide coatings can be an advantage in antibacterial properties of coatings, once, as previously refered, despite silver being a well-known antimicrobial agent, and having a broad-spectrum of activity, its mechanism of action is not fully understood [72,73]. However, it is suggested that the antimicrobial behavior of silver can be achieved by: i) the release of Ag^+ ions, ii) the interaction of bacteria with silver nanoparticles and iii) the formation of reactive oxygen species (ROS) [53,57,61,74].

ROS can be generated inside or outside the cell and are byproducts of respiring organisms' metabolism. Induction of ROS formation leads to the synthesis of highly reactive radicals that can cause the mitochondrial damage of the microorganism, accelerating the cell death or dysfunction. It is reported that silver can generates ROS, potentially including superoxide ($O_2^{\cdot -}$), hydroxyl radicals ($^{\cdot}OH_{\cdot}$), singlet oxygen ($^1O_2$) and the most stable ROS (H_2O_2) [85].

Hence, it should be also possible to improve silver antibacterial characteristics by forming reactive oxygen species, which leads to a most effective antibacterial behavior of silver, due to the toxic character of these species to bacterial cells, as demonstrated by Ferreri *et al.* [72] that used oxidized nano-silver to achieve antibacterial behavior.

Thus, it is important to evaluate the influence of oxygen content on the functional properties of the films, namely the antibacterial effect. As a result, the main objective of this part of the work is to produce and characterize silver and silver oxides thin films, by reactive magnetron sputtering, with the main aim of designing a coating that provide antibacterial properties to medical devices such as cardiovascular stents. The oxygen flow variation, during the coatings deposition process, was studied, in order to understand the influence of the oxygen content on the physical, chemical and structural properties of coatings and its effect on the antibacterial activity against *S. epidermidis*, since this bacterium showed more sensitivity to silver oxide antibacterial properties.

2. Materials and Methods

2.1. Production of silver and silver oxide coatings

Ag and Ag_xO coatings were deposited onto stainless steel 316L and silicon substrates by reactive pulsed dc magnetron sputtering. In order to remove impurities and minimize contamination,

substrates were ultrasonically cleaned with distillate water, ethanol and acetone, during 10 minutes in each solution, before deposition. Additionally, similar to previously depositions, the substrates and the silver target (200 x 100 mm^2) were cleaned by an argon plasma etching process prior to each deposition. The etching process was performed in an argon atmosphere (80 sccm), using a pulsed dc power supply at 0.4 A, 1536 ns of reverse time and 200 kHz applied to the substrate holder and a dc power supply, with a current density of 0.5 mA cm^{-2}, applied to the Ag target.
During the deposition process, the sputtering atmosphere consisted of a constant argon flow (**Φ**Ar = 60 sccm) and an O_2 flow (**Φ**O2) that varied from 0 scmm to 15 sccm, (increasing 1.5 sccm per deposition), corresponding to a variation in the fraction of oxygen in the discharge [127] (fO_2 = **Φ**O_2 /(**Φ**O_2 + **Φ**Ar) from 0 to 0.2). Total pressure inside the chamber varied from $5.8x10^{-1}$ Pa until $7.8x10^{-1}$ Pa, with the increase of the O_2 flow. A pulsed dc power supply was connected to the silver target, applying a current density of 1 $mA.cm^{-2}$, and the reverse time and the frequency were kept at 1536 ns and 200 kHz, respectively. The samples were placed in a substrate holder, located 70 mm away from the target and rotating at a constant velocity of 7 rpm. The deposition time (8 h) was maintained constant for all the coatings. Deposition process was performed at room temperature. Silver oxide coatings deposited in reactive sputtering mode were labelled as AgO following by the percentage of O_2 flow used in the deposition, while silver coating was labelled as Ag. Thus, AgO10 corresponds to a deposition with 10% of the total O_2 flow (corresponding to 1.5 sccm) AgO20 corresponds to a deposition with 20% of the total O_2 flow (corresponding to 3 sccm), etc.

2.2. Characterization of silver and silver oxide coatings

Regarding coatings' characterization, and similar to section 2.2. of Chapter III, XPS analysis was performed on coated silicon, in order to obtain information about binding state of the samples. However, it should be pointed out that no previous sputter cleaning was performed before the XPS analysis in order to avoid the preferential sputtering of oxygen. The morphology and thickness of the coatings deposited on silicon, were evaluated by SEM in a NanoSEM – FEI nova200 equipment, being analyze three different regions, but only present a representative micrograph. EDS was performed for the detection of coatings bulk composition, with an energy of interaction between electron beam and material of 10 keV. Despite the use of EDS for chemical composition, it is widely known that the quantification of oxygen is not always accurate with EDS and the thickness of samples is to low, once the interaction of electron beam and the sample can be 1 micrometer. However, a correlation between all the results from XRD, XPS and EDS is made, in order to elucidate the type of oxide present in the samples. Thus, the procedure followed to obtain accurate composition should be interpreted as the combination of the techniques, where the XRD shows the crystalline phases, the XPS the bonding states of the elements and the EDS a ratio between the content of O and Ag. EDS measurements were performed at SEMAT-UM (Serviço de Caracterização de Materiais at Universidade do Minho).

Structure and phase distribution of coatings was assessed by XRD analysis in a PANalytical X'Pert PRO MPD system, using CuKα (λ=0.154056nm), as previously described in section 2.2 of Chapter III.

Contact angle measurements were performed with the view to investigate the samples hydrophobic behavior, using the van Oss approach, in 8 measurements of each coating, through the sessile drop contact angle technique, using an automated contact angle measurement apparatus (OCA 15 Plus; Dataphysics, Germany). For this purpose, water, formamide and α- bromonaphtalene were used, as already described in section 2.2 of Chapter III. For statistical analysis, one- way ANOVA analysis was used, by applying Tukey multiple comparisons test, using GraphPad Prism 6 software. All tests were performed with a confidence level of 95%.

2.3. Preliminary antibacterial evaluation

Halo inhibition zone tests, against *S. epidermidis* (IE 186), were performed in order to evaluate, as a qualitative measure, antibacterial activity. The conditions of the tests were described in section 2.2 of Chapter III. All the assays were run in triplicate.

Furthermore, ICP-OES (inductively coupled plasma optical emission spectrometry) was performed in order to quantify the silver ion release from coatings. With that intuit, coated SS316L were placed in a falcon with 50 mL of 0.95 (w/v) NaCl and incubated at 37 ^{o}C, for 24 h. After that, 2 mL of this solution was taken and diluted in 4 mL of 5% (w/v) HNO_3, once this acid could lead to the formation of $AgNO_3$ and the production of more Ag ions. Previously, a calibration curve was prepared, using silver standard solution for ICP. The release of Ag ions was measure using a PERKINELMER, ICP-OES OPTIMA 8000, with a 6106PE POLYSCIENCE refrigerator and a S10 PERKINELMER automatic sampler. All the tests were run in triplicate and performed at Centro de Engenharia Biológica at Universidade do Minho.

3. Results and Discussion

3.1. Characterization of silver and silver oxide coatings

The variation of Ag target voltage and pressure in deposition chamber according with the fraction of oxygen is presented in Figure 41. It reveals that the target voltage increases up, with a tendency to stabilize, from 86.9 V up to 92.4 V. As the fO_2 increased, an increase in the total pressure and in the silver target voltage is observed, once the reactive gas is not totally consumed during the growth of thin films, which leads to a formation of a compound (Ag-O) in the target surface, associated with a variation in effective secondary electron emission yield (SEEY), reaching a poisoned mode.

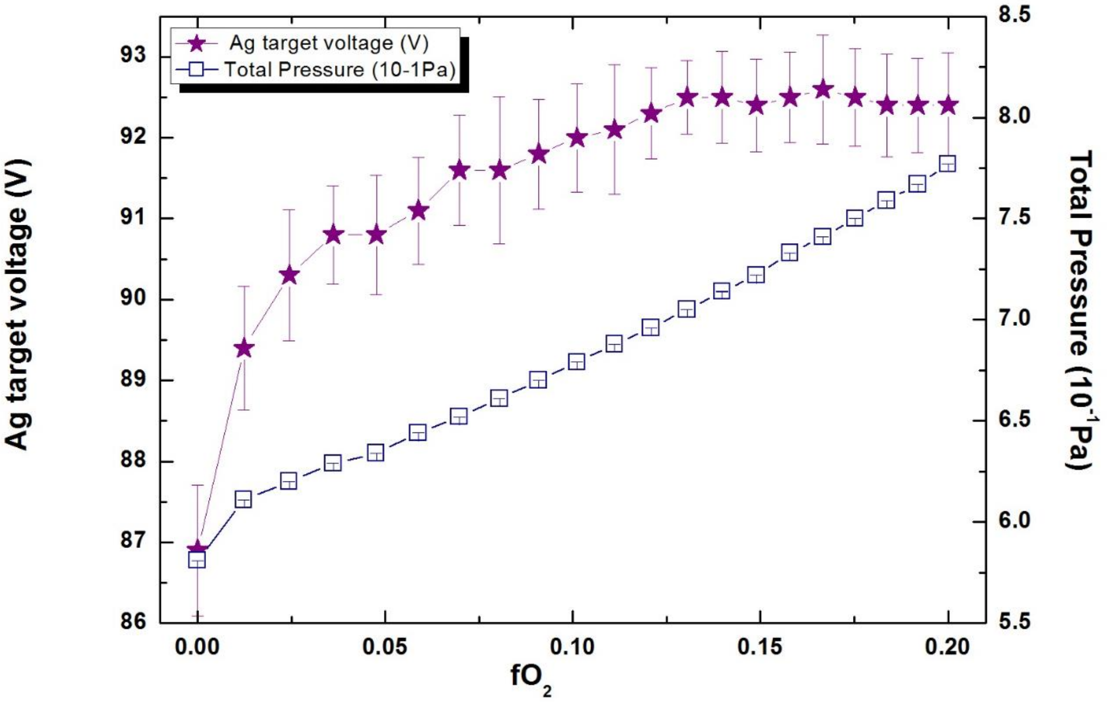

Figure 41- Variation of Ag target voltage and total pressure in deposition chamber for different oxygen fractions in the discharge.

The deposition rate of the films (see Figure 42) was calculated from the thickness (observed by SEM) and deposition time, revealing an increase for the film deposited with the lowest oxygen flow rate and continuously decreasing as oxygen is incorporated. This behavior is attributed to the introduction of oxygen, which in an initial phase, contributes along with silver films growth, leading to an increase of deposition rate with the introduction of oxygen. However, for higher amounts of oxygen, silver target is poisoned with oxygen, leading to deposition of silver oxides, and, consequently, to lower deposition rates, once silver oxides have lower sputtering yield, when compared with pure silver [137]. A closer look on the deposition rate for the Ag film on this series of samples (≅ 20 nm.h^{-1}) indicates that the deposition rate is clearly lower than the deposition rate for the Ag film, from previous series (≅ 660 nm.h^{-1}). The differences cannot be explained by the differences on the current density, which change from 1 mA.cm^{-2} to 2.5 mA.cm^{-2}. Even the target condition, cannot be claimed so different, since the target potential change from 86.9 to 250 V, somehow expected by the increase on the current density. However, it seems clear that the low deposition rate of Ag film on this section should indicate that the target current density applied can be in the limit of the plasma maintenance.

Regarding the silver oxide samples with higher content of oxygen (fO_2=0.2) in both series, differences in deposition rates can be observed. As reported by Snyders *et al.* [127] partial pressure of oxygen influences the conditions of deposition and the deposition rate, and the partial pressure of oxygen are in fact different in both series. In previous series the input oxygen partial pressure was 1.50*10^{-1} Pa while in this series was 1.60*10^{-1} Pa. This difference can leads to different conditions in the target and in the mean free path, leading to different deposition conditions and, consequently, to a different growth of the film.

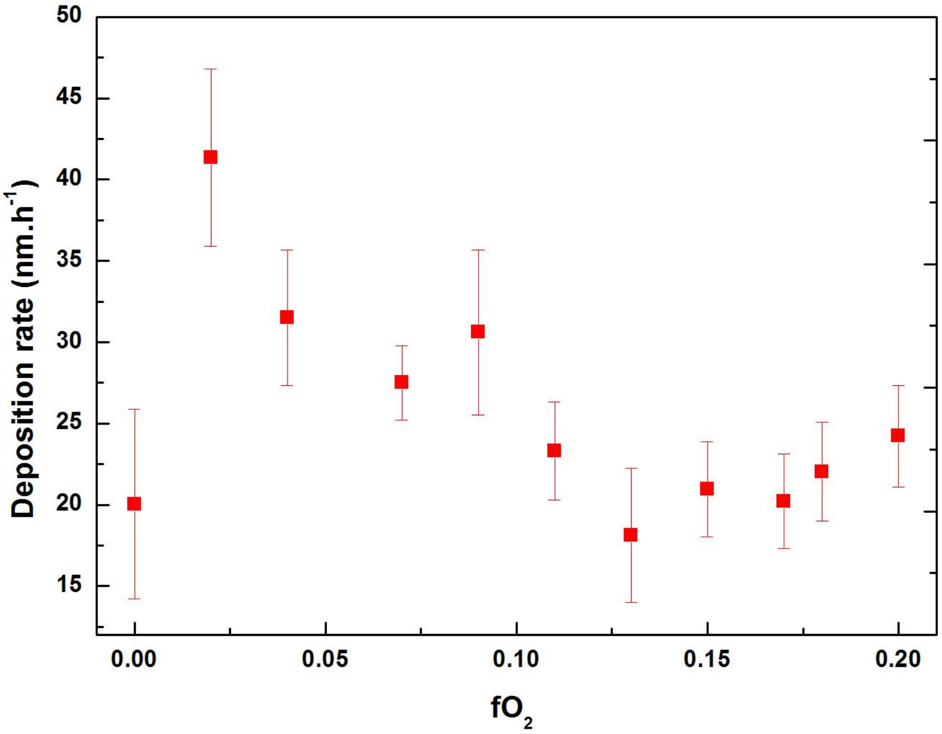

Figure 42 -Variation of deposition rate for different oxygen fractions in the discharge.

A bulk composition of the coatings was performed by EDS analysis, indicating an excess of silver for AgO10 and AgO20 coatings, while for the remaining coatings the amount of silver and oxygen are similar, suggesting an AgO composition (Figure 43 and Table 17).

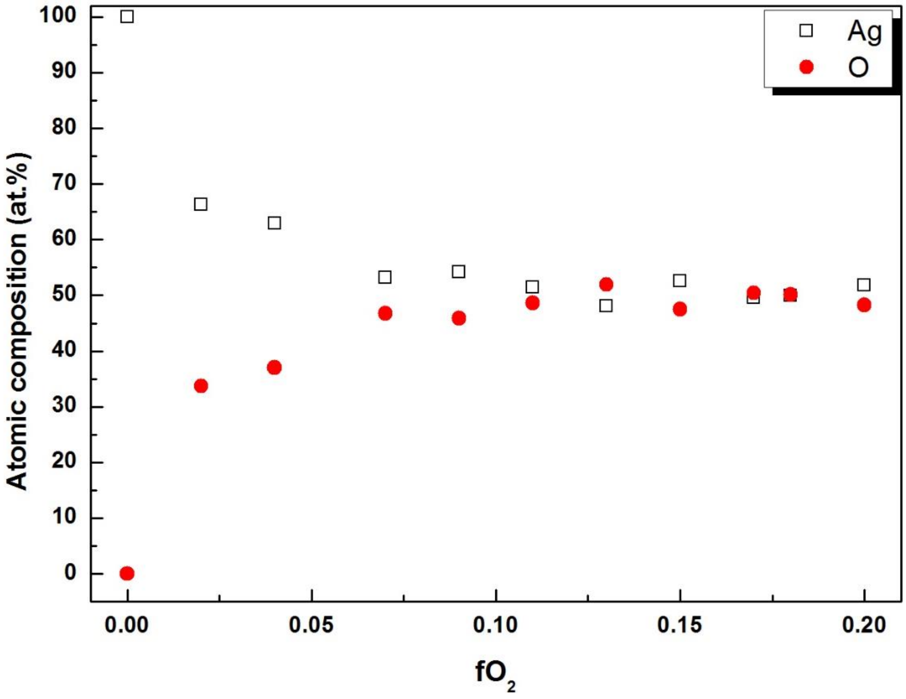

Figure 43-EDS composition for silver and silver oxide coatings

Figure 41 reveal that with the increase of the fraction of oxygen in the discharge, the pressure in the chamber increases linearly in the entire range of oxygen fraction. The increase of oxygen also leads to an increment in the Ag target voltage, but the voltage stabilizes, approximately after fO_2= 0.09. The same tendency is observed (see also Table 17) in atomic composition of the coatings, where the percentage of oxygen increases, until fO_2= 0.09, stabilizing after that.

Table 17-Thickness and of Ag/O ratio composition of silver oxide coatings

Nomenclature	**O_2 flow (%)**	**O_2 flow (sccm)**	**$p_{O2,in}$ $(10^{-1} Pa)$**	**$fO_2 = \frac{\Phi_{O2}}{\Phi_{Ar}+\Phi_{O2}}$**	**Ag/O ratio**	**Thickness (nm)**
Ag	0	0	-	-	-	160
AgO10	10	1.5	0.12	0.02	2.0	329
AgO20	20	3	0.24	0.04	1.7	253
AgO30	30	4.5	0.46	0.07	1.1	219
AgO40	40	6	0.60	0.09	1.2	242
AgO50	50	7.5	0.76	0.11	1.1	185
AgO60	60	9	0.92	0.13	0.9	146
AgO70	70	10.5	1.08	0.15	1.1	166
AgO80	80	12	1.26	0.17	1.0	163
AgO90	90	13.5	1.37	0.18	1.0	175
AgO100	100	15	1.60	0.20	1.0	195

SEM results (Figure 44) suggest the presence of a compact film in Ag coating contrary to Ag_xO coatings that present some porosity. Ag_xO coatings show a more columnar structure, compared to the pure Ag coating; however, the increase of oxygen fraction minimizes the porosity, producing more compact films and with lower column size. Comparing the silver oxide coatings with silver oxide thin film from the previous series of samples it is clear that they present different morphologies, once the two series present different deposition (in first series of samples it was 3600 s while in the second series of samples it was 28800 s).

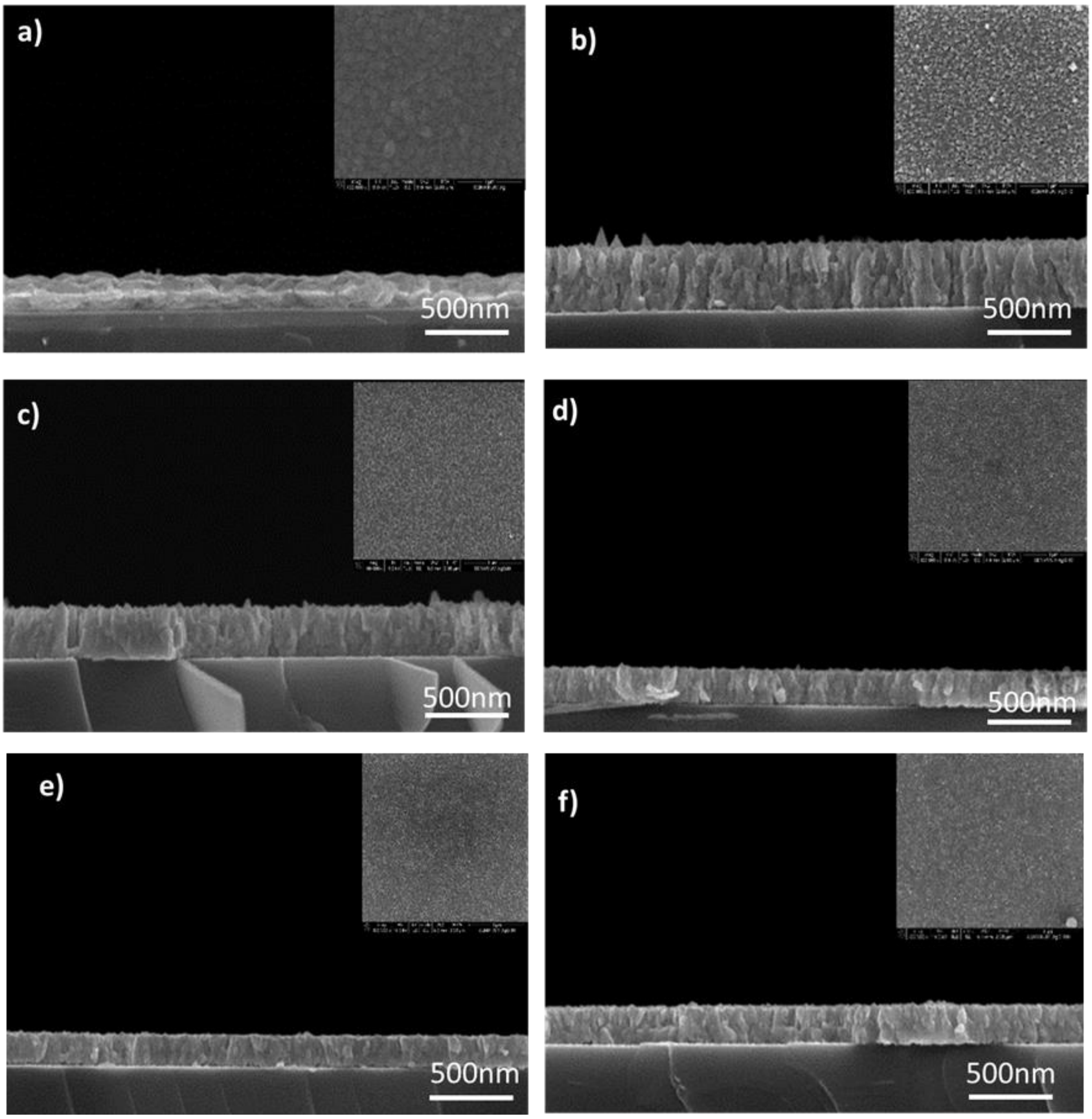

Figure 44 -SEM films cross section detailed view (recorded in SE mode at 100kX) and top-view micrographs (recorded in SE mode at 100kX) (a) to f) referent to Ag, AgO10, AgO20, AgO50, AgO80 and AgO100, respectively.

In order to obtain a more detailed information about the coatings structure, XRD analysis was performed. The XRD diffraction patterns of Ag, AgO10, AgO20, AgO40, AgO60, AgO80 and AgO100 coatings are presented in Figure 45. The XRD spectrum evidenced three different structures in the films. The Ag films present a typical face-centered cubic (FCC) polycrystalline structure (ICDD card no 00-004-0783), with randomly oriented crystallites with grain sizes of 79 nm, calculated by Scherrer formula (equation 17).

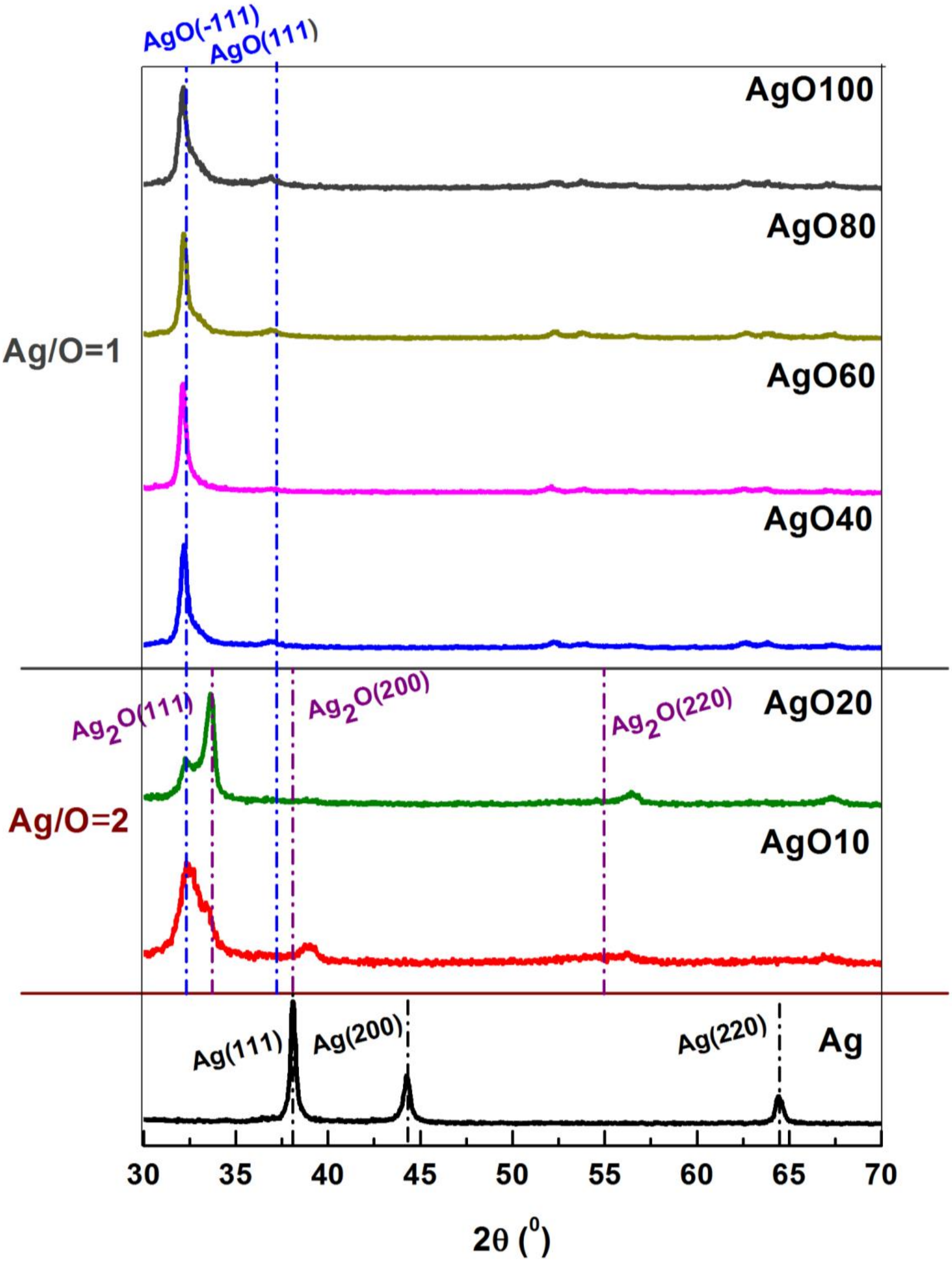

Figure 45-XRD patterns of Ag and AgxO coatings, according to ratio of Ag/O composition estimated by EDS.

For Ag_xO films, on the other hand, two distinctive behaviors are noticed. For large oxygen fractions (AgO40 to AgO100), a monoclinic AgO phase is easily identified (ICDD card no 00-043-1038), which is in agreement with the composition of the films, where the ratio between Ag and O is close to the unit, as previously discussed. Once again, a different behavior can be observed when compared this series of oxide silver samples with the first series of samples. In this series, for samples with higher content of oxygen, a stoichiometric silver oxide, seems to be achieved, which not occurred in the previous series. Afresh, the conditions in two depositions series are different.

Nonetheless, for low oxygen fractions (AgO10 and AgO20) at least two scenarios can be considered. In the first case, a pure monoclinic AgO phase was fitted, where residual stresses in the films may slightly increase the lattice parameter. This variation results in a shift of the (002) plane towards lower angles. The simulation predict a variation from 0.549 to 0.559 nm, in the lattice parameter, which is likely to occur for grains preferentially orientated in the (002) direction and films in compressive stress. These results can simulate the spectra obtained for sample AgO10. Yet, there is still a lack of fit for AgO20, where the diffraction peak corresponding to 56.3 degrees is not included in the fitted spectrum, as shown in Figure 46 a). Additionally, the excess of silver in those films would not explain the pure AgO phases.

As a result, a second scenario is proposed, considering a mixture of Ag_2O FCC (ICDD card no 00-043-0997) and monoclinic AgO phases and the result are shown in Figure 46 b). In this case, the diffraction occurring at 56.3 degrees is included as the (022) diffraction of the Ag_2O phase, decreasing the fitting deviation. However, the cell parameter for the cubic structure showed a slight deviation from the theoretically value, showing a difference of 0.009 nm (from 0.471 nm to 0.463 nm). This variation may be due to the lack of stoichiometry of the compound, where instead of pure Ag_2O, an Ag_xO phase is formed. This has been previously reported in silver oxide nanostructures [161].

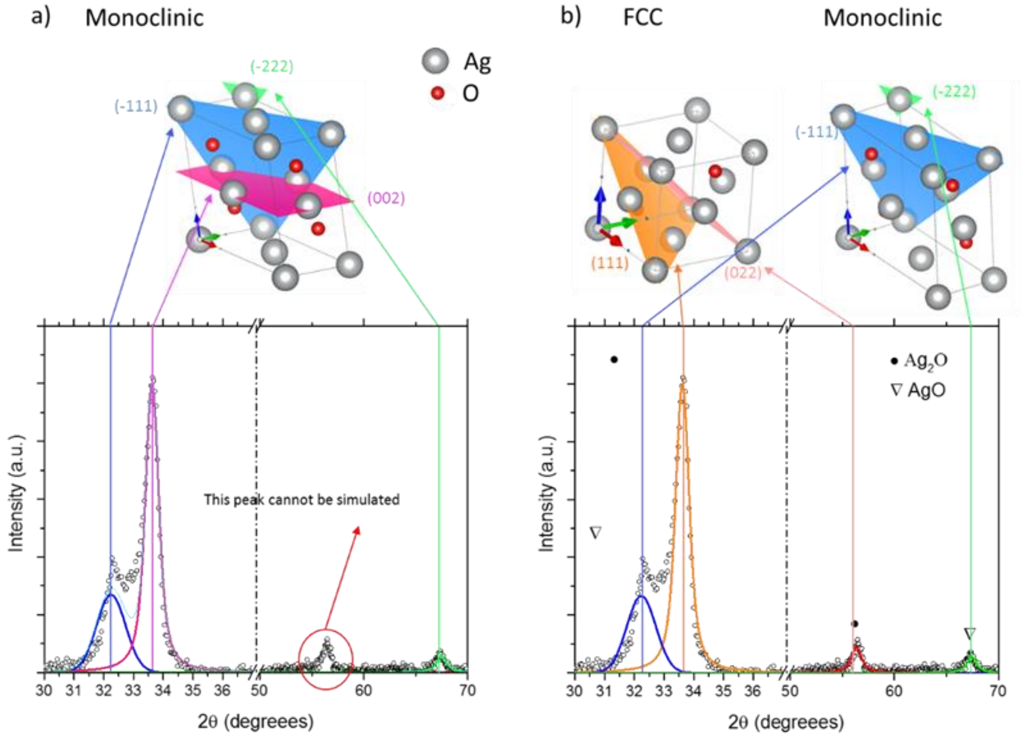

Figure 46-AgO20 XRD pattern fitted using a monoclinic AgO structure, b) AgO20 XRD pattern fitted using a mixture of Ag_2O and AgO phases. The symbols correspond to the experimental results and the color lines to the fitted lattice planes for the identified structures.

Considering the previous analysis, silver oxide coatings AgO10 and AgO20 are identified as a mixture of sub-stoichiometric Ag_xO FCC phase, with composition close to Ag_2O, and AgO monoclinic phases. For higher oxygen fractions (AgO40 to AgO100), Ag_2O disappears and coatings only present a single AgO monoclinic phase. These results are in agreement with the composition of the films, where for high oxygen fractions there is sufficient oxygen to form a pure AgO compound, as previously mentioned. The difference observed in silver oxides, with the increase of oxygen fraction, can be justified by the availability of oxygen in the reaction zone, resulting in the formation of different valence states of metal oxide [158].

According to Figure 41 and the compositional, structural and morphological results presented, four samples were chosen to continue the study of chemical bonding and antibacterial characterization (Ag, AgO10, AgO20 and AgO100). The remaining samples were discarded for further analysis due to their similar composition, morphology and structure with samples AgO100.

In order to confirm the chemical state and binding energy of the coatings surface and the phase composition, XPS analyses were carried out. Nevertheless, XPS analysis of silver and silver oxides is very complex, once the binding energies of metallic silver and its oxides are reported with low dispersion of values, or even superposition.

In order to facilitate the identification of oxidation states, the Auger Parameter (AP) was used, since it is considered to be more reliable that finding the correct binding energy of each state of oxidation [140]. AP does not depend on the sample charge shift, avoiding charge correction, and AP peaks present larger chemical shifts than photoelectron peaks [140]. Despite the fact that this parameter allows distinguishing the reduced form Ag^{o} from its oxidized forms, it cannot distinguish Ag (I) form from other oxidation states, and thus other parameter such as the FWHM of the peak should be considered. Hence, XPS analysis of coatings were carried out with binding energy for Ag3d and kinetic energy for Ag MNN, as observed in Figure 47.The bonding types, binding energies, APs and possible structures are summarized in Table 18.

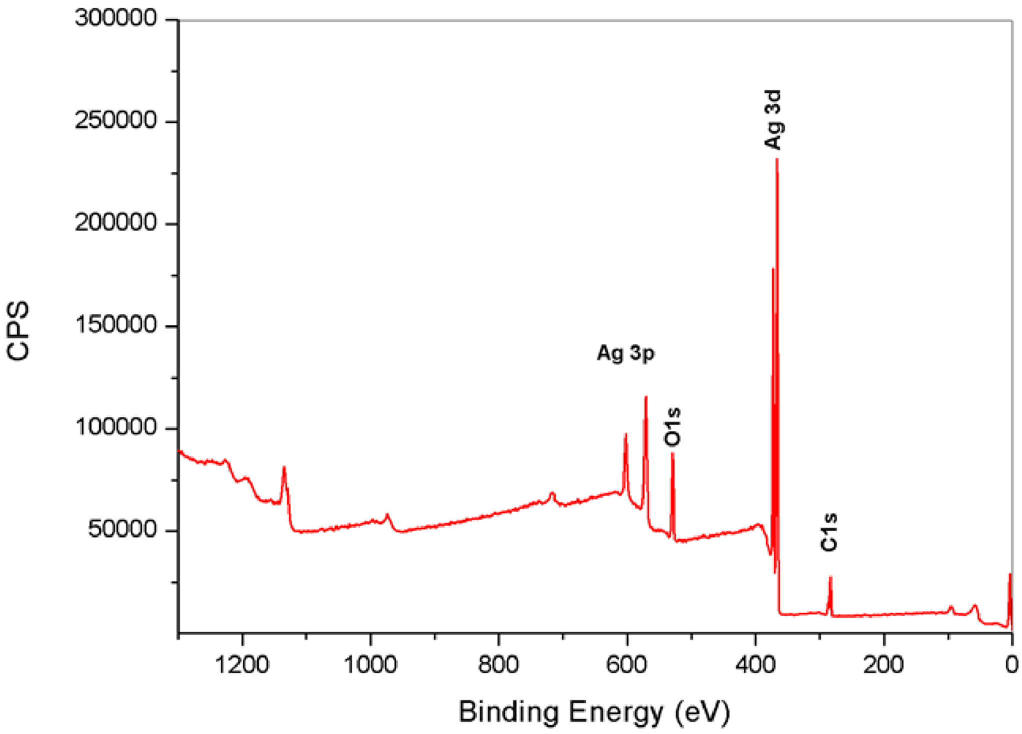

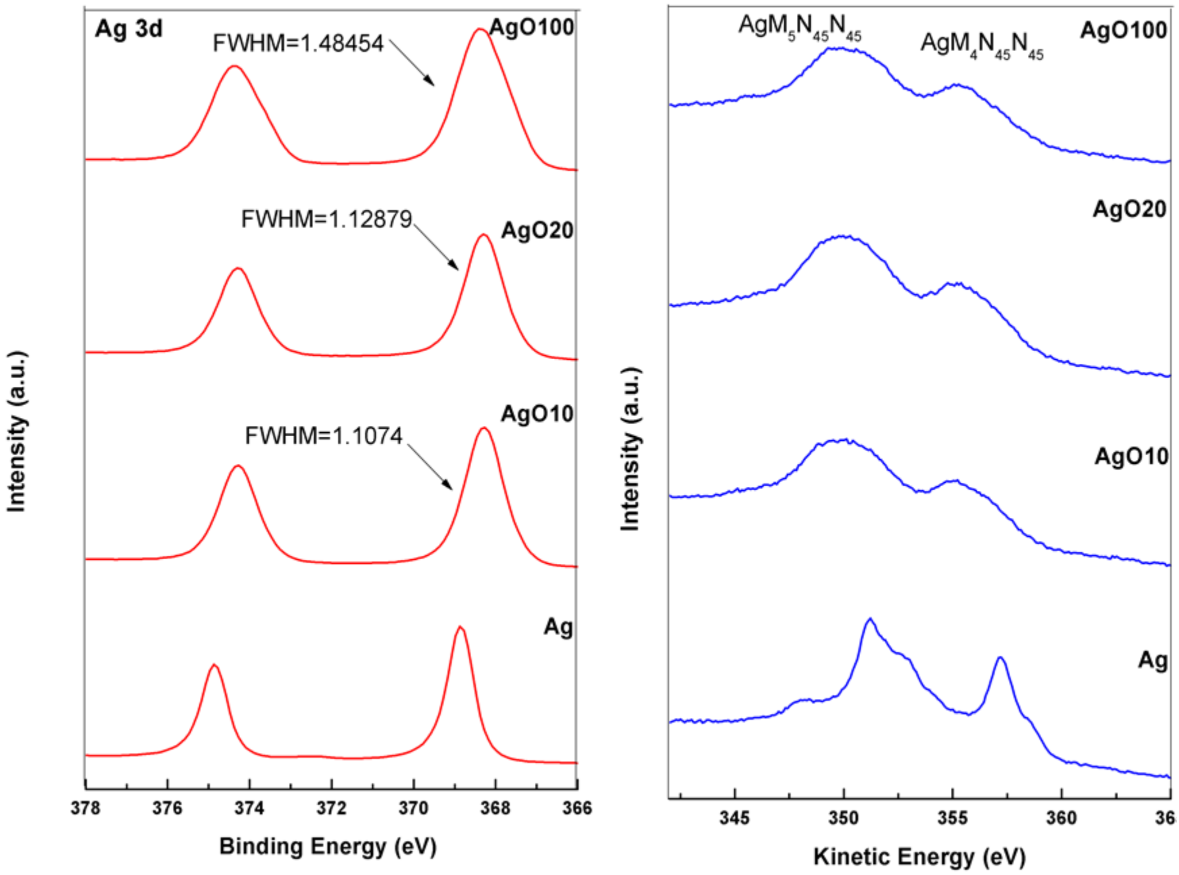

Figure 47-XPS survey spectra and detailed regions of Ag3d (left) and Ag MNN (right) for Ag and AgOX thin films.

Table 18-XPS analysis of different coatings [140,162–164]

Coating	**Bonding**	**Binding Energy (eV)**	**Auger parameter (eV)**	**Compatible with:**
Ag	Ag-Ag	368.86	726.09	Ag
AgO10	Ag-O	368.28	723.36	AgO/Ag_2O
AgO20	Ag-O	368.28	723.41	AgO/Ag_2O
AgO100	Ag-O	368.31	723.37	AgO/Ag_2O

For Ag coating, the spectra suggest the presence of a doublet with the Ag 3d5/2 peak located at 368.86 eV. This fact, combined with auger parameter, is reported to correspond to Ag-Ag bond in metallic state [139,164]. On the other hand, Ag-O bonds at 368.28eV [165], for transition mode coatings (AgO10 and AgO20), and at 368.31 eV for the coating in the reactive mode (AgO100).

These binding energies are compatible with silver oxides. According to Ferraria *et. al* [140], the doublet assignable to Ag 3d have different characteristics in AgO, Ag_2O and in a mixture of those two phases, regarding binding energy and FWHM. In fact, the Ag 3d doublet, reported in such study, is slightly shifted in AgO coating (0.4±0.1 eV) and presents the largest FWHM, when compared with a mixture of Ag_2O and AgO powders [140]. This behavior is observed in sample AgO100, when compared to AgO10 and AgO20 coatings, as shown in Figure 47 ,supporting the idea of a mixture of AgO +Ag_2O phases for AgO10 and AgO20 coatings and a single AgO phase for AgO100 coating, observed by XRD, and corroborated by compositional analysis.

Furthermore, XPS spectra to O 1s and C 1s are presented in Figure 48. Some residual oxygen and carbon are associated with surface contamination, since no previous sputter cleaning was performed in order to avoid preferential sputtering of O and any structural damage in the coatings. Additionally to the contamination, O-Ag peak (529.3 eV), associated to the bonding of silver oxide, was identified in the AgO_x coatings, which has been reported to shift to lower binding energies for pure AgO phases, observed in AgO100 coating, when compared with Ag_2O and their mixture [140].

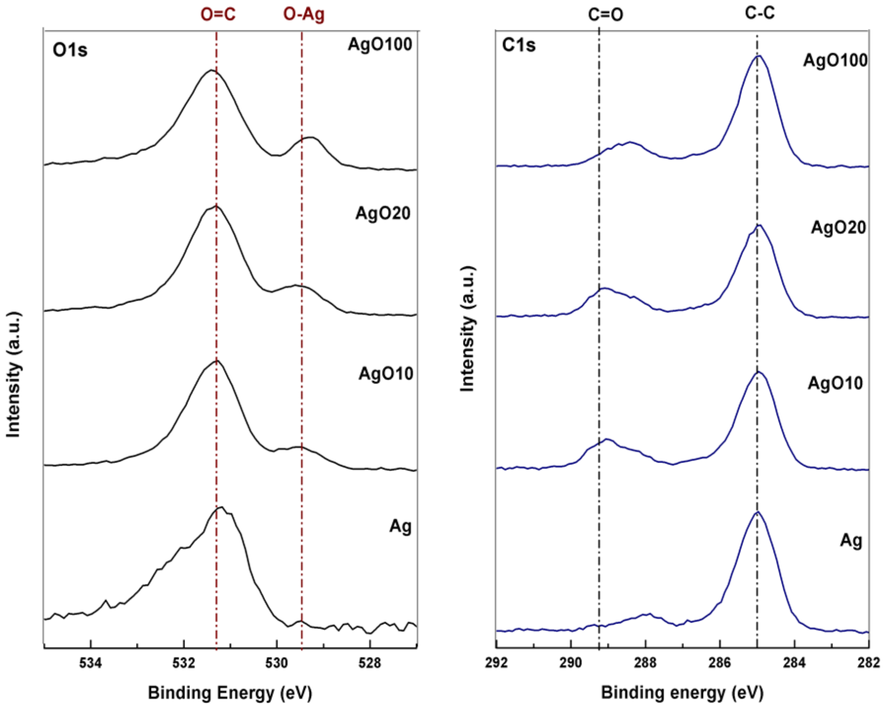

Figure 48- XPS O1 (left) and C 1s (right) spectra for Ag and Ag_xO thin films.

As referred in section 3.1 of Chapter III, the measurement of contact angle allows the evaluation of the hydrophobicity character of a surface. Table 19 shows the contact angles, surface energy parameters and degree of hydrophobicity of all the coatings. The results evidence that all coatings present a hydrophobic surface, since the water contact angles are above 90^0 and ΔG_{mwm} present negative values. AgO100 coating is statistically different from the others ($p<0.05$).

By the literature the wettability of coatings is strongly dependent on the oxygen partial pressure and films morphology [145,147].

Regarding silver oxide thin films, different states of oxidation of the films leads to changes in their affinity toward water. Mirzaeian *et al.* [147] reported that the increase in oxygen flow rate increases the wettability of the films toward water, due to further, changes in the electronic properties of the surface caused by the increase in the oxidation state of the films. This is a result of clustering of electrons in polar molecules of water around the oxides at a higher oxidation state.

However, as discussed by SEM micrographs before, higher oxygen flow rates result in smooth and dense films which leads to a slightly decrease on the wettability with water, as observed to AgO100 coating.

Additionally, all coatings present a monopolar surface. Higher density of apolar areas in material's surface can promote an attachment of microorganism via the hydrophobic effect, due to the increment of hydrophobic interactions [144].

Table 19-Water (θ_w), formamide (θ_F) and α-bromonaphtalene ($\theta_{\alpha\text{-}B}$) contact angles, surface energy components (apolar Lifshitz-van der Walls surface free energy component, Υ^{lw} ; electron acceptor surface free energy component, Υ_i^+; electron donor surface free energy component, Υ_i^-

Coating	**Contact Angle ± S.D.(º)**			**Surface energy components (mJ.m-²)**			**ΔG_{mwm} (mJ.m⁻²)**
	θ_w	**θ_F**	**$\theta_{\alpha\text{-}B}$**	**Υ^{lw}**	**Υ^+**	**Υ^-**	
Ag	102±1	95±2	53±1	28.7	0.0	5.1	-57±4
AgO10	101±3	88±6	44±2	32.6	0.0	3.3	-68±6
AgO20	99±4	87±1	40±1	34.4	0.0	4.4	-63±5
AgO100	107±2	90±3	50±3	29.9	0.0	1.1	-82±9

3.2. Preliminary antibacterial evaluation

Halo inhibition tests were performed in order to evaluate the existence of antibacterial properties of the coatings, against *S. epidermidis*. The results obtained are present in Figure 49. A halo zone (zone of inhibition of bacteria growth) in oxide coatings is clearly observed. On the other hand, in Ag coating the halo is not visible, which means the pure Ag continuous film did not present antibacterial activity against *S. epidermidis*.

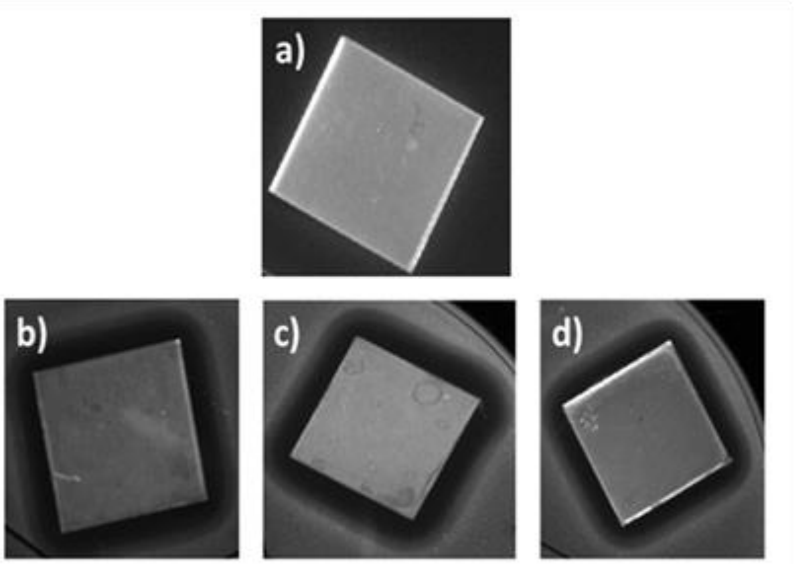

Figure 49-Results of antibacterial tests for: Ag (a)); AgO10 (b)); AgO20 (c)) and AgO100 (d)).

As previously suggested, the form of silver can influence the antibacterial efficiency. The presence of Ag nanoparticles tends to ionize more easily, when compared with a compact film, and also interact, directly, with bacteria, promoting their destruction [157]. Once in studied coatings there is no evidence of silver nanoparticles, the antibacterial behavior of the silver oxide coatings should be due to a higher silver ion release of those coatings. In order to verify the amount of silver ions release of the coatings, ICP-OES was performed after 24 h period of contact of coatings with NaCl 0.9%. In Figure 50 it is possible to analyze the Ag^+ release from coatings and it is possible to observe that silver oxides did not present a high silver ion release, which means that are not the silver ions the direct responsible from the different antibacterial characteristics presented by silver and silver oxides coatings.

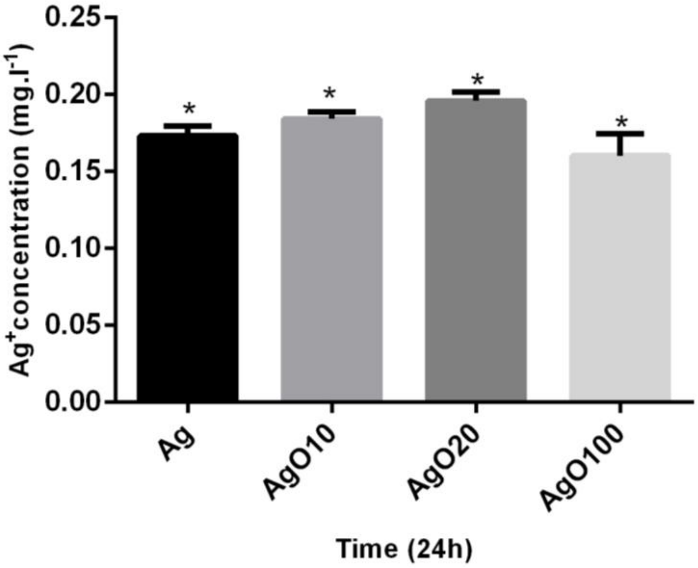

Figure 50- Results of ICP-OES test. The data are expressed as mean ± standard deviations. One way ANOVA was used with significant level of 95% (* $p<0.05$).

In Chapter III it is shown that in silver thin films, Ag ionization is insufficient or non-existent and, consequently, no antibacterial activity was observed, contrary to Ag_xO thin films. In this series of samples, the same results are achieved (only silver oxide samples presented antibacterial activity). However, once there is not higher silver ionization in silver oxide coatings, when compared to silver coatings, and no nanoparticles are present in this series of sample, it should be the presence of the silver oxide the responsible for the antibacterial behavior of silver oxide thin films.

By the literature it has been proposed that it is the specific characteristics of silver morphology the main responsible for the production of ROS and silver oxide promotes the formation of ROS [54,74,162]. So, according with ICP-OES and halo tests results, it is suggested that the formation of ROS (equation 18) [74] is, probably, the agent responsible for the antibacterial properties of silver oxides.

$$Ag + O_2 \rightarrow Ag \dots O_2 \rightarrow^{H^+} Ag^+ + ROS + Ag \rightarrow Ag^+ + H_2O \qquad (18)$$

Ninganagouda *et al.* [163] demonstrated that Ag nanoparticles when in contact with bacteria inhibited their growth, due to ROS formation. However, when it was added an antioxidant to Ag nanoparticles, the antibacterial behavior was not observed. This study determined that the antioxidant agent prevented the formation of a silver oxide layer on Ag nanoparticles' surface, and consequently, inhibited the antibacterial activity. Thus, the use of a silver oxide coating can be an advantage in ROS formation and explain antibacterial results.

Furthermore, as demonstrated by Ferreri *et al.* [72], the incorporation of oxidized silver on coatings can inhibit the bacterial growth, since allows the synthesis of OH^- in aqueous environments (equation 19 and equation 20).

$$Ag_2O + H_2O \leftrightarrow 2Ag^+ + 2OH^- \tag{19}$$

$$AgO + H_2O \leftrightarrow Ag^+ + 2OH^- \tag{20}$$

Antibacterial tests demonstrated that the formation of reactive oxygen species could be the principal motive to achieve antibacterial properties, since silver oxide coatings presented antibacterial activity unlike continuous silver coating.

4. Partial Conclusions

Ag and Ag_xO coatings were deposited by non-reactive and reactive pulsed dc magnetron sputtering, respectively. The O_2 flow and, consequently, oxygen fraction during the deposition process, was varied in order to evaluate the influence of oxygen species in coatings properties.

The structural and morphological characterizations revealed that Ag coating forms a continuous layer, composed by crystalline FCC-Ag phase. The incorporation of oxygen in the deposition atmosphere leads to the formation of a coating composed by a mixture of Ag_2O+ AgO phases. As the amount of oxygen fraction increase, the observed thin film became, only, AgO, with a monoclinic crystalline phase.

Halo inhibition testes revealed the antibacterial behavior of Ag_xO coating unlike Ag coating. The differences on coating behavior may be attributed to film composition (the incorporation of oxygen leads to a higher formation of ROS and, consequently, to an antibacterial behavior), as summarized in Figure 51.

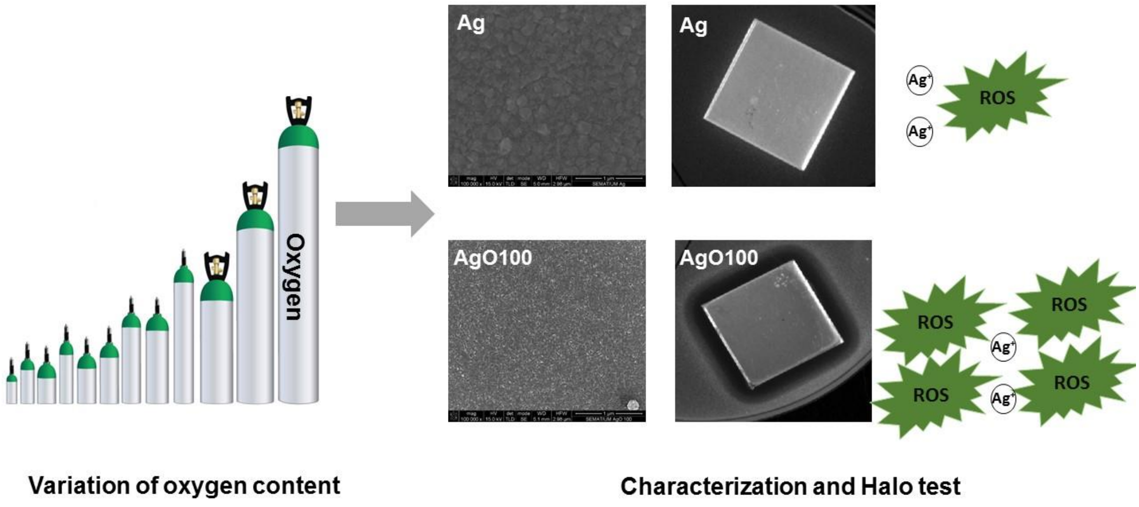
Oxygen
Ag
Ag
Ag+
Ag+
ROS
AgO100
AgO100
ROS
ROS
ROS
ROS
Ag+
Ag+
Variation of oxygen content
Characterization and Halo test

Figure 51-Summary of the variation of the oxygen content and its influence on film's characterization and antibacterial properties.

The results suggest that Ag_xO coating deposited by dc magnetron sputtering have potential to be used in coronary stents.

CHAPTER V

Fibrous Stents with Antibacterial Coatings: Functional Properties Study

This chapter is based on the publication:

R. Rebelo, M. Fernandes, R. Fangueiro, M. Henriques, and S. Carvalho, "Antimicrobial Silver-based Coatings on Fibrous Braided Coronary Stents", ready for submission.

1. Introduction

Taking into account the disadvantages of commercial metallic stents previously reported, there is a growing need for the development of biocompatible stents that avoid the corrosion and restenosis events associated to metallic stents and polymeric coatings. Additionally, apart from restenosis, coronary stent infection has been described as an unusual but severe complication of coronary artery stenting procedures with associated alarmingly high mortality [166–169].

As mention in Chapter II, a polyester stent (PES270A35D6) was developed and presented good mechanical properties (0.23 N of force in longitudinal compression, 1.29 N of force in radial compression, 80% of porosity and 85,5% of unchanged diameter in bending tests), when compared with nitinol commercial stents. Furthermore, considering the promise results in antibacterial activity, against Gram-positive *Staphylococcus epidermidis*, for silver oxide coatings developed in Chapter III and Chapter IV, in this chapter we intend to functionalize the PES270A35D6 stent with silver and silver oxide coatings. The mechanical properties of the coated stent, the coating's performance when subjected to mechanical tests, the obtained antibacterial properties as well as the biocompatibility will be thoroughly studied.

The ultimate objective of this study is to achieve the optimal conditions for obtaining a fibrous stent that fulfil the mechanical requirements when compared with commercially available nitinol stents and provide it with antibacterial properties [14].

2. Materials and Methods

2.1. Production of silver and silver oxide coatings

After the production and mechanical characterization of PES270A35D6 braided stent (see Chapter II), silver and silver oxide coatings were deposited on stents by non-reactive and reactive pulsed dc magnetron sputtering, taking in account previously antibacterial results obtained for these coating in stainless steel (Chapter III and Chapter IV). In order to remove impurities and avoid contamination, stents were previously cleaned ultrasonically, during 1 h, with petroleum ether.

Ag, AgO10, AgO20 and AgO100 coatings were, once again, deposited by non-reactive and reactive magnetron sputtering in PES270A35D6 with the conditions described in section 2.1. of Chapter IV and Table 17 in section 3.1 of Chapter IV. Samples of stainless steel were placed along the stents, in order to easily characterize the coating, in cytotoxicity assays.

2.2. Characterization of silver and silver oxide coatings

The morphology of coated stents with silver and silver oxide, were evaluated by SEM analysis in an EDAXNova nano-SEM200 equipment. Three different regions of stents' surface were analyzed and a representative micrograph was taken. Samples were mounted on aluminum bases with carbon tape, sputter-coated with gold/palladium before observation.

In order to evaluate the potential application of stents in human body, cytotoxicity and antibacterial tests were performed. Thus, coated stents were sterilized at 121 ^{0}C during 15min in autoclave, before all the biological assays. The biological assays were realized in Centro de Engenharia Biológica at Universidade do Minho.

Concerning the cytotoxicity evaluation, assays were taken adapting ISO 10993-5 [170] and CellTiter 96® AQueous One Solution Cell Proliferation protocol and it was used fibroblast 3T3 cells (CCl-163) obtained from American Type Cell Collection [171]. Fibroblast cells were grown in Dulbecco Modified Eagle Medium (DMEM) containing 1% of penicillin streptomycin (PS, Gibco) and 10% of fetal bovine serum (FBS-Gibco) until obtaining 80% of confluence. After detachment of cells, 50 µl of cell suspension with $1x10^5$ cells.ml^{-1} were added to each plate of a 96 well's plate and incubated for 24h. At the same time, coated stainless steel coupons were placed in six well plates with 3 ml of DMEM and incubated with 5% of CO_2 at 37 ^{0}C for 24 h, 48 h, 168 h and 720 h. After the pre determinate time, 50 µl of the medium in contact with the coated samples were removed for each well and added to 96 well plate with cells, being incubated with 5% of CO_2 at 37 ^{0}C for 24 h. After the incubation, 20 µl of MTS (3-(4,5-dimethylthiazol-2-yl)-5-(3-carboxymethoxyphenyl)-2-(4-sulfophenyl)-2H-tetrazolium) inner salt (Promega CellTiter 96® Aqueous Non-Radioactive Cell Prolifaration Assay) was added, in the dark, to each well of the 96 wells plate. The plate was incubated with 5% of CO_2 at 37 ^{0}C for 1 h and after that the absorbance of the resulting solution was measured at 490 nm. MTS assay is accurate, fast and reliable method [54,172]. The MTS tetrazolium compound is bioreduced by cells into a colored formazan product, through the mitochondrial activity of viable cells. This conversion is probably accomplished by NADPH or NADH produced by dehydrogenase enzymes in metabolically active cells [171].

The number of living cells in culture is directly proportional to the amount of formazan produced by enzymes [54,172].

Cellular viability was measured taking in account the ratio of the difference between cell grown in control (samples without coating - 100%) and coated samples over the control growth (equation

21). Assays were run in triplicate, three different times. Stainless steel was used in cytotoxicity tests, once the aim is to test the coating cytotoxicity and using square samples of stainless steel there is a major contact area between coating and medium and a less complex geometry, when compared to braided stents.

$$\% \, cell \, viability = \frac{sample}{control} * 100 \tag{21}$$

Regarding antibacterial activity, it was tested against the clinical isolated *Staphylococcus epidermidis* (IE 186) and the assays were realized by the adaptation of Standard Japanese Industrial Standard (JIS) Z 2801 [173]. Bacterium was grown in tryptic Soy Agar (TSA, Merck, Germany), during 24 h at 37 ^{0}C. *S. epidermidis* was inoculated in tryptic soy broth (TSB, Merck, Germany) and incubated for 18 h at 37 °C under agitation (120 rpm). Subsequently, bacterial concentration was adjusted to 1x10^6 cells.mL^{-1}, via absorbance readings at 640 nm, using the correspondent calibration curve. Coated and uncoated (control) PES stents were inserted in falcons with 3 ml of cellular suspension and incubated, for 24 h, at 37 ^{0}C and a constant agitation of 120 rpm. After incubation period, stents were transferred for new falcons and 5 ml of a saline solution with a non-ionic surfactant was added. Samples were vortexed 5 times for 5 seconds, each, in order to detach bacteria from stent's surface. Serial dilutions were performed and bacteria were plated in TSA plates at 37 ^{0}C, during 24 h. Thereafter the number of colonies forming unites (CFU's) were counted. All assays were run in triplicate and in three independent times.

At the same time, some samples were taken out after incubation period and, consequently, biofilm formation was expected, and were dehydrated by an immersion in increasing ethanol concentration solutions of 70, 95 and 100% (v/v) for 10, 10 and 20 minutes, respectively, for further observation in SEM.

For statistical analysis, one-way ANOVA analysis was used, by applying Tukey multiple comparisons test, using the software GraphPad Prism 6. All tests were performed with a confidence level of 95%.

Mechanical properties after stent functionalization were evaluated, once stents' therapeutic efficacy is several influenced by their mechanical behavior. Thus, in order to keep, adequately, their function, stents should present a good mechanical behavior [174]. Mechanical behavior, including: cover factor and porosity, radial and longitudinal compression and bending tests, of coated stents were tested and compared with PES stents (previously reported and tested in Chapter II) with the intention of understand and study the influence of silver and silver oxide coatings in mechanical performance. In mechanical testes were used samples with 4 cm of length.

3. Results and Discussion

3.1. Coating's Characterization

In Figure 52 it is possible to observe the PES stent produced (PES270A35D6), as well as PES stent coated with silver and silver oxide (Ag and AgO100, respectively).

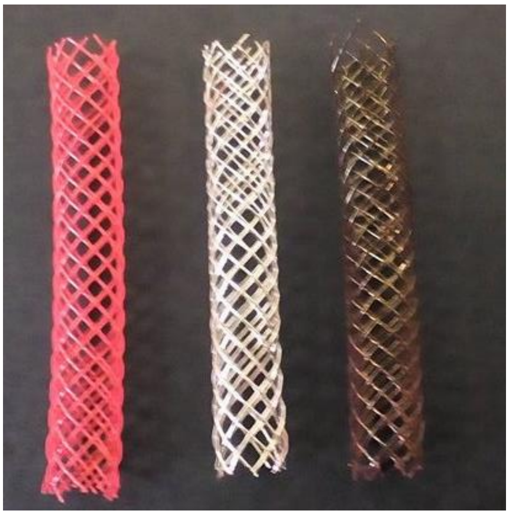

Figure 52-Braided PES stents uncoated, and coated with Ag and AgO100, by the same order.

SEM analysis were performed, with the intention of study coating's morphology and chemical composition. SEM analysis on coated stents, presented in Figure 53, shows a homogenous coating in all samples, meaning a successful deposition on a 3D substrate.

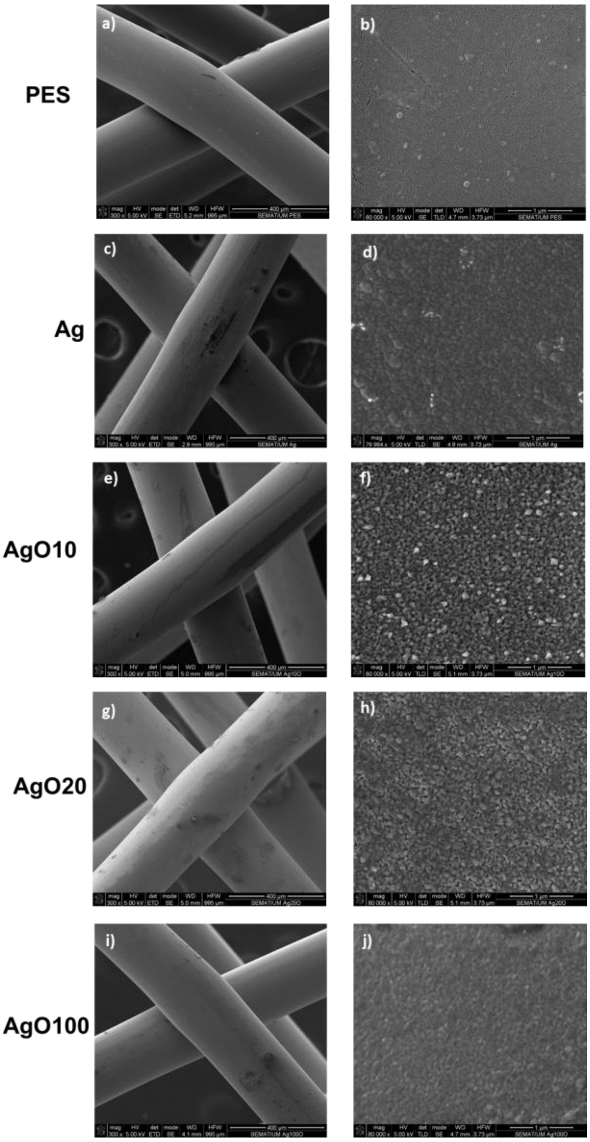

Figure 53- SEM micrographs of uncoated (a) and b)) and coated (c), d), e), f), g), h), i) and j)) polyester stents and a more detailed view of surfaces.

Biological Characterization

Firstly, with the purpose to analyze the applicability of the coatings as a biomaterial, silver and silver oxide coated stainless steel coupons cytotoxicity was assessed in fibroblast cells, through MTS assay, which gives the samples' toxicity on cells in a precise, fast and reliable way. Cellular viability of coatings, over time, can be observed in Figure 54.

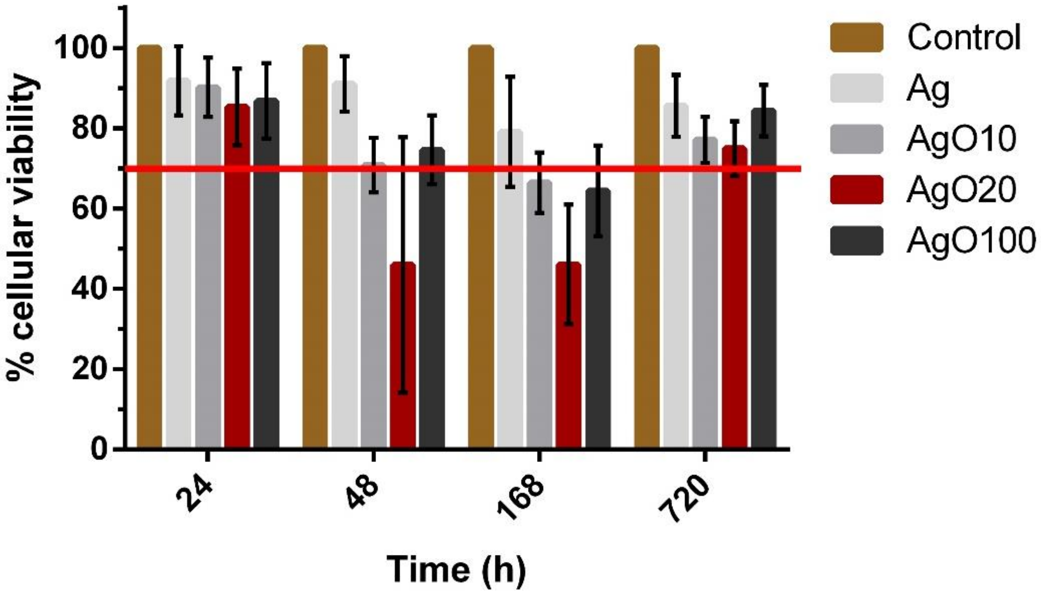

Figure 54- Rate of fibroblast cell viability, over time, for the different coatings.

Despite the several studies highlighting the toxicity of silver to several cultured cells, at least, Ag and AgO100 coatings presented a cellular viability superior to 70%, which is the limit of cytotoxicity determined by International Standard ISO 10993-5. Concerning silver oxide coatings, AgO100 sample is the one with lower silver at. %, which is expected to be the sample with lower cytotoxicity. Thus, according to cytotoxicity results, Ag and AgO100 stents are viable to insert in human body and being used as a biomaterial. So, for now on, the remained biological and mechanical tests will be performed only for these coatings.

Regarding antibacterial properties, an antibacterial assay were performed in order to evaluate antibacterial properties of the coated stents against *S. epidermidis* that is reported as bacterium with propensity to form biofilms [59,175,176]. The results obtained, regarding logarithm of bacterial concentration (CFU.ml^{-1}), are presented in Figure 55, as well as, SEM images for respectively biofilm’s formation.

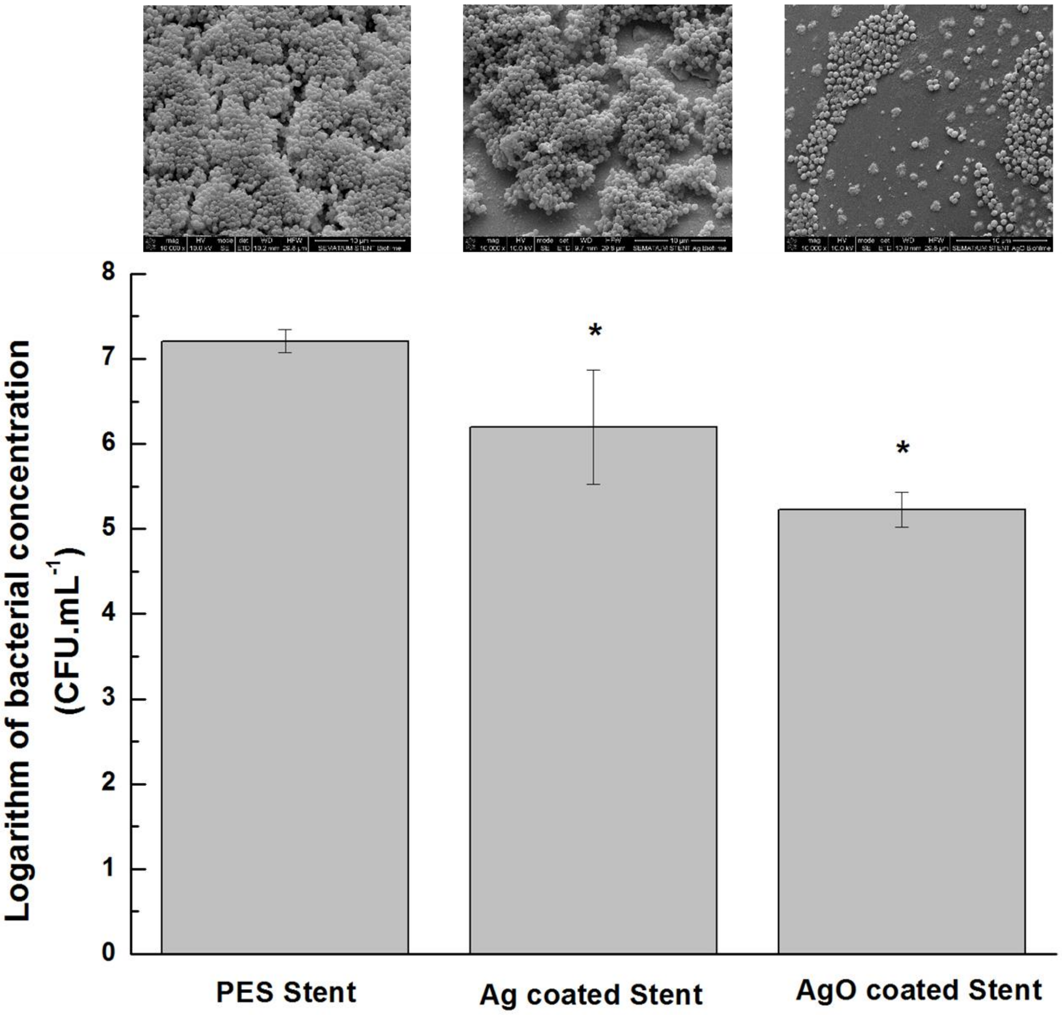

Figure 55- Logarithm of bacterial concentration after 24h of contact between stents and *Staphylococcus epidermidis* and SEM images of biofilm's formation. Concentrations that are significantly different (* $p<0.05$) of each compound compared to control.

From the observation of Figure 55 it is possible to verify that the addition of silver promotes significant decrease ($p<0.05$) in stent's bacterial adhesion, however, this decrease is not sufficient to provide antibacterial properties to silver coated stents, once according to JIS Z 2801 it is necessary a logarithmic difference of 2 values between antibacterial products and untreated products. On the other hand, the logarithmic difference between PES stents and coated stents with silver oxide is 2 values, which means that PES stents coated with silver oxide present antibacterial properties. Thus, as expected, the formation of biofilm is higher in uncoated stents and decreases with the introduction of silver and silver oxide coatings.

As already discussed in Chapter III and IV, the antibacterial effect of silver and the exact mechanism of actuation is poorly understood. Nonetheless, the antibacterial behavior of silver oxide coated stents should be attributed to a higher formation of ROS, which leads to a most effective antibacterial behavior due to the toxic character of these species to bacterial cells.

In Figure 56 there are present the results of logarithm of bacterial concentration (CFU.ml^{-1}) from cellular suspension which was in contact with PES stents coated and uncoated. It is possible to observe that bacterial concentration statistical decreases with the incorporation of silver and even more with the incorporation of silver oxide ($p<0.05$), which leads to the conclusion that coated stents not only decreases the bacterial adhesion in stents' surface but even diffuse the silver to the medium and, consequently, causing the death of bacteria.

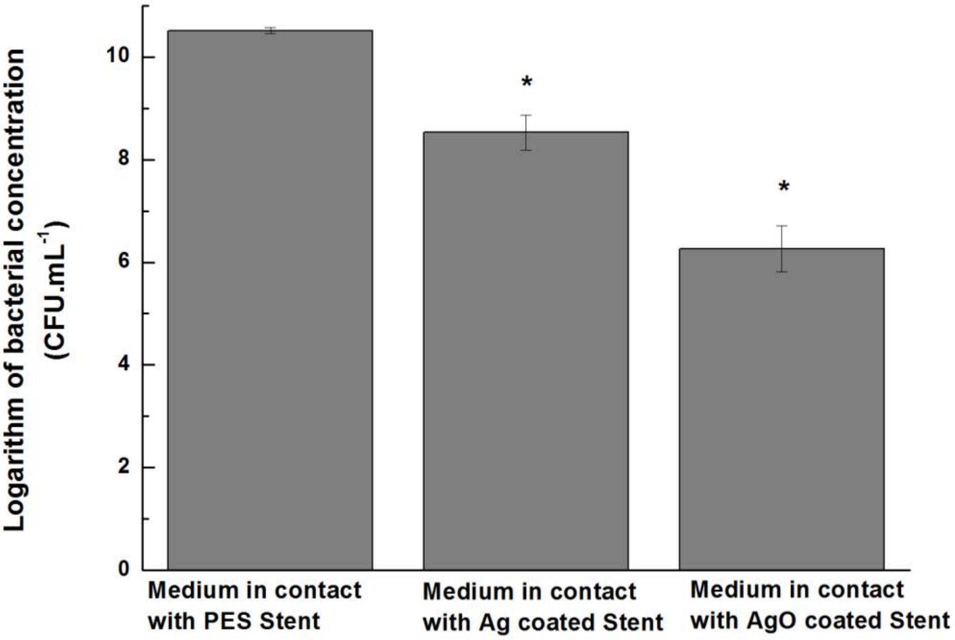

Figure 56-Logarithm of bacterial concentration in bacterial suspension after 24h of contact between stents and *Staphylococcus epidermidis*. Concentrations that are significantly different (*$p<0.05$) of each compound compared to control.

Mechanical Behavior

After stents functionalization and characterization, it was necessary to observe not only the mechanical behavior of stents but also the coatings behavior during mechanical efforts, ensuring, this way that no coating delamination occurs.

Porosity and cover factor for PES stents and coated PES stents are similar once those parameters are calculated through equations 8 and 9, since these parameters are not influenced by a nanocoating (thicknesses lower than 160 nm for silver coatings and 195 nm for silver oxide coatings), taking in account the dimensions of the stent structure and monofilament thickness (270 µm). Stents presented a good percentage of porosity and cover factor, once they showed a porosity of 80% and a consequently cover factor of 20%, which is a good value and allows the stent to maintain mechanical performance required, avoiding collapse [41]. Porosity and cover factor depends on monofilament's diameter and mandrel's diameter, as demonstrated by equation 8 and equation 9 (Chapter II). The good results on porosity and cover factor can be attributed to the lower diameter of the used monofilaments (270 μm) that cover less area on mandrel surface than higher diameters. Furthermore, a high mandrel diameter, as the used one (6 mm) leads to a less deposition of yarns on the mandrel and, consequently, a reduction in mandrel's cover area.

In Figure 57 it is possible to observe that mechanical behavior of PES and coated stents, regarding longitudinal and radial compressions. It is possible to observe that all samples present a linear trend during compression, which means that for the required extension stents remained in elastic domain, with no permanent alteration in the structure. However, a different behavior is observed, when a comparison is made between the polyester and coated stents. In longitudinal compression, it is clear that the material is influencing the mechanical behavior. Thus, with the addition of a coating, the stiffness of the material increases, from 0.02 $N.mm^{-1}$ (PES) to 0.03 $N.mm^{-1}$ and 0.05 $N.mm^{-1}$ (AgO and Ag coated stents, respectively), and, consequently, a higher force is required for the same elongation. On the other hand, in radial compression, materials' type do not play the main contribution to the mechanical behavior, but the structure itself. In radial compression, the contact area between the stent and the applied force is much higher, and thus, the structure has a more important role in this type of compression. For radial compression, Ag coated stent present a stiffness of 0.36 $N.mm^{-1}$ that increase to 0.55 $N.mm^{-1}$ for PES stent and to 0.90 $N.mm^{-1}$ for AgO coated stent. Furthermore, silver coatings are considered lubricants [153,177]. Thus, and once in radial compression the structure has the main contribution, the incorporation of silver coatings can lead to a slippage between the monofilaments and, this way, decrease the necessary force to the required compression.

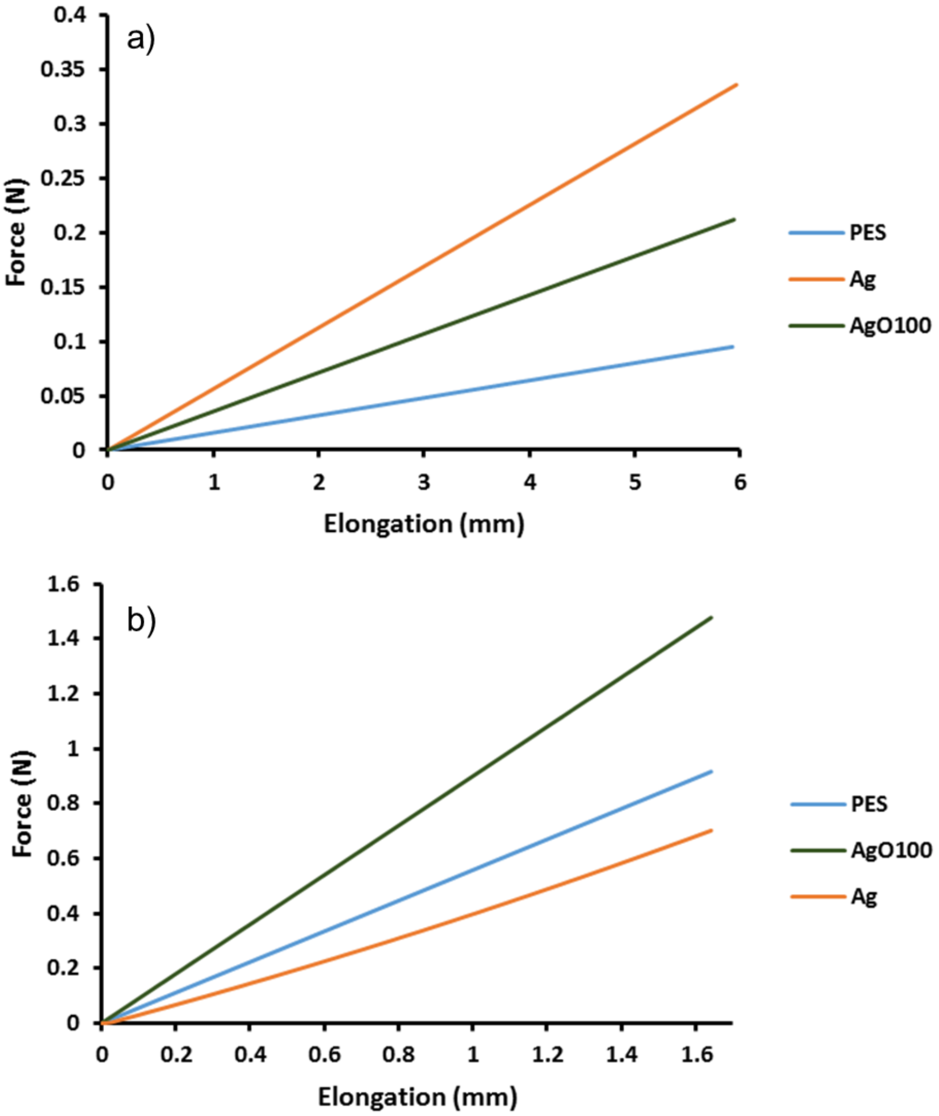

Figure 57-Relationship between force and extension for longitudinal (a)) and radial (b)) compression.

Coated stents were observed in SEM before and after mechanical testing, in order to evaluate damage in coatings. From the analysis of Figure 58, it is possible to observe differences in morphology of silver coated stent, before and after mechanical tests, due to the rearrangement of silver columns, once it is a ductile coating, in order to accumulate the tensions to which it is subject. No other significant changes, like delamination, are visible in silver and silver oxide coatings, after the mechanical tests. These results suggest that these coatings are suitable to stents applications, since there is no evidence of delamination of the coating or even loss of adhesion, indicating that coatings will support adequately the mechanical forces and since there is no delamination, the dangerous of delivering parts of coating for blood current will not occur.

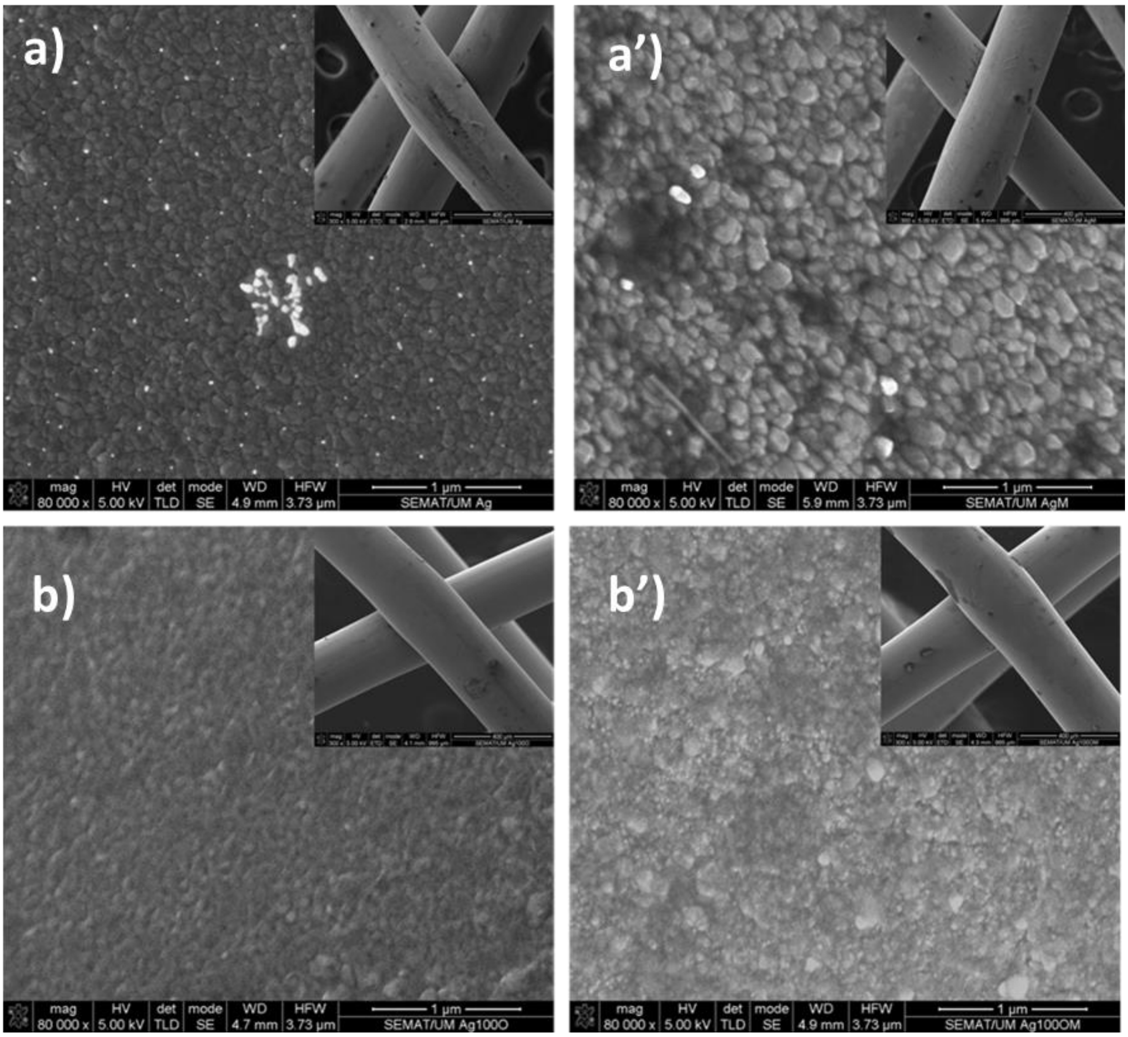
a)
a')
b)
b')
mag 80 000 x HV 5.00 kV det TLD mode SE WD 4.9 mm HFW 3.73 µm 1 µm SEMAT/UM Ag
mag 80 000 x HV 5.00 kV det TLD mode SE WD 5.9 mm HFW 3.73 µm 1 µm SEMAT/UM AgM
mag 80 000 x HV 5.00 kV det TLD mode SE WD 4.7 mm HFW 3.73 µm 1 µm SEMAT/UM Ag100O
mag 80 000 x HV 5.00 kV det TLD mode SE WD 4.9 mm HFW 3.73 µm 1 µm SEMAT/UM Ag100OM

Figure 58- SEM micrographs of silver and silver oxide coated stents before (a) and b)) and after (a') and b')) mechanical tests, respectively.

Combining all the biological and mechanical tests, polyester stent coated with silver oxide (AgO100) seems to be an excellent candidate to be inserted in human body and replace, actual metallic stents, with the advantage of providing antibacterial properties.

4. Partial Conclusions

A 100% polyester braided stent (PES270A35D6) was functionalize with Ag and Ag_xO coatings through dc non-reactive and reactive magnetron sputtering, in order to substitute and minimize the disadvantages of metallic stents used nowadays.

Cytotoxicity assays revealed that both Ag and AgO100 are not cytotoxic and can be used in human body.

Antibacterial tests revealed the antibacterial behavior of AgO100 coating unlike Ag coating, probably due to a higher formation of ROS by silver oxide coating.

Mechanical tests were performed and coated stents morphology before and after tested were assessed by SEM and no delamination or poor adhesion were notice.

Considering all tests performed, polyester coated stent with silver oxide seems to present a great potential to be applied as a biomaterial or medical device and be a candidate of substitution of nitinol commercial stents, as summarize in Figure 59.

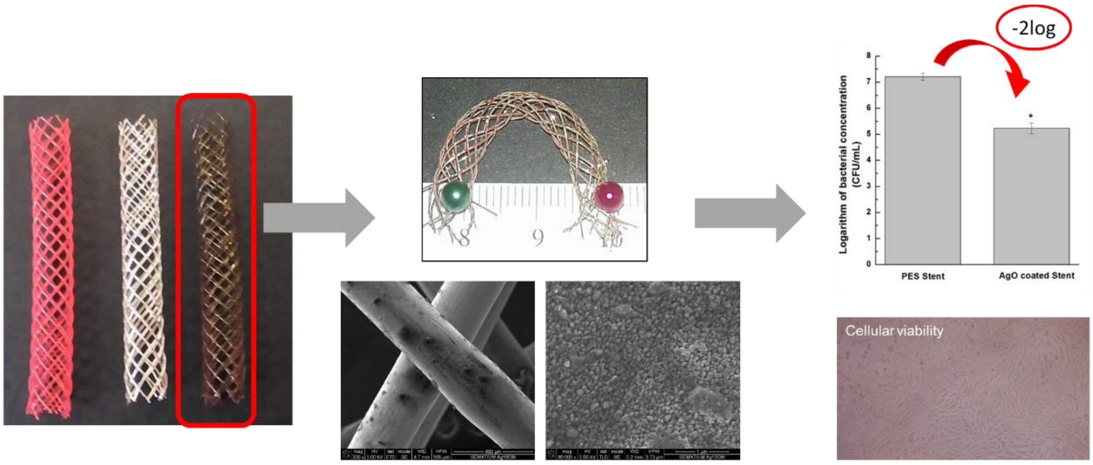

Production of Ag_xO coated stent

Evaluation of mechanical properties

Evaluation of biological properties

Figure 59- Summary of the mechanical and biological behavior of polyester coated stent with silver oxide.

Silver oxide coated stents present a good mechanical behavior, when compared with commercial nitinol stents and as an advantage it provides antibacterial properties, without causing any damage to human organism.

CHAPTER VI

Conclusions and Future Work

1. Main Conclusions

The main objective of this study was to develop a 100% fibrous stent, with antibacterial properties, able to minimize the disadvantages associated to metallic. Thus, primarily, it was necessary to study and characterize different fibrous materials (monofilaments) in order to develop fibrous braided stents, with different braided parameters. Those stents were subject to mechanical tests, and were compared to the stents available in the market. After obtaining a fibrous stent able to compete, mechanically, with the metallic ones, fibrous stents were coated, through dc magnetron sputtering, with silver and silver oxides with the intuit to achieve antibacterial properties. During the deposition process, oxygen content was varied, in order to understand the influence of oxygen on physical, chemical and structural properties of coatings and its effect on the antibacterial behavior. Finally, coated stents were, again, mechanical tested, and biological properties, as antibacterial evaluation, cytotoxicity and biofilm formation, were studied to confirm a possible application of the coating in cardiovascular stents.

Along the work, some relevant conclusions were obtained, specifically:

i) Within this work, 100% fibrous stents were developed using braiding technology and the influence of different material, process and structural parameters such as fiber type and diameter, braiding angle and mandrel diameter on their performance was thoroughly investigated. Regarding fiber diameter and braiding angle, it is possible to conclude that the increase in these parameters leads to higher radial and longitudinal compression resistance, however, the porosity is reduced. On the other hand, the increase in the mandrel diameter improves the porosity but reduce the mechanical performance.

ii) According to the experimental results, the best performance (i.e properties closely matched with those of commercial metallic stents) was achieved for polyester stents with 270 μm yarn diameter, braiding angle of 35^0 and mandrel diameter of 6 mm, providing the values of radial compression, longitudinal compression, porosity and unchanged bending diameter of 1.29 N, 0.23 N, 80% and 85.5%, respectively. The properties of these 100% fibrous stents are in the range offered by commercial metallic stents.

iii) Silver and silver oxide thin films were deposited by non-reactive (for Ag thin film) and reactive (for Ag_xO thin films) pulsed dc magnetron sputtering. The structural and morphological characterizations revealed that Ag thin film forms a continuous layer, while the incorporation of oxygen in the deposition atmosphere lead to the formation of a thin film composed by a mixture of two crystalline phases: Ag and silver oxide. The latter thin film was characterized by the presence of islands with several hundreds of nanometers surrounded by smaller nanoparticles with tens of nanometers. The halo inhibition zone tests revealed the antibacterial behavior of Ag_xO thin films against *S. epidermidis* and *S. aureus*; conversely no antibacterial effect was found in Ag thin film. The differences between these two coatings might be related not only to the presence of silver oxide phase, but also to the differences found in coatings growth mode; with Ag coatings forming a continuous layer and Ag_xO forming islands surrounded by smaller nanoparticles that should promote silver ion release (known as antimicrobial agent). Thus, in order to better understand the mechanism that rules the antimicrobial activity of the Ag_xO coatings new depositions were performed.

iv) Different Ag_xO coatings, were deposited with different O_2 flow, during the deposition process. The structural and morphological characterizations revealed that, Ag coating forms a continuous layer, composed by crystalline FCC-Ag phase. The incorporation of oxygen in the deposition atmosphere leads to the formation of a coating composed by a mixture of Ag_2O+ AgO phases. As the amount of oxygen flow increases, the observed continuous thin film became, only, AgO, with a monoclinic crystalline phase. Halo inhibition testes revealed the antibacterial behavior of Ag_xO coating unlike Ag coating. By ICP-OES measurements the Ag^+ release is similar for the silver and silver oxide coatings. So a new mechanism for the observed antimicrobial activity was proposed. The incorporation of oxygen leads to a higher formation of ROS and, consequently, to an antibacterial behavior. The obtained results suggest that Ag_xO coating, deposited by dc magnetron sputtering has potential to be used in coronary stents.

v) Stents functionalized with silver and silver oxide coatings demonstrated that silver oxide stents present antibacterial behavior. Cytotoxicity assays revealed that both silver and silver oxide coated stents are not cytotoxic and can be used in human body.

Considering all tests performed, polyester coated stent with silver oxide seems to present a great potential to be applied as a biomaterial and be a candidate of substitution of nitinol commercial stents. Silver oxide coated stents present a good mechanical behavior, when compared with nitinol stents available in the market and as an advantage it is provide with antibacterial properties, without causing any harm to human body.

2. Future Work

Despite the promised results obtained in this work, and considering the final application, some suggestions of future investigation can be proposed.

Thus, it will be necessary to evaluate the mechanical behavior of stent in a simulated body fluid, as well as execute fatigue tests in stents, in order to evaluate the performance of the stents over the time and the behavior of coatings, when subject to repeated loads. Furthermore, biological assays should be realized in order to confirm the major production of ROS species from silver oxide coatings, when compared with silver coatings.

Once, medical devices can be colonized by several species, antibacterial assays against other species, like *Escherichia coli* and *Pseudomonas aeruginosa* should be carried out. Furthermore, another coatings should be studied and incorporate in the stent's surface, like anti-inflammatory coatings, with the sense of minimize an inflammatory response from the human body. Additionally, studies regarding stent's sensing should be performed, for non-invasive follow-up of the stent location, function and integration in the patient.

Finally, it would be important to develop a stent able to provide mechanical support, and antibacterial properties, only while it is needed and then disappear from the vessel, allowing its natural healing and avoiding the risks associated with having a permanent implant in place. Consequently, bioabsorbable material should be considered for further studies.

References

[1] M. Nichols, N. Townsend, P. Scarborough, M. Rayner, Cardiovascular disease in Europe 2014 - Epidemiological update, Eur. Heart J. 35 (2014) 2950–2959.

[2] N. Vila, Braided Hybrid Stents Design, 2009.

[3] J.H. Kim, T.J. Kang, W.R. Yu, Mechanical modeling of self-expandable stent fabricated using braiding technology, J. Biomech. 41 (2008) 3202–3212.

[4] S. Rajendran, S.C. Anand, J.F. Kennedy, Medical Textiles and Biomaterials for Healthcare, 2006.

[5] Z. Paszenda, Use of coronary stents - material and biophysical conditions, 43 (2010) 125–135.

[6] L.H.G. França, A.H. Pereira, Update on vascular endoprostheses (stents):from experimental studies to clinical pratice, J. Vasc. Bras. 7 (2008) 351–363.

[7] Z. Paszenda, Use of coronary stents - material and biophysical conditions, J. Chievements Mater. Manuf. Eng. 43 (2010) 125–135.

[8] J. Sheldrake, Drug-eluting stents begin to replace bare metal, (2003).

[9] T. Simard, B. Hibbert, F.D. Ramirez, M. Froeschl, Y.X. Chen, E.R. O'Brien, The Evolution of Coronary Stents: A Brief Review, Can. J. Cardiol. 30 (2014) 35–45.

[10] H.G. Puskas JE, Muñoz-Robledo LG, Hoerr RA, Foley J, Schmidt SP, Evancho-Chapman M, Dong J, Frethem C, Drug-eluting stent coatings, Wiley Interdiscip. Rev. Nanomedicine Nanobiotechnology. 4 (2009) 451–462.

[11] X. Ma, T. Wu, M.P. Robich, Drug - eluting Stent Coatings, 4 (2012) 73–83.

[12] R. Rebelo, R. Fangueiro, S. Carvalho, M. Henriques, S. Rana, Methods of incorporation antimicrobial agents in stents, Int. J. Eng. Sci. Innov. Technol. 3 (2014) 409–422.

[13] J.E. Sousa, M. a Costa, A. Abizaid, a S. Abizaid, F. Feres, I.M. Pinto, et al., Lack of neointimal proliferation after implantation of sirolimus-coated stents in human coronary arteries: a quantitative coronary angiography and three-dimensional intravascular ultrasound study., Circulation. 103 (2001) 192–195.

[14] R. Rebelo, N. Vila, R. Fangueiro, S. Carvalho, S. Rana, Influence of design parameters on the mechanical behavior and porosity of braided fibrous stents, Mater. Des. 86 (2015) 237–247.

[15] S.A. Shabalovskaya, J.W. Anderegg, A. Undisz, M. Rettenmayr, G.C. Rondelli, Corrosion resistance, chemistry, and mechanical aspects of Nitinol surfaces formed in hydrogen

peroxide solutions, J. Biomed. Mater. Res. - Part B Appl. Biomater. 100 B (2012) 1490–1499.

[16] I. Milošev, B. Kapun, The corrosion resistance of Nitinol alloy in simulated physiological solutions: Part 1: The effect of surface preparation, Mater. Sci. Eng. C. 32 (2012) 1068–1077.

[17] M. Saugo, D.O. Flamini, L.I. Brugnoni, S.B. Saidman, Silver deposition on polypyrrole films electrosynthesised onto Nitinol alloy. Corrosion protection and antibacterial activity, Mater. Sci. Eng. C. 56 (2015) 95–103.

[18] C. Trépanier, L. Zhu, J. Fino, A.R. Pelton, Corrosion Resistance of Oxidized Nitinol, in: Proc. SMST-2003, 2004: pp. 367–373.

[19] C.C. Shih, S.J. Lin, Y.L. Chen, Y.Y. Su, S.T. Lai, G.J. Wu, et al., The cytotoxicity of corrosion products of nitinol stent wire on cultured smooth muscle cells, J. Biomed. Mater. Res. 52 (2000) 395–403.

[20] S. Kujala, Biocompatibility and Biomechanical Aspects of Nitinol Shape Memory Metal Implants, Academic Dissertation, Faculty of Medicine, University of Oulu, 2003.

[21] J.R.P.D. Hendra Hermawan, Dadan Ramdan, Metals for biomedical applications, in: Biomed. Eng. - From Theory to Appl., InTech, 2011: pp. 411–430.

[22] B. O'Brien, W. Carroll, The evolution of cardiovascular stent materials and surfaces in response to clinical drivers: A review, Acta Biomater. 5 (2009) 945–958.

[23] A. Kastrati, J. Mehilli, J. Dirschinger, F. Dotzer, H. Schuhlen, F.-J. Neumann, et al., Intracoronary Stenting and Angiographic Results : Strut Thickness Effect on Restenosis Outcome (ISAR-STEREO) Trial, Circulation. 103 (2001) 2816–2821.

[24] C. Briguori, C. Sarais, P. Pagnotta, F. Liistro, M. Montorfano, A. Chieffo, et al., In-stent restenosis in small coronary arteries : Impact of strut thickness, J. Am. Coll. Cardiol. 40 (2002) 403–409.

[25] F. Airoldi, A. Colombo, D. Tavano, G. Stankovic, S. Klugmann, V. Paolillo, et al., Comparison of diamond-like carbon-coated stents versus uncoated stainless steel stents in coronary artery disease, Am. J. Cardiol. 93 (2004) 474–477.

[26] G.C.X. Meireles, L.M. de Abreu, A.A.D.C. Forte, M.K. Sumita, J.H. Sumita, J.D.C.S. Aliaga, Randomized comparative study of diamond-like carbon coated stainless steel stent versus uncoated stent implantation in patients with coronary artery disease., Arq. Bras. Cardiol. 88 (2007) 343–347.

[27] Y.H. Kim, C.W. Lee, M.K. Hong, S.W. Park, S.J. Tahk, J.Y. Yang, et al., Randomized comparison of carbon ion-implanted stent versus bare metal stent in coronary artery disease: The Asian Pacific Multicenter Arthos Stent Study (PASS) trial, Am. Heart J. 149 (2005) 336–341.

[28] M. Unverdorben, B. Sippel, R. Degenhardt, K. Sattler, R. Fries, B. Abt, et al., Comparison of a silicon carbide-coated stent versus a noncoated stent in human beings: the Tenax versus Nir Stent Study's long-term outcome., Am. Heart J. 145 (2003) e17.

[29] S. Windecker, R. Simon, M. Lins, V. Klauss, F.R. Eberli, M. Roffi, et al., Randomized comparison of a titanium-nitride-oxide-coated stent with a stainless steel stent for coronary revascularization - The TiNOX trial, Circulation. 111 (2005) 2617–2622.

[30] S. Irsale, Design and Characterization of Polymeric Stents, J. Ind. Text. 35 (2006) 189–200.

[31] A.F.D.P. Freitas, M.D. de Araujo, W.W. Zu, R.M.E. Fangueiro, Development of weft-knitted and braided polypropylene stents for arterial implant, J. Text. Inst. 101 (2010) 1027–1034.

[32] A. Avino, B. Johnson, D. Bandyk, M. Back, S. Roth, B. Kudryk, et al., Does prosthetic covering of nitinol stents alter healing characteristics or hemodynamics?, J. Endovasc. Ther. 7 (2000) 469–478.

[33] B. Marty, A.J. Leu, A. Mucciolo, L.K. von Segesser, Biologic fixation of polyester- versus polyurethane-covered stents in a porcine model., J. Vasc. Interv. Radiol. 13 (2002) 601–607.

[34] H. Tamai, K. Igaki, E. Kyo, K. Kosuga, A. Kawashima, S. Matsui, et al., Initial and 6-Month Results of Biodegradable Poly-l-Lactic Acid Coronary Stents in Humans, Circulation. 102 (2000) 399–404.

[35] S. Nishio, K. Kosuga, K. Igaki, M. Okada, E. Kyo, T. Tsuji, et al., Long-term (>10 Years) clinical outcomes of first-in-human biodegradable poly-l-lactic acid coronary stents: Igaki-Tamai stents, Circulation. 125 (2012) 2343–2352.

[36] S. Garg, P.W. Serruys, Coronary stents: Current status, J. Am. Coll. Cardiol. 56 (2010) S1–42.

[37] J.A. Ormiston, P.W. Serruys, E. Regar, D. Dudek, L. Thuesen, M.W. Webster, et al., A bioabsorbable everolimus-eluting coronary stent system for patients with single de-novo coronary artery lesions (ABSORB): a prospective open-label trial, Lancet. 371 (2008)

899–907.

[38] J. Cruz, S. Rana, R. Fangueiro, R. Guedes, Designing artificial anterior cruciate ligaments based on novel fibrous structures, Fibers Polym. 15 (2014) 181–186.

[39] W. Zhong, Applications Braided Structures in Medical Fields, Braided Strctures and Composites: production, Properties, Mechanics, and Technical Applications, CRC Press, 2015.

[40] S. Zhao, X. (Cheryl) Liu, L. Gu, The Impact of Wire Stent Fabrication Technique on the Performance of Stent Placement, J. Med. Device. 6 (2012) 011007–1–011007–4.

[41] Y. Hoi, C.N. Ionita, R. V. Tranquebar, K.R. Hoffmann, H.W. Scott, D.B. Taulbee, et al., Flow modification in canine intracranial aneurysm model by an asymmetric stent: studies using digital subtraction angiography (DSA) and image-based computational fluid dynamics (CFD) analyses, in: Proceedings of the Society of Photo-Optical Instrumentation Engineers, 2006.

[42] J. Hyun Kim, T. Jin Kang, W.R. Yu, Simulation of mechanical behavior of temperature-responsive braided stents made of shape memory polyurethanes, J. Biomech. 43 (2010) 632–643.

[43] C.M.F. Dias, Design de Estruturas Fibrosas Híbridas para Aplicação Técnica, Universidade do Minho, 2009.

[44] R.F. e H.H. Mário de Araújo, Têxteis Técnicos – Materiais do Novo Milénio, Vol. I – Visão Geral, Williams/DGI, Lda., 2000.

[45] S. Rana, R. Fangueiro, Braided Structures and Composites: Production, Properties, Mechanics, and Technical Applications, CRC Press, 2016.

[46] P. Potluri, A. Rawal, M. Rivaldi, I. Porat, Geometrical modelling and control of a triaxial braiding machine for producing 3D preforms, Compos. Part A Appl. Sci. Manuf. 34 (2003) 481–492.

[47] N. Hoiby, T. Bjarnsholt, M. Givskov, S. Molin, O. Ciofu, Antibiotic resistance of bacterial biofilms, Int. J. Antimicrob. Agents. 35 (2010) 322–332.

[48] D. Pavithra, M. Doble, Biofilm formation, bacterial adhesion and host response on polymeric implants–issues and prevention., Biomed. Mater. 3 (2008) 1–13.

[49] M.L.W. Knetsch, L.H. Koole, New strategies in the development of antimicrobial coatings: The example of increasing usage of silver and silver nanoparticles, Polymers (Basel). 3 (2011) 340–366.

[50] M.E. Cortés, J.C. Bonilla, R.D. Sinisterra, Biofilm formation, control and novel strategies for eradication, Sci. against Microb. Pathog. Commun. Curr. Res. Technol. Adv. (2011) 896–905.

[51] M. Elieson, T. Mixon, C. John, Coronary Stent Infections : A Case Report and Literature Review, Hear. Inst. J. 39 (2012) 884–889.

[52] R.A. dos R.M. Cardoso, As infeções associadas aos cuidados de saúde, Universidade de Coimbra, 2015.

[53] L.R. Rodrigues, Inhibition of Bacterial Adhesion on Medical Devices, Exp. Med. Biol. 715 (2011) 351–367.

[54] I.M.F. de G. e Silva, Antibacterial properties of multifunctional coatings Ag-ZrCN for biomedical devices: a novel approach, University of Minho, 2016.

[55] R.M. Donlan, Biofilms and device-associated infections, Emerg. Infect. Dis. 7 (2001) 277–281.

[56] L. Montanaro, S. Pietro, C. Davide, R. Stefano, C. Ilaria, P. Giampiero, et al., Scenery of Staphylococcus implant infections in orthopedics, Future Microbiol. 6 (2011) 1329–1349.

[57] I. Carvalho, M. Henriques, J.C. Oliveira, C.F. Almeida Alves, A.P. Piedade, S. Carvalho, Influence of surface features on the adhesion of Staphyloccocus epidermidis to Ag–TiCN thin films, Sci. Technol. Adv. Mater. 14 (2013) 1–10.

[58] F. Fitzpatrick, H. Humphreys, E. Smyth, C.A. Kennedy, J.P. O'Gara, Environmental regulation of biofilm formation in intensive care unit isolates of Staphylococcus epidermidis, J. Hosp. Infect. 42 (2002) 212–218.

[59] I. Carvalho, Development of antimicrobial multifunctional coatings based on Ag-Ti(C,N), University of Minho, 2014.

[60] P. Singleton, D. Sainsbury, Dictionary of Microbiology and Molecular Biology, Third edition, 3rd ed., John Wiley &Sons, Ltd, 2006.

[61] W.M.P.F. Bosman, B.L.S. Borger van der Burg, H.M. Schuttevaer, S. Thoma, P.P. Hedeman Joosten, Infections of intravascular bare metal stents: a case report and review of literature., Eur. J. Vasc. Endovasc. Surg. 47 (2014) 87–99.

[62] S.P. Hawser, S.K. Bouchillon, D.J. Hoban, M. Dowzicky, T. Babinchak, Rising incidence of Staphylococcus aureus with reduced susceptibility to vancomycin and susceptibility to antibiotics: A global analysis 2004-2009, Int. J. Antimicrob. Agents. 37 (2011) 219–224.

[63] P. Thevenot, W. Hu, L. Tang, Surface Chemistry Influence Implant Biocompatibility, Curr.

Top. Med. Chem. 8 (2008) 270–280.

[64] B. Thierry, F.M. Winnik, Y. Merhi, J. Silver, M. Tabrizian, Bioactive coatings of endovascular stents based on polyelectrolyte multilayers, Biomacromolecules. 4 (2003) 1564–1571.

[65] G.A. Sotiriou, S.E. Pratsinis, Antibacterial Activity of Nanosilver Ions and Particles, Environ. Sci. Technol. 44 (2010) 5649–5654.

[66] M.A. Kohanski, D.J. Dwyer, J.J. Collins, How antibiotics kill bacteria: from targets to networks., Nat. Rev. Microbiol. 8 (2010) 423–435.

[67] M. Chen, Q. Yu, H. Sun, Novel strategies for the prevention and treatment of biofilm related infections, Int. J. Mol. Sci. 14 (2013) 18488–18501.

[68] World Health Organization, Antimicrobial resistance, 2014.

[69] L.D. de Melo, Partículas e filmes híbridos de polímeros e compostos de amônio quaternário com atividade antimicrobiana, Faculdade de Ciências Farmacêuticas da Universidade de São PAulo, 2010.

[70] T. Thorsteinsson, T. Loftsson, M. Masson, Soft antibacterial agents., Curr. Med. Chem. 10 (2003) 1129–36.

[71] M. Rai, A. Yadav, A. Gade, Silver nanoparticles as a new generation of antimicrobials, Biotechnol. Adv. 27 (2009) 76–83.

[72] I. Ferreri, S. Calderon V, R. Escobar Galindo, C. Palacio, M. Henriques, A.P. Piedade, et al., Silver activation on thin films of Ag-ZrCN coatings for antimicrobial activity., Mater. Sci. Eng. C. 55 (2015) 547–555.

[73] D.-H. Song, S.-H. Uhm, S.-B. Lee, J.-G. Han, K.-N. Kim, Antimicrobial silver-containing titanium oxide nanocomposite coatings by a reactive magnetron sputtering, Thin Solid Films. 519 (2011) 7079–7085.

[74] B. Reidy, A. Haase, A. Luch, K.A. Dawson, I. Lynch, Mechanisms of silver nanoparticle release, transformation and toxicity: A critical review of current knowledge and recommendations for future studies and applications, Materials (Basel). 6 (2013) 2295–2350. doi:10.3390/ma6062295.

[75] N.K. Vu, A. Zille, F.R. Oliveira, N. Carneiro, A.P. Souto, Effect of particle size on silver nanoparticle deposition onto dielectric barrier discharge (DBD) plasma functionalized polyamide fabric, Plasma Process. Polym. 10 (2013) 285–296.

[76] L. Yang, S. Whiteside, P.A. Cadieux, J.D. Denstedt, Ureteral stent technology : Drug-eluting

stents and stent coatings, Asian J. Urol. 2 (2015) 194–201.

[77] M. Lachine, A. El-Nahas, E. Elsawy, A. Mosbah, H. El-Kappany, A randomized controlled trial comparing antimicrobial coated (silver sulfadiazine) ureteral stents with non-coated stents, Eur. Urol. Suppl. 15 (2016) e1038.

[78] W. Wen, L.-M. Ma, W. He, X.-W. Tang, Y. Zhang, X. Wang, et al., Silver-nanoparticle-coated biliary stent inhibits bacterial adhesion in bacterial cholangitis in swine, Hepatobiliary Pancreat. Dis. Int. 15 (2016) 87–92.

[79] B. Atiyeh, M. Costagliola, S.N. Hayek, S.A. Dibo, Effect of silver on burn wound in infection control and healing: Review of the literature, Burns. 33 (2007) 139–148.

[80] S.W.P. Wijnhoven, W.J.G.M. Peijnenburg, C. a Herberts, W.I. Hagens, A.G. Oomen, E.H.W. Heugens, et al., Nano-silver – a review of available data and knowledge gaps in human and environmental risk assessment, Nanotoxicology. 3 (2009) 109–138.

[81] J.T. Seil, T.J. Webster, Antimicrobial applications of nanotechnology: Methods and literature, Int. J. Nanomedicine. 7 (2012) 2767–2781.

[82] G. Nam, S. Rangasamy, B. Purushothaman, J.M. Song, The Application of Bactericidal Silver Nanoparticles in Wound Treatment, Nanomater. Nanotechnol. (2015).

[83] W.-R. Li, X.-B. Xie, Q.-S. Shi, S.-S. Duan, Y.-S. Ouyang, Y.-B. Chen, Antibacterial effect of silver nanoparticles on Staphylococcus aureus, Biometals. 24 (2011) 135–141.

[84] K. Nakano, K. Egashira, S. Masuda, K. Funakoshi, G. Zhao, S. Kimura, et al., Formulation of Nanoparticle-Eluting Stents by a Cationic Electrodeposition Coating Technology. Efficient Nano-Drug Delivery via Bioabsorbable Polymeric Nanoparticle-Eluting Stents in Porcine Coronary Arteries, JACC Cardiovasc. Interv. 2 (2009) 277–283.

[85] D. He, A.M. Jones, S. Garg, A.N. Pharm, T.D. Waite, Silver nanoparticle– reactive oxygen species interactions: application of a charging– discharging model, J. Phys. Chem. C. 115 (2011) 5461–5468.

[86] R. Snyders, M. Wautelet, R. Gouttebaron, J.P. Dauchot, M. Hecq, Experimental and theoretical studies of the DC reactive magnetron sputtering deposition of silver oxide thin films, Surf. Coatings Technol. 174 -175 (2003) 1282–1286. doi:10.1016/S0257-8972.

[87] J.F. Pierson, C. Rousselot, Stability of reactively sputtered silver oxide films, Surf. Coatings Technol. 200 (2005) 276–279.

[88] G.A. Kumar, M.V.R. Reddy, K.N. Reddy, Structural and Optical Properties of AgO Thin Films Grown by RF Reactive Magnetron Sputtering Technique, in: Int. Conf. Adv.

Nanomater. Emerg. Eng. Technol., 2013: pp. 354–356.

[89] P.N. Reddy, M.H.P. Reddy, J.F. Pierson, S. Uthanna, Characterization of Silver Oxide Films Formed by Reactive RF Sputtering at Different Substrate Temperatures, ISRN Opt. 2014 (2014) 1–7.

[90] H.Y. Lee, H.K. Park, Y.M. Lee, K. Kim, S.B. Park, A practical procedure for producing silver nanocoated fabric and its antibacterial evaluation for biomedical applications., Chem. Commun. (2007) 2959–2961.

[91] S.Y. Park, J.W. Chung, R.D. Priestley, S.-Y. Kwak, Covalent assembly of metal nanoparticles on cellulose fabric and its antimicrobial activity, Cellulose. 19 (2012) 2141–2151.

[92] X. Wang, Thin Functional Plasma Polymer and Metal / Plasma Polymer Nanocomposite Films, Ruhr-Universitat Bochum, 2007.

[93] Y. Wang, A.S. Angelatos, F. Caruso, Template Synthesis of Nanostructured Materials via Layer-by-Layer Assembly, Chem. Mater. 20 (2008) 848–858.

[94] M. Michel, V. Toniazzo, D. Ruch, V. Ball, Deposition Mechanisms in Layer-by-Layer or Step-by-Step Deposition Methods: From Elastic and Impermeable Films to Soft Membranes with Ion Exchange Properties, ISRN Mater. Sci. 2012 (2012) 1–13.

[95] S. Hossfeld, A. Nolte, H. Hartmann, M. Recke, M. Schaller, T. Walker, et al., Bioactive coronary stent coating based on layer-by-layer technology for siRNA release, Acta Biomater. 9 (2013) 6741–6752.

[96] A.W. Martinez, E.L. Chaikof, Microfabrication and nanotechnology in stent design, Wiley Interdiscip. Rev. Nanomedicine Nanobiotechnology. 3 (2011) 256–268.

[97] A. Mahapatro, D.M. Johnson, D.N. Patel, M.D. Feldman, A.A. Ayon, C.M. Agrawal, The use of alkanethiol self-assembled monolayers on 316L stainless steel for coronary artery stent nanomedicine applications: an oxidative and in vitro stability study, Nanomedicine Nanotechnology, Biol. Med. 2 (2006) 182–190.

[98] W. Gan, B. Xu, H.L. Dai, Activation of thiols at a silver nanoparticle surface, Angew. Chemie - Int. Ed. 50 (2011) 6622–6625.

[99] F. Lewis, P. Horny, P. Hale, S. Turgeon, M. Tatoulian, D. Mantovani, Study of the adhesion of thin plasma fluorocarbon coatings resisting plastic deformation for stent applications, J. Phys. D. Appl. Phys. 41 (2008) 045310 (7pp).

[100] D. Roman, Deposição de Filmes Finos de Nitreto de Zircônio para Aplicação em

Biomateriais, Universidade de Caxias do Sul, 2010.

[101] S. Carvalho, Propriedades mecânicase características microestruturais de filmes finos nanocompósitos de (Ti,Al,Si)N preparados por pulverização catódica reactiva em magnetrão, Universidade do Minho, 2004.

[102] D.M. Mattox, Handbook of Physical Vapor Deposition (PVD) Processing, Noyes Publications, 1998.

[103] V. Loureiro, Modificação da superfície de implantes neuronais superfície de implantes neuronais, Universidade de Coimbra, 2010.

[104] P.V. Kashtanov, B.M. Smirnov, R. Hippler, Magnetron plasma and nanotechnology, Physics-Uspekhi. 50 (2007) 455–488.

[105] S.T. Shishiyanu, T.S. Shishiyanu, P.S. Stefanov, V.K. Gueorguiev, DLC Thin Films for Cardiovascular Stents, in: Int. Symp. Biomed. Eng. Med. Physics, IFMBE Proc., 2013: pp. 198–200.

[106] A.P. Piedade, J. Nunes, M.T. Vieira, Thin films with chemically graded functionality based on fluorine polymers and stainless steel, Acta Biomater. 4 (2008) 1073–1080.

[107] N. Elmrabet, N. Botterill, D.M. Grant, P.D. Brown, Characterisation of Mg biodegradable stents produced by magnetron sputtering, J. Phys. Conf. Ser. 644 (2015).

[108] J.G. Guillén, Fibras Textiles – Propriedades y descripcion, Editora Terrasa, 1991.

[109] D. Ramos, Têxteis Cirúrgicos Reutilizáveis E Seu Impacte Ambiental, Universidade do Minho, 2003.

[110] International Organization for Standardization, Textiles- Yarns from packages-Determination of Single-end Breaking Force and Elongation at Break, ISO 2062, (1993).

[111] Têxteis : fios - determinação da massa linear (massa por unidade de comprimento)-Método da meada,NP EN ISO 2060, (1996).

[112] Standard Test Method for Coefficient of Friction , Yarn to Solid Material, ASTM 3108, (2007).

[113] P. Gill, T.T. Moghadam, B. Ranjbar, Differential scanning calorimetry techniques: applications in biology and nanoscience., J. Biomol. Tech. 21 (2010) 167–193.

[114] M.E. Yüksekkaya, Analysis of Elastic Deformation of Braided Tubular Structures for Medical Applications, J. Eng. Sci. (2001) 277–285.

[115] G. Leibundgut, M. Gick, A. Toma, C. Valina, N. Löffelhardt, H.J. Büttner, et al., Longitudinal compression of the platinum-chromium everolimus-eluting stent during

coronary implantation: Predisposing mechanical properties, incidence, and predictors in a large patient cohort, Catheter. Cardiovasc. Interv. 81 (2013) 206–214.

[116] I. W. L. Gore & Associates, Mechanical Properties of Nitinol Stents and Stent-grafts: Comparison of 6mm Diameter Devices, (2007) 1–11.

[117] T. Moon, D. Hong, H.J. Chun, K.B. Lee, Analytical models for predicting mechanical properties of mesh-type self-expandable metal stents with cover membrane, Curr. Appl. Phys. 9 (2009) 92–100.

[118] P. Poncin, J. Proft, Stent Tubing: Understanding the Desired Attributes, Proc. ASM Conf. Mater. Process. Med. Devices. (2003).

[119] O. Lyutakov, I. Goncharova, S. Rimpelova, K. Kolarova, J. Svanda, V. Svorcik, Silver release and antimicrobial properties of PMMA films doped with silver ions, nano-particles and complexes, Mater. Sci. Eng. C. 49 (2015) 534–540.

[120] P. Dallas, V.K. Sharma, R. Zboril, Silver polymeric nanocomposites as advanced antimicrobial agents: Classification, synthetic paths, applications, and perspectives, Adv. Colloid Interface Sci. 166 (2011) 119–135.

[121] J.A. Spadaro, S.E. Chase, D.A. Webster, Bacterial inhibition by electrical activation of percutaneous silver implants., J. Biomed. Mater. Res. 20 (2004) 565–577.

[122] S.B. Sant, K.S. Gill, R.E. Burrell, The nature of chemical species in novel antimicrobial silver films deposited by magnetron sputtering, Philos. Mag. A. 82 (1999) 1115–1136.

[123] M. Anzano, A. Tosti, M. Lasagni, A. Campiglio, D. Pitea, E. Collina, Antimicrobial activity of thin metallic silver flakes,waste products of a manufacturing process, 23 (2011) 1570–1577.

[124] C.-N. Lok, C.-M. Ho, R. Chen, Q.-Y. He, W.-Y. Yu, H. Sun, et al., Silver nanoparticles: partial oxidation and antibacterial activities., J. Biol. Inorg. Chem. 12 (2007) 527–534.

[125] S.B. Sant, K.S. Gill, R.E. Burrell, Nanostructure, dissolution and morphology characteristics of microcidal silver films deposited by magnetron sputtering, Acta Biomater. 3 (2007) 341–350.

[126] H. Palza, Antimicrobial polymers with metal nanoparticles, Int. J. Mol. Sci. 16 (2015)

[127] R. Snyders, J.-P. Dauchot, M. Hecq, Synthesis of Metal Oxide Thin Films by Reactive Magnetron Sputtering in Ar/O2 Mixtures: An Experimental Study of the Chemical Mechanisms, Plasma Process. 4 (2007) 113–126.

[128] S.M. Marques, N.K. Manninen, S. Lanceros-Mendez, S. Carvalho, Ag-TiNx electrodes

deposited on piezoelectric poly(vinylidene fluoride) for biomedical sensor applications, Sensors Actuators, A Phys. 234 (2015) 1–8.

[129] S.M. da S. Marques, Development of multifunctional coatings deposited on polymers based sensors for biomedical applications, University of Minho, 2016.

[130] R.E. Whan, ASM Handbook :Materials characterization, 1986.

[131] L.A.C.G. Cunha, Estudo dos mecanismos de degradação em revestimentos PVD baseados em nitretos metálicos no processamento de materiais plásticos, University of Minho, 2000.

[132] D.M. Smilgies, Scherrer grain-size analysis adapted to grazing-incidence scattering with area detectors, J. Appl. Crystallogr. 42 (2009) 1030–1034.

[133] C.J. van Oss, R.F. Giese, The hydrophilicity and hidrophobicity of clay minerals, Clays Clay Miner. 43 (1995) 474–477.

[134] B. Janczuk, E. Chibowski, J.M. Bruque, M.L. Kerkeb, F.G. Caballero, On the Consistency of Surface Free Energy Components as Calculated from Contact Angles of Different Liquids: An Application to the Cholesterol Surface, J. Colloid Interface Sci. 159 (1993) 421–428.

[135] D. Carter, H. Walde, G. McDonough, G. Roche, Parameter optimization in pulsed DC reactive sputter deposition of aluminum oxide, 45th Annu. Tech. Conf. Proceedings. (2002) 570–577. http://www.advanced-energy.com/en/upload/File/Reprints/Param Opt in Plsd DC Reac Sputt Dep Alum Ox.pdf.

[136] D. Depla, J. Haemers, R. De Gryse, Discharge voltage measurements during reactive sputtering of oxides, Thin Solid Films. 515 (2006) 468–471.

[137] J.F. Pierson, D. Wiederkehr, A. Billard, Reactive magnetron sputtering of copper, silver, and gold, Thin Solid Films. 478 (2005) 196–205.

[138] F. Paladini, R.A. Picca, M.C. Sportelli, N. Cioffi, A. Sannino, M. Pollini, Surface chemical and biological characterization of flax fabrics modified with silver nanoparticles for biomedical applications, Mater. Sci. Eng. C. 52 (2015) 1–10.

[139] S. Calderon V, R.E. Galindo, N. Benito, C. Palacio, A. Cavaleiro, S. Carvalho, Ag + release inhibition from ZrCN–Ag coatings by surface agglomeration mechanism: structural characterization, J. Phys. D. Appl. Phys. 46 (2013).

[140] A.M. Ferraria, A.P. Carapeto, A.M. Botelho Do Rego, X-ray photoelectron spectroscopy: Silver salts revisited, Vacuum. 86 (2012) 1988–1991.

[141] C. Vicent, Handbook of Monochromatic XPS Spectra, The Elements of Native Oxides, Wiley, 2000.

[142] V.K. Kaushik, XPS core level spectra and Auger parameters for some silver compounds, J. Electron Spectros. Relat. Phenomena. 56 (1991) 273–277.

[143] E.A. Vogler, Protein adsorption in three dimensions, Biomaterials. 33 (2012) 1201–1237.

[144] I. Carvalho, M. Henriques, S. Carvalho, New strategies to fight bacterial adhesion, Microb. Pathog. Strateg. Combat. Them Sci. Technol. Educ. (2013) 170–178.

[145] A.M. Meier, P. Chidambaram, G.R. Edwards, A comparison of the wettability of copper-copper oxide and silver-copper oxide on polycrystalline alumina, J. Mater. Sci. 30 (1995) 4781–4786.

[146] P. Dutheil, A.L. Thomann, T. Lecas, P. Brault, M. Vayer, Sputtered Ag thin films with modified morphologies: Influence on wetting property, Appl. Surf. Sci. 347 (2015) 101–108.

[147] M. Mirzaeian, A.A. Ogwu, H.F. Jirandehi, S. Aidarova, Z. Ospanova, N. Tsendzughul, Surface characteristics of silver oxide thin film electrodes for supercapacitor applications, Colloids Surfaces A Physicochem. Eng. Asp. (2016).

[148] R. Bayston, L. Vera, A. Mills, W. Ashraf, O. Stevenson, S.M. Howdle, In vitro antimicrobial activity of silver-processed catheters for neurosurgery, J. Antimicrob. Chemother. 65 (2010) 258–265.

[149] C. Gorzelanny, R. Kmeth, A. Obermeier, A.T. Bauer, N. Halter, K. Kümpel, et al., Silver nanoparticle-enriched diamond-like carbon implant modification as a mammalian cell compatible surface with antimicrobial properties, Sci. Rep. 6 (2016).

[150] N. Tran, M.N. Kelley, P.A. Tran, D.R. Garcia, J.D. Jarrell, R.A. Hayda, et al., Silver doped titanium oxide-PDMS hybrid coating inhibits Staphylococcus aureus and Staphylococcus epidermidis growth on PEEK, Mater. Sci. Eng. C. 49 (2015) 201–209.

[151] N. Duran, P.D. Marcato, R. De Conti, O.L. Alves, F.T.M. Costa, M. Brocchi, Potential Use of Silver Nanoparticles on Pathogenic Bacteria, their Toxicity and Possible Mechanisms of Action, J. Braz. Chem. Soc. 21 (2010) 949–959.

[152] A.A. Ivanova, R.A. Surmenev, M.A. Surmeneva, T. Mukhametkaliyev, K. Loza, O. Prymak, et al., Hybrid biocomposite with a tunable antibacterial activity and bioactivity based on RF magnetron sputter deposited coating and silver nanoparticles, Appl. Surf. Sci. 329 (2015) 212–218.

[153] L. Incerti, A. Rota, S. Valeri, A. Miguel, J.A. García, R.J. Rodríguez, et al., Nanostructured self-lubricating CrN-Ag films deposited by PVD arc discharge and magnetron sputtering, Vacuum. 85 (2011) 1108–1113.

[154] W.C. Chiang, I.S. Tseng, P. Møller, L.R. Hilbert, T. Tolker-Nielsen, J.K. Wu, Influence of silver additions to type 316 stainless steels on bacterial inhibition, mechanical properties, and corrosion resistance, Mater. Chem. Phys. 119 (2010) 123–130.

[155] J.-B. Ricco, O. Assadian, Antimicrobial Silver Grafts for Prevention and Treatment of Vascular Graft Infection, Semin. Vasc. Surg. 4 (2011) 234–241.

[156] S. Ferraris, S. Perero, M. Miola, E. Vern??, A. Rosiello, V. Ferrazzo, et al., Chemical, mechanical and antibacterial properties of silver nanocluster/silica composite coated textiles for safety systems and aerospace applications, Appl. Surf. Sci. 317 (2014) 131–139.

[157] J.J. Hu, C. Muratore, A.A. Voevodin, Silver diffusion and high-temperature lubrication mechanisms of YSZ-Ag-Mo based nanocomposite coatings, Compos. Sci. Technol. 67 (2007) 336–347.

[158] N. Ravi Chandra Raju, K. Jagadeesh Kumar, A. Subrahmanyam, Physical properties of silver oxide thin films by pulsed laser deposition: effect of oxygen pressure during growth, J. Phys. D. Appl. Phys. 42 (2009) 135411–135416.

[159] U.K. Barik, S. Srinivasan, C.L. Nagendra, A. Subrahmanyam, Electrical and optical properties of reactive DC magnetron sputtered silver oxide thin films: Role of oxygen, Thin Solid Films. 429 (2003) 129–134.

[160] D. Dellasega, A. Facibeni, F. Di Fonzo, V. Russo, C. Conti, C. Ducati, et al., Nanostructured high valence silver oxide produced by pulsed laser deposition, Appl. Surf. Sci. 255 (2009) 5248–5251.

[161] W. Wei, X. Mao, L. a. Ortiz, D.R. Sadoway, Oriented silver oxide nanostructures synthesized through a template-free electrochemical route, J. Mater. Chem. 21 (2011) 432–438.

[162] J. Liu, D.A. Sonshine, S. Shervani, R.H. Hurt, Controlled release of biologically active silver from nanosilver surfaces, ACS Nano. 4 (2010) 6903–6913.

[163] S. Ninganagouda, V. Rathod, D. Singh, J. Hiremath, A.K. Singh, J. Mathew, et al., Growth kinetics and mechanistic action of reactive oxygen species released by silver nanoparticles from Aspergillus niger on Escherichia coli, Biomed Res. Int. 2014 (2014).

[164] C.J. Powell, Recommended Auger parameters for 42 elemental solids, J. Electron Spectros. Relat. Phenomena. 185 (2012) 1–3. doi:10.1016/j.elspec.2011.12.001.

[165] L.J. Gerenser, Photoemission investigation of silver/poly(ethylene terephthalate) interfacial chemistry: The effect of oxygen-plasma treatment, J. Vac. Sci. Technol. A. 8 (1990).

[166] O. Leroy, E. Martin, A. Prat, E. Decoulx, H. Georges, J. Guilley, et al., Fatal infection of coronary stent implantation, Cathet. Cardiovasc. Diagn. 39 (1996) 168–170.

[167] B.A. Kaufmann, C. Kaiser, M.E. Pfisterer, P.O. Bonetti, Coronary stent infection: A rare but severe complication of percutaneous coronary intervention, Swiss Med. Wkly. 135 (2005) 483–487.

[168] E. Gonda, A. Edmundson, T. Mann, Late Coronary Stent Infection: A Unique Complication after Drug-Eluting Stent Implantation, J Invasive Cardiol. 19 (2007) 307–308.

[169] R.S. Dieter, Coronary artery stent infection, Clin. Cardiol. 23 (2000) 808–810.

[170] International Organization for Standardization, Biological Evaluation of Medical Devices Part 5: Tests for In Vitro Cytotoxicity, ISO 10993-5, 2009.

[171] Promega Corporation, CellTiter 96 ® AQueous One Solution Cell Proliferation Assay, Tech. Bull. (2012) 2014–12–15. www.promega.com/protocols/.

[172] G. Malich, B. Markovic, C. Winder, The sensitivity and specificity of the MTS tetrazolium assay for detecting the in vitro cytotoxicity of 20 chemicals using human cell lines, Toxicology. 124 (1997) 179–192.

[173] Antimicrobial products- test for antimicrobial activity and efficacy. Japanese Industrial Standard JIS Z 2801:2000, 2000.

[174] J. Tambaca, S. Canic, M. Kosor, R.D. Fish, D. Paniagua, Mechanical behavior of fully expanded commercially available endovascular coronary stents., Tex. Heart Inst. J. 38 (2011) 491–501.

[175] C. Sousa, P. Teixeira, R. Oliveira, The role of extracellular polymers on Staphylococcus epidermidis biofilm biomass and metabolic activity, J. Basic Microbiol. 49 (2009) 363–370.

[176] N. Cerca, G.B. Pier, M. Vilanova, R. Oliveira, J. Azeredo, Quantitative analysis of adhesion and biofilm formation on hydrophilic and hydrophobic surfaces of clinical isolates of Staphylococcus epidermidis, Res. Microbiol. 156 (2005) 506–514.

[177] J.J. Hu, C. Muratore, A.A. Voevodin, Silver diffusion and high-temperature lubrication mechanisms of YSZ-Ag-Mo based nanocomposite coatings, Compos. Sci. Technol. 67

(2007) 336–347.